UNIVERSITY OF CALIFORNIA

Los Angeles

Carbon Efficient Conversion of Methanol to Higher Alcohols

A dissertation submitted in partial satisfaction of the

requirements for the degree Doctor of Philosophy

in Chemical Engineering

by

Chang-Ting Chen

2018

ABSTRACT OF THE DISSERTATION

Carbon Efficient Conversion of Methanol to Higher Alcohols

by

Chang-Ting Chen

Doctor of Philosophy in Chemical Engineering

University of California, Los Angeles, 2018

Professor James C. Liao

Methanol, a common derivative of natural gas, is increasingly attractive as a chemical feedstock due to its low cost and abundance. Among the technologies that converts methanol to value added chemicals, biological conversion has the advantage of mild reaction conditions low capital cost. Several methanol assimilation pathways can be found in nature. However, carbon yield for production of acetyl-CoA derived products using these pathways has intrinsic limits due to CO_2 lost in pyruvate decarboxylation or ATP requirement. To address the carbon yield problem, as our first Aim, a synthetic pathway termed methanol condensation cycle (MCC) was designed and demonstrated. MCC is an ATP-independent pathway that is capable of stoichiometric conversion of methanol to acetyl-CoA, a precursor to many longer chain products. With a cell-free system, a catalytic cycle of MCC was confirmed using ^{13}C labeled methanol. The *in vitro* production was further optimized by adjusting the key enzymes to avoid "kinetic

trap", where excess amount of certain enzymes would reduce the robustness of the cycle. As a result, the Aim was accomplished by demonstrating conversion of methanol to ethanol and 1-butanol with high carbon yield (80% and 50%, respectively).

During our work in realizing MCC, poor catalytic efficiency of NAD-dependent methanol dehydrogenase (Mdh) had been a major hurdle. The enzyme catalyzes a thermodynamically unfavorable methanol oxidation reaction and has higher activity towards ethanol and 1-butanol instead of methanol. Therefore, our second Aim was to bioprospect and engineer Mdhs for improved methanol oxidation activity. We first identified and characterized Mdh2 from *Cupriavidus necator* N-1 with significant activity towards methanol. We then employed directed evolution with high-throughput screening to further enhance methanol activity and specificity. As a result, the engineered Mdh2 variant CT4-1 showed 6-fold higher K_{cat}/K_m for methanol and 10-fold lower K_{cat}/K_m for 1-butanol.

With the experience in *in vitro* methanol conversion to chemical products and Mdh engineering, our third Aim was to engineer *E. coli* for methanol dependent growth and production. We constructed an *E. coli* strain that couples methanol assimilation to growth. By disrupting ribulose-phosphate 3-epimerase or ribose-5-phosphate isomerase in the pentose phosphate pathway, the strain was unable to utilize xylose or ribose as sole carbon source. Expression of methanol assimilation enzymes from the ribulose monophosphate pathway allowed the strain to co-utilize methanol with either one of the pentoses. This strain was termed as "synthetic methanol auxotrophy" since it cannot grow without methanol. This strain allowed us to optimize methanol assimilation by evolving for faster methanol-dependent growth. Our best strains were able to utilize methanol for growth to an OD_{600} of 4.0 in 30 hrs with methanol

and xylose co-assimilation at a molar ratio of about 1:1. Genome sequencing and reversion of mutations indicates that mutations on genes encoding for adenylate cyclase (*cyaA*) and the fromaldehyde detoxification operon (*frmABR*) are necessary for the growth phenotype. The methanol auxotrophy strain was further engineered to produce ethanol or 1-butanol to final titers of 4.6 g/L and 2.0 g/L, respectively. We also demonstrated the utility of this strain as a selection platform to significantly decrease residual methanol amount in growth medium. The synthetic methanol auxotrophy strain represents a useful platform for engineering methanol conversion.

The dissertation of Chang-Ting Chen is approved.

Harold G. Monbouquette

Yvonne Y. Chen

Beth A. Lazazzera

James C. Liao, Committee Chair

University of California, Los Angeles,

2018

To my loving family

University of California, Los Angeles

2018

Table of Contents

List of Figures

List of Tables

Chang-Ting Chen

EDUCATION

Ph.D. candidate, Chemical Engineering, UCLA
M.S., Chemical Engineering, National Taiwan University, July 2011
B.S., Chemical Engineering, National Taiwan University, June 2009

FIELDS OF INTEREST

Biofuel and Biochemical Production Using Methanol, Synthetic Pathway Design, Metabolic Engineering, High-Throughput Screening, Protein Engineering

RESEARCH EXPERIENCE

Doctoral Student, ***2012- 2018***
Dr. James Liao, UCLA, Department of Chemical Engineering

- Developed a novel methanol conversion pathway for high yield ethanol and 1-butanol production *in vitro*
- Optimized the production pathway by analyzing kinetic and redox problem
- Bioprospected and characterized pathway enzymes to enhance efficiency
- Designed & implemented a high-throughput screening process to engineer bottleneck enzyme
- Created a protein structure model to guide site-directed mutagenesis
- Engineered *E. coli* strain for methanol assimilation and constructed production pathways for ethanol and 1-butanol

Master Degree Student, ***2009-2011***
Dr. Hsyue-Jen Hsieh, National Taiwan University, Department of Chemical Engineering
Dr. Danny Ling Wang, Institute of Biomedical Sciences , Academia Sinica

- Studied the effect of shear stress on hydrogen sulfide (H_2S) production in endothelial cells
- Investigated the roles of H_2S in shear-induced physiological response
- Studied regulation mechanisms of shear stress on H_2S production

PUBLICATIONS

Igor W. Bogorad*, **Chang-Ting Chen***, Matthew K. Theisen*, Tung-Yun Wu*, Alicia R. Schlenz, Albert T. Lam, and James Liao, Building Carbon-carbon Bonds Using a Biocatalytic Methanol Condensation Cycle. *Proc. Natl Acad. Sci. USA* 111, 15928-15933 (2014). *Contributed equally to this work

Chang-Ting Chen, and James Liao, Frontiers in Microbial 1-Butanol and Isobutanol Production. *FEMS Microbiol. Lett.* 363 (2016)

Tung-Yun Wu*, **Chang-Ting Chen***, Jessica Tse-Jin Liu, Igor W. Bogorad, Robert Damoiseaux, and James Liao, Characterization and Evolution of an Activator-Independent Methanol Dehydrogenase from *Cupriavidus Necator* N-1. *Appl. Microbiol. Biotechnol.* 100, 4969-4983 (2016). *Contributed equally to this work

Bin Huang, **Chang-Ting Chen**, Chi-Shia Chen, Yun-Ming Wang, Hsyue-Jen Hsieh, and Danny Ling Wang, Laminar Shear Flow Increases Hydrogen Sulfide and Activates a Nitric Oxide Producing Signaling Cascade in Endothelial Cells. *Biochem. Biophys. Res. Commun* 464, 1254-1259 (2015)

FELLOWSHIPS AND AWARDS

Jul 2008 – Feb 2009

Undergraduate Student Research Fellowship, National Science Council, Taiwan

Sept 2012 – Jun 2014

Bowie Lee Fellowship, LCY Chemical Corp., Taiwan

1. Introduction

C1 substrates such as methanol derived from biogas or natural gas may become an attractive raw material for production of chemicals. Biological conversion of methanol to value-added products has advantages such as higher capital efficiency due to its inherent low scale and therefore allows to access resources in smaller scale (James M. Clomburg et al., 2017; Haynes and Gonzalez, 2014). Bioconversion of methanol to products such as amino acids (Hagishita et al., 1996; Motoyama et al., 2001, 1994, 1993), polyamine monomers (Naerdal et al., 2015), vitamins (Ivanova et al., 2006), and terpenoids (Sonntag et al., 2015) has been demonstrated using methylotrophic bacteria, a group of microorganisms that can use single carbon compounds such as methanol as their sole carbon source for growth. Despite these previous successes, many obstacles remained to be overcome for industrial application. In particular, improvement of genetic tools and study of cell physiology are required for further strain engineering (Bennett et al., 2018; Schrader et al., 2009). A promising alternative is to engineer industrial friendly organisms such as *Escherichia coli*. Theoretically, "synthetic methylotrophy" can be achieved by expressing three key enzymes from ribulose monophosphate (RuMP) pathway that assimilates methanol to form central metabolites: methanol dehydrogenase (Mdh) that oxidize methanol to formaldehyde, 3-hexulose-6-phosphate synthase (Hps) that condenses formaldehyde with ribulose 5-phosphate to produce *arabino*-3-hexulose 6-phosphate (H6P), and 6-phospho-3-hexuloisomerase (Phi) that isomerize H6P to fructose 6-phosphate. However, using RuMP pathway for production of chemicals derived from acetyl-coA suffers from intrinsic carbon yield limitation due to CO_2 lost. Furthermore, although methanol incorporation to central metabolites has been demonstrated in model organisms such as *E. coli* (Bennett et al., 2017; Gonzalez et al.,

2017; Jonas E N Müller et al., 2015; Whitaker et al., 2017), *Saccharomyces cerevisiae* (Dai et al., 2017), and *Corynebacterium glutamicum* (Leßmeier et al., 2015; Witthoff et al., 2015), none of these strains can grow solely on methanol or utilize methanol as main carbon source for production. Therefore, the overall goal of my Ph.D. thesis has been to improve the current scheme of methanol bioconversion using *Escherichia coli,* in the aspect of pathway carbon efficiency, key enzyme kinetics, and *in vivo* biochemical production.

Chapter 2 will address the intrinsic carbon yield limit for production of acetyl-CoA derived products. As one of the key metabolites, acetyl-CoA plays a pivotal role in biosynthesis of many industrially interesting products. Current methanol assimilation pathways found in nature has limited carbon yield due to CO_2 lost or ATP requirement. Our first goal was to address this problem with a design of synthetic pathway. As such, a novel pathway termed Methanol Condensation Cycle (MCC) was designed with 100% theoretical carbon yield. After pathway optimization, our *in vitro* production was able to produce ethanol and 1-butanol with carbon yield of 80% and 50%, respectively.

Chapter 3 discusses the bottleneck enzyme methanol dehydrogenase (Mdh) and related engineering results. Mdh catalyzed the thermodynamically unfavorable methanol oxidation reaction and is a hurdle of engineering methanol bioconversion. Here we identified the Mdh2 from *Cupriavidus necator* N-1 that showed significant activity towards methanol. We have developed a high-throughput screening method to further improve the enzyme with directed enzyme evolution. The resulting Mdh2 variant CT4-1 demonstrated 6-fold higher K_{cat}/K_m for methanol and 10-fold lower K_{cat}/K_m for 1-butanol.

Chapter 4 describes our effort in engineering *E. coli* for *in vivo* methanol conversion to ethanol and 1-butanol. Here we designed and constructed an *E. coli* strain that assimilates methanol as essential carbon source for growth when ribose or xylose is provided. The so-defined "methanol auxotrophy" strain allowed us to optimize methanol-utilization based on growth. By adaptive evolution, we were able to improve the cell to grow on methanol and xylose to OD_{600} of 4 in 30 hours. Deleterious mutation on adenylate cyclase (*cyaA*) and truncation of the fromaldehyde detoxification operon (*frmABR*) are identified as key genome modifications that contributed to the improved growth phenotype. The strain was further engineered to demonstrate ethanol and 1-butanol production from methanol to final titers of 4.6 g/L and 2.0 g/L, respectively.

2. Building carbon-carbon bonds using a biocatalytic methanol condensation cycle

Disclaimer: This chapter was originally published with the same title in *PNAS* **111** (2014) 15928-15933.

This publication had equal 1st co-authorship between myself, Dr. Igor W. Bogorad, Dr. Matthew K. Theisen, Dr. Tung-Yun Wu. Chang-Ting demonstrated methanol conversion to ethanol and 1-butanol with GC-FID. Dr. Theisen performed the EMRA analysis and carried out the ^{13}C labeling experiment of formaldehyde to acetate. Dr. Wu conducted large scale protein purifications and enzyme characterization. Dr. Bogorad invented the pathway and performed the ^{13}C tracing experiment of formaldehyde conversion to ethanol. All 1st-coauthors participated in the manuscript writing. Alicia R. Schlenz and Albert T. Lam were laboratory technicians who assisted with *in vitro* assays and protein purification.

Author contributions: I.W.B., C.-T.C., M.K.T., T.-Y.W., and J.C.L. designed research; I.W.B., C.-T.C., M.K.T., T.-Y.W., A.R.S., and A.T.L. performed research; I.W.B., C.-T.C., M.K.T., T.-Y.W., and J.C.L. wrote the paper; and I.W.B. and J.C.L. invented the MCC pathway.

2.1 Abstract

Methanol is an important intermediate in the utilization of natural gas for synthesizing other feedstock chemicals. Typically, chemical approaches for building C–C bonds from methanol require high temperature and pressure. Biological conversion of methanol to longer carbon chain compounds is feasible; however, the natural biological pathways for methanol utilization involve carbon dioxide loss or ATP expenditure. Here we demonstrated a biocatalytic

pathway, termed the methanol condensation cycle (MCC), by combining the nonoxidative glycolysis with the ribulose monophosphate pathway to convert methanol to higher-chain alcohols or other acetyl-CoA derivatives using enzymatic reactions in a carbon-conserved and ATP-independent system. We investigated the robustness of MCC and identified operational regions. We confirmed that the pathway forms a catalytic cycle through ^{13}C-carbon labeling. With a cell-free system, we demonstrated the conversion of methanol to ethanol or 1-butanol. The high carbon efficiency and low operating temperature are attractive for transforming natural gas-derived methanol to longer-chain liquid fuels and other chemical derivatives.

2.2 Significance statement

With the recent discoveries of large reserves of natural gas, the efficient utilization of one-carbon compounds for chemical synthesis would reduce the raw material cost for the petroleum- based chemical industry. Methanol is produced industrially from methane and is a feedstock chemical for the synthesis of higher carbon compounds. However, current chemical synthesis of higher carbon compounds from methanol requires high temperature and pressure. Natural biological pathways for methanol utilization are carbon and ATP inefficient. Here we constructed a synthetic biocatalytic pathway that allows the efficient con- version of methanol to higher-chain alcohols or other higher carbon compounds without carbon loss or ATP expenditure. The high carbon efficiency and favorable operating conditions are attractive for industrial applications.

2.3 Introduction

Methanol is industrially produced from synthetic gas-derived olefins and alkanes (Bjørgen et al., 2008; Chang, 1983; Jones, 2000; McCann et al., 2008; Ott et al., 2012; Stöcker, 1999; Summers et al., 1986). These reactions typically involve high temperatures and pressures that require large capital investment (Conrado and Gonzalez, 2014; Haynes and Gonzalez, 2014). The condensation of methanol to higher-chain alcohols such as ethanol or 1-butanol is thermodynamically favorable ($\Delta G^{\circ\prime} = -68$ and -182 kJ/mol, respectively), but the direct condensation of methanol to higher-chain alcohols has been quite challenging. Using the Guerbet reaction, methanol can upgrade short alcohols (such as n-propanol) to longer alcohols; however, methanol cannot self-couple (Kozlowski and Davis, 2013). Metal acetylides can convert methanol to isobutanol, although this process was demonstrated to be noncatalytic (Fox et al., 1984).

Nature has evolved several distinct ways to assimilate methanol to form metabolites necessary for growth. In principle, metabolites resulting from these methylotrophic pathways can be used to form higher-chain alcohols, although inherent pathway limitations prevent complete carbon conservation (Figure 2-5). In the ribulose monophosphate pathway (RuMP), three formaldehydes condense to pyruvate, which is decarboxylated to form acetyl-CoA and CO_2, reducing the carbon efficiency to 67%. The serine pathway requires an external supply of ATP to drive otherwise unfavorable reactions. Similarly, oxidation of methanol to CO_2 followed by CO_2 fixation using the Calvin–Benson–Bassham (CBB) cycle also requires additional ATP. To generate the required ATP input, extra carbon must be spent to drive oxidative phosphorylation. To our knowledge, natural methylotrophs are not capable of using the reductive acetyl-CoA

pathway, which can produce acetyl-CoA without carbon loss or ATP requirement through carbon reassimilation after complete oxidation of methanol. This route is extremely oxygen sensitive and difficult to engineer due to the complex cofactors involved, and achieving carbon conservation would require that CO_2 produced in methanol oxidation is completely reassimilated. Thus, in all native pathways some carbon must be lost during the production of acetyl-CoA, the precursor for n-alcohols.

Here we constructed an enzymatic cycle to achieve the catalytic condensation of methanol to higher alcohols with complete carbon conservation and ATP independence. This pathway is modified from the combination of RuMP coupled with a non-native pathway, nonoxidative glycolysis (NOG) (Bogorad et al., 2013) shown in Figure 2-1A. However, the combined pathway, which we call the methanol condensation cycle (MCC), can be simplified to become completely ATP independent. A thorough list of reactions is given in Table 2-1. The first step in MCC is the oxidation of methanol to formaldehyde. This reaction can be catalyzed by three classes of enzymes: alcohol oxidase (Roggenkamp et al., 1975), quinone-dependent methanol dehydrogenase (Anthony and Zatman, 1967), and NAD-dependent methanol dehydrogenase (Arfman et al., 1989). Only the last class of enzymes provides the correct reducing equivalents, which can be used to drive the reductive portion of MCC for ethanol or 1-butanol formation (Figure 2-6).

The core portion of MCC is the biochemical condensation of two formaldehydes with a CoA to form acetyl-CoA and water (Figure 2-1 B and C). Similar to the initial steps in the RuMP pathway, formaldehyde combines with ribulose-5 phosphate (Ru5P) to produce hexulose-6-phosphate, which is isomerized to fructose- 6-phosphate (F6P). The formaldehyde assimilation is

catalyzed by hexulose-6-phosphate synthase (Hps) and phosphohexulose isomerase (Phi), respectively. A similar conversion could be achieved using dihydroxyacetone synthase (Bogorad et al., 2013) and fructose-6-phosphate aldolase (Schürmann and Sprenger, 2001) as shown in Figure 2-6. Once fructose-6-phosphate is formed, half of the molecules are saved for carbon rearrangement to regenerate Ru5P, whereas the rest are cleaved irreversibly by phosphoketolase (F/Xpk). This promiscuous enzyme can cleave either F6P (Fpk) or X5P (Xpk) to acetyl-phosphate and its corresponding sugar phosphate (Schramm et al., 1958). Although Xpk activity is higher, both Xpk and Fpk can be used to achieve the same net conversion. F/Xpk is able to conserve ATP by phosphorylating the two carbon keto group cleaved from F6P or X5P using inorganic phosphate. The produced acetyl-phosphate can be readily converted to acetyl-CoA by the phosphate acetyltransferase (Pta). By avoiding pyruvate decarboxylation to form acetyl-CoA, no carbon is lost. The E4P produced then reacts with F6P through a series of reactions involving transaldolase (Tal), transketolase (Tkt), ribose-5 phosphate isomerase (Rpi), and ribulose 5-phosphate epimerase (Rpe), to regenerate two molecules of Ru5P to complete the cycle. MCC does not involve an essential RuMP enzyme (phosphofructokinase) and avoids three NOG enzymes: triose phosphate isomerase (Tpi), fructose-1,6-bisphosphate aldolase (Fba), and fructose-1, 6-bisphosphatase (Fbp).

A unique feature of MCC is the conservation of phosphates in the cycle. The sum of all sugar phosphates remains constant throughout the catalytic cycle as long as no nonenzymatic degradation reactions occur to deplete the sum. No new sugar phosphate intermediates are generated or degraded by pathway reactions. Other pathways like CBB and RuMP do not conserve phosphate groups and instead lose these high energy bonds by the action of

phosphatases. The final phase in MCC involves the reduction of acetyl-CoA to alcohols Figure 2-7. Ethanol can be directly produced from acetyl-CoA by an acylating aldehyde dehydrogenase and an alcohol dehydrogenase. The biosynthesis of 1-butanol can be accomplished by a pathway previously established (Shen et al., 2011) that involves reactions similar to the one use by *Clostridia*.

2.4 Results

To demonstrate the feasibility of MCC, we first focused on the core portion from formaldehyde to acetate using purified enzymes (primers listed in Table 2-2). Each enzyme was demonstrated to have activity in individual assays. Similar to other non-linear metabolic cycles (like TCA or CBB), an initial pool of intermediates was needed to prime the pathway. ^{13}C-labeled formaldehyde was used to detect the carbon flow. According to MCC, double-labeled acetic acid (MW = 62) was expected if ^{13}C-formaldehyde was catalytically converted and the ribulose-5-phosphate was regenerated. Unfortunately, after buffer optimization even this core pathway could not be demonstrated. No difference in double labeled acetate was observed with or without carbon rearrangement enzymes.

2.4.1 Robustness of MCC to Enzyme Variation

The failure of these initial tests prompted us to examine the robustness of the pathway. Since the cycle enzymes involve bifurcating branches, unbalanced enzyme activities may have led to failure of the cycle. We used Ensemble Modeling for Robustness Analysis (EMRA) to determine if the cycle is robust against loss of steady-state due to non-linear effects (Lee et al.,

2014). The analysis showed that the MCC cycle is most robust using intermediate levels of phosphoketolase (Figure 2-2A), and will produce less acetyl-phosphate as the enzyme amount increases or decreases. At excessive levels of phosphoketolase, a kinetic "trap" occurs that significantly diminishes the total acetyl-phosphate produced since an accumulation of G3P or E4P occurs. This phenomenon was only predicted for phosphoketolase, while other enzymes were immune to this trap at high amounts (Figure 2-8). To further investigate the kinetic trap, we simulated the effect of increasing phosphoketolase on conversion of ^{13}C-formaldehyde and unlabeled R5P to acetic acid (Figure 2-2B). All enzymes were modeled using Michaelis-Menten kinetics and a batch simulation was solved using a set of ordinary differential equations in Matlab. Enzyme parameters were chosen at random except for V_{max} of phosphoketolase which was varied systematically. The average of ten parameter sets was calculated and a maximum amount of acetic acid was predicted at intermediate levels F/Xpk.

2.4.2 Cell-Free Verification of Kinetic Trap.

To experimentally verify the kinetic trap, we varied the amount of phosphoketolase using ^{13}C-formaldehyde and R5P as substrates to produce acetylphosphate. By using glucose phosphorylation to recycle the ADP, acetyl-phosphate was converted to acetate to enable GC-MS analysis (Kien et al., 1990). GC-MS allowed us to see the distribution of 60, 61, and 62 acetate isotopes. The maximum amount of acetate was observed when F/Xpk was around 90 mg/L (Figure 2-2C). Consistent with our previous simulations, increasing the amount of phosphoketolase above this observed maximum caused a twofold decrease in total acetic acid. Single and unlabeled acetic acid both increased at higher F/Xpk values since the initial R5P

could isomerize to X5P. The total acetic acid and isotope distribution from the cell-free experiment matched the trend shown in the simulation as the amount of phosphoketolase is varied.

2.4.3 Demonstration of the Catalytic Cycle using ^{13}C Tracing.

Since sugar phosphates must be added to prime the cycle, it is important establish whether the carbon in the final product comes from formaldehyde or the initial sugar phosphate pool. Having optimized the amount of F/Xpk in the core portion of MCC, we then extended the pathway further to ethanol using an external source of reducing equivalents. Phosphate acetyltransferase (Pta from *Bacillus subtilis*) was used to convert acetyl-phosphate to acetyl-coA, which can be reduced by a bifunctional alcohol dehydrogenase (AdhE). Yet, this enzyme is known to be oxygen labile and forms long rod-like structures (Kessler et al., 1992; Nnyepi et al., 2007), making in-vitro purification difficult. Instead, the oxygen-tolerant acylating acetaldehyde dehydrogenase (PduP) from *Salmonella enterica* (Lan et al., 2013) can be used in a two-step reduction process via an aldehyde intermediate. We used a homologue of PduP from *Bacillus methanolicus* for converting acetyl-CoA to acetaldehyde, and a commercial Adh (*Saccharomyces cerevisiae*) for producing ethanol. Instead of starting from methanol, here we used formic acid and formate dehydrogenase from *Candida boidinii* (Shaked and Whitesides, 1980) to provide the NADH needed reduce acetyl-CoA to ethanol. This strategy allowed us to optimize the pathway from formaldehyde to ethanol independently without the complication of Mdh. To verify that the carbon rearrangement is essential, we compared the full pathway to a control without Tal. ^{13}Carbon labeled formaldehyde was used to track the carbon flow (Figure

2-9). Since there is an initial pool of pentose phosphates, some unlabeled ethanol can form by cleavage of X5P. Additionally, a single pass of formaldehyde assimilation would produce a single labeled [2-^{13}C]- ethanol. However, if the MCC is functional, fully labeled [1,2-^{13}C]- ethanol can be made. Using the complete cycle, the pentose phosphates can be regenerated and fully-labeled ethanol can be produced. The fragmentation pattern of ethanol leads to a $[M-1]^+$ ion that is roughly three times more abundant compared to the molecular ion $[M]^+$. This ratio of $[M-1]^+$ to $[M]^+$ ions was consistently observed for all four ethanol isotopes (Figure 2-3A). The full pathway produced mostly double-labeled ethanol as determined by the ratio of 48 to 47 ions (Figure 2-3B). In this cell-free system, no 48 ion could be detected in the "No Tal" control (Figure 2-3C). Some unlabeled carbon was still present since the 46 ion, which is absent in the double-labeled ethanol standard, could be detected. The presence of the 48 ion demonstrates a catalytic MCC cycle.

2.4.4 Continuous Production of Ethanol

Next, we attempted to show that the production of ethanol can be continuous if there is constant supply of formaldehyde. The optimal productivity was achieved when formaldehyde was added at a rate of 6 mM CH_2O/hour (Figure 2-4A). Though feeding R5P should not be necessary since it can theoretically be replenished, improved production was achieved also fed at low levels (0.5 mM/hour). Since MCC should have conserved metabolites, this suggested that the pool of intermediates was degraded during the course of the reaction. To identify the distribution of metabolites and possible bottlenecks, we used high-performance ion chromatography (HPIC) with pulsed amperometric detection (PAD) (Groussac et al., 2000; Park

et al., 2011) to quantify the sugar phosphates (Figure 2-4B). Within the first minute, the R5P quickly rearranges to other intermediates. Between the first and twentieth minutes, the overall pool decreases to a third of the initial point (through relative quantities remain about the same) indicating substrate degradation. G3P is known to be fairly unstable and was not detected in this system (Ye et al., 2012). The decrease in pool of intermediates explains why feeding low levels of R5P was required to maintaining continuous ethanol production from formaldehyde.

2.4.5 Production of Ethanol and 1-Butanol from Methanol

Finally, we aimed to demonstrate the conversion of methanol to ethanol and 1-butanol. Since a NAD-dependent methanol dehydrogenase (EC 1.1.1.244) is only found from *B. methanolicus* (Arfman et al., 1989; de Vries et al., 1992), our initial target was to use this unique enzyme. However its low specific activity (< 1 U/mg) and high K_m (>100 mM) in the optimized buffer conditions, led to trace amounts of alcohols. We purified six methanol dehydrogenases from *B. methanolicus* and constructed activator-insensitive mutants for each homolog. A single point mutation has been shown to make Mdh forty times more active in the absence of the Nudix activator (Hektor et al., 2002). Additionally, we bioprospected a wide variety of predicted NAD dependent alcohol dehydrogenases from other organisms. Unfortunately, all purified enzymes demonstrated relatively poor activity towards methanol with higher specificity towards longer chain alcohols, consistent with previous results (Krog et al., 2013). We chose the commercial alcohol dehydrogenase from *S. cerevisiae*, which is the same enzyme used for ethanol production. Although it does not have the highest activity towards methanol, its availability made it a more reasonable option than purifying large amounts other enzymes. The optimal production was

identified by mapping a 2-dimensional parameter space (Figure 2-9), varying F/Xpk and Adh (*S. cerevisiae*). This condition was used for a 24 hour time course (Figure 2-4C). We tested several methanol concentrations and 200 mM methanol was chosen since it produced the highest carbon yield. After five hours, the productivity decreases and this led to a final titer of 610 mg/L (13.3 mM) ethanol from 6200 mg/L (200 mM) methanol. The carbon yield was 80% (33.5 mM methanol consumed), exceeding the theoretical yield (66%) from the native pathway RuMP followed by EMP.

We then extended the pathway to 1-butanol by including the enzymes from acetyl-CoA to 1-butanol. These include thiolase (*Escherichia. coli*), 3-hydroxybutyryl-CoA dehydrogenase (*Clostridia acetobutylicium*), crotonase (*C. acetobutylicum*), trans-enoyl-CoA reductase (*Treponema denticola*), acylating aldehyde dehydrogenase (PduP from *Salmonella enterica*), and alcohol dehydrogenase (*S. cerevisiae*). Starting with 6200 mg/L (200 mM) of methanol, the final titer for 1-butanol was 170 mg/L (2.3 mM). Since only 21.1 mM of methanol was consumed, this represents a 50% carbon yield (Figure 2-4D). Remaining carbons were in ethanol (about 15%), acetate, and possibly some degradation products of sugar phosphates. Here we used the same alcohol dehydrogenase for methanol oxidation as well as ethanol and 1-butanol production. Interestingly, even though this enzyme is reversible and has higher activity towards 1-butanol and ethanol oxidation than methanol oxidation, the thermodynamic driving force (Figure 2-10) effectively drives the reaction towards the longer chain alcohol.

2.5 Discussion

The above results demonstrate that MCC is indeed functional, although kinetics of the cycle needs to be tuned to avoid the kinetic trap. We expect that with some moderate protein engineering, the activities of Mdh, Fpk, and PduP could be improved to enable substantially higher fluxes (Table 2-3). Because MCC is completely redox balanced and independent of ATP, a cell-free system could be a viable application for larger-scale production after optimizing the conditions for enzyme and intermediates stability. Unlike microbial systems, cell-free conversion can achieve high theoretical yields, achieve high productivity, and are easier to control (Welch and Scopes, 1985; Zhang et al., 2010, 2007). Alternatively, MCC could be engineered into a variety of hosts because all of the enzymes are oxygen tolerant. Because of the abundance of natural gas, methanol is expected to become an abundant feedstock (Caballero and Pérez, 2013). The building of specific C-C bonds with high carbon and energy efficiency from methanol is of high interest.

2.6 Materials and methods

For details and full list of abbreviations see page 23 (supplementary text).

Chemicals and Reagents. All reagents were purchased from Sigma-Aldrich unless otherwise stated. The following enzymes were also purchased from Sigma-Aldrich: hexokinase (*S. cerevisiae*), phosphoglucose isomerase (*S. cerevisiae*), glucose-6-phosphate dehydrogenase (*S. cerevisiae*), and alcohol oxidase (*Pichia pastoris*). Alcohol dehydrogenase (*S. cerevisiae*) and formate dehydrogenase (*C. boindii*) were purchased from Worthington Biochemical Corporation.

Simulation of MCC Robustness and ^{13}C-Tracing Prediction. For details, see page 23 (supplementary text).

Cloning and Purification MCC Enzymes. All enzymes were cloned onto the pQE9 (Qiagen) backbone and purified on a Ni-NTA column. Large-scale purification (500 mL) typically produced about 10-50 mg of for each enzyme. For primers and details, see Table 2-2.

Formaldehyde to Acetate Assay with F/Xpk Variation. A 200 μL reaction contained 50 mM Tris-HCl buffer pH = 7.5, 25 mM potassium phosphate buffer, 10 mM MgCl2, 48 μg Tkt, 76 μg Tal, 24 μg Rpe, 70 μg Hps, 15 μg Phi, 20 μg Rpi, 1 mM R5P, 0.5 mM thiamine pyrophosphate, 5 mM 13C-formaldehyde, 0.1 mM ATP, 5.4 μg Ack, 2.5 U hexokinase, and 5 mM glucose.

Various amounts of F/Xpk were used. The reaction time for formaldehyde to acetate assays was 3 hours and the reactions were conducted at room temperature.

Continuous Ethanol Production. A 200 μL reaction contained 50 mM Potassium Phosphate pH 7.5, 0.2 mM NAD+, 0.2 mM CoA, 10 mM MgCl2, and 1 mM TPP. The enzyme amounts were: 30 μg Hps, 10 μg Phi, 100 μg Tkt, 60 μg Tal, 10 μg Rpi, 10 μg Rpe, 15 μg F/Xpk, 10 μg Pta, 50 μg PduP (Bm), 0.01 U Adh, and 0.1 U Fdh. The initial substrates were 6 mM ^{13}C- formaldehyde,

0.5 mM R5P, 10 mM sodium formate. The same amount of substrates were feed at 1 hour and 2 hours. Tal was excluded for the control. Samples were analyzed by GC-MS every 30 minutes for three hours.

Methanol to Ethanol Assays. The buffer conditions were changed since methanol oxidation by alcohol dehydrogenase is extremely slow at pH 7.5. Diglycine buffer (pH 8.5) was chosen as a compromise between optimal activity for Mdh and F/Xpk. Since F/Xpk is slower at pH 8.5, more enzyme was added to compensate. A 550 µL reaction contained 100 mM Diglycine buffer pH = 8.5, 1 mM dipotassium phosphate, 10 mM MgCl2, 1 mM NAD^+, 1 mM thiamine pyrophosphate, 0.2 mM Coenzyme A, 200 mM 13C-methanol, 4 mM F6P. The enzyme amounts were: 55 µg Tkt, 431 µg Tal, 53 µg Rpe, 79 µg Rpi, 393 µg Hps, 431 µg Phi, 344 µg Fpk, 55 µg Pta, 297 µg PduP (Bm), 2.75 mg Adh. Reaction was carried out at 37°C. At each time point, 120 µL of sample was taken out and mixed with 12 µL of 8 M urea to quench the reaction. Samples were subject to filtration (Costar Centrifuge Devices, cellulose acetate, 0.22 µm, Corning, Amsterdam, The Netherlands) if precipitation occurs. After 2 minutes, 120 µL of 1g/L 1- pentanol were added as internal standard for GC analysis. The samples were kept in -20°C before further analysis.

Methanol to 1-butanol assays. The buffer and components of reaction mixture were identical to methanol to ethanol assay except for the enzymes. In a 550 µL reaction, the following enzymes were added: 55 µg Tkt, 431 µg Tal, 53 µg Rpe, 79 µg Rpi, 393 µg Hps, 431 µg Phi, 344 µg Fpk, 55 µg Pta, 743 µg AtoB, 88 µg Hbd, 38 µg Crt, 30 µg Ter, 59 µg PduP (Se), and 2.75 mg Adh (Sc). The procedure of sample preparation for GC is identical to methanol to ethanol assay.

Analytical methods. Individual assays followed spectrophotometrically using a Beckman Coulter DU 800 (Beckman Coulter, Pasadena, CA, USA) or Agilent 8453 UV-Vis

Spectrophotometer (Agilent Technologies, Santa Clara, California, USA). Acetic acid, ethanol, and n-butanol were analyzed by GC-FID or GC-MS (Agilent Technologies, Santa Clara, California, USA). Details given in SI Text.

Sugar Phosphate Analysis. Sugar phosphates were analyzed by a modified method from Groussac et. al.

2.7 Figures

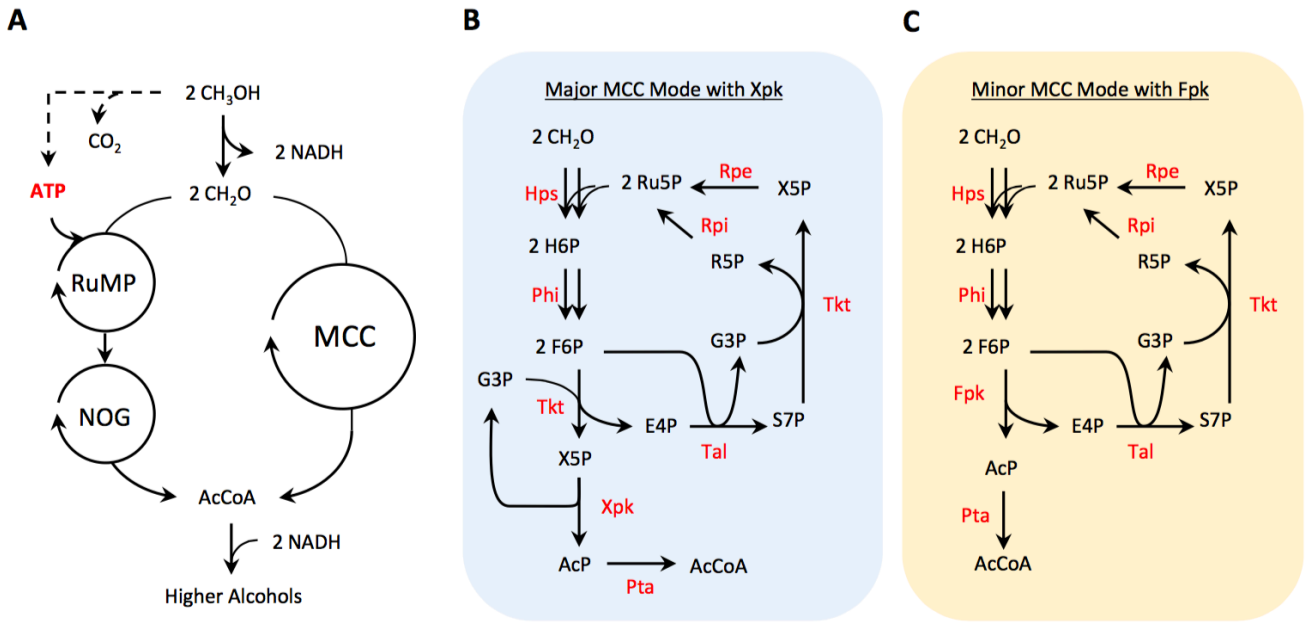

Figure 2-1. Conversion of methanol to higher n-alcohols

(A) The MCC is the combination of RuMP with NOG that bypasses ATP dependency. See Table 2-1 for details. (B) The major MCC mode uses the more active X5P-phosphoketolase (Xpk). (C) The minor MCC mode can achieve the same result with the less active F6P-phosphoketolase (Fpk). This figure was created by Dr. Igor W. Bogorad.

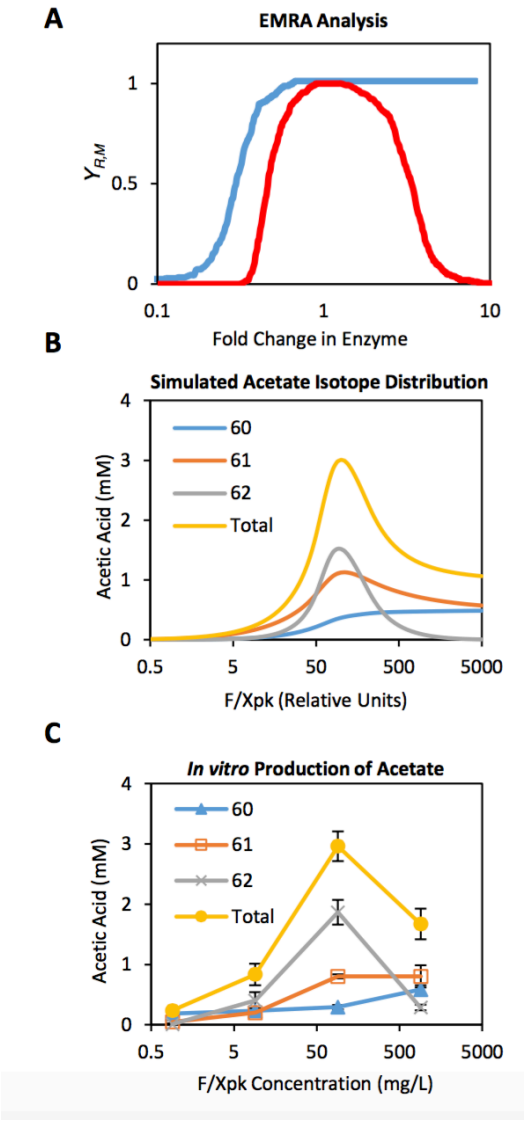

Figure 2-2. Simulation and *in vitro* demonstration of a kinetic trap

(A) Ensemble model robustness analysis (EMRA) of the core MCC pathway 84. YR,M is the fraction of robust models constrained to a steady state. The variation of phosphoketolase is shown in red and variation of transaldolase in blue. (B) Simulated distribution of acetic acid isotopes using ^{13}C-formaldehyde as the substrate (C) In vitro production of acetic acid and GC-MS analysis using 13C-formaldehyde as substrate. Seven enzymes (Hps, Phi, Tkt, Tal, Rpe, Rpi, and F/Xpk) were used to produce acetyl-phosphate from ^{13}C-formaldehyde. For GC analysis, the AcP was then converted to acetate by acetate kinase using ATP recycling by glucokinase. An acetate standard curve was established with R^2 = 0.998 up to 5 mM to ensure reliable quantitation. Assays were independently run in triplicate (n = 3) with error bars representing SD. The data and simulations in this figure were generated by Dr. Matthew K. Theisen.

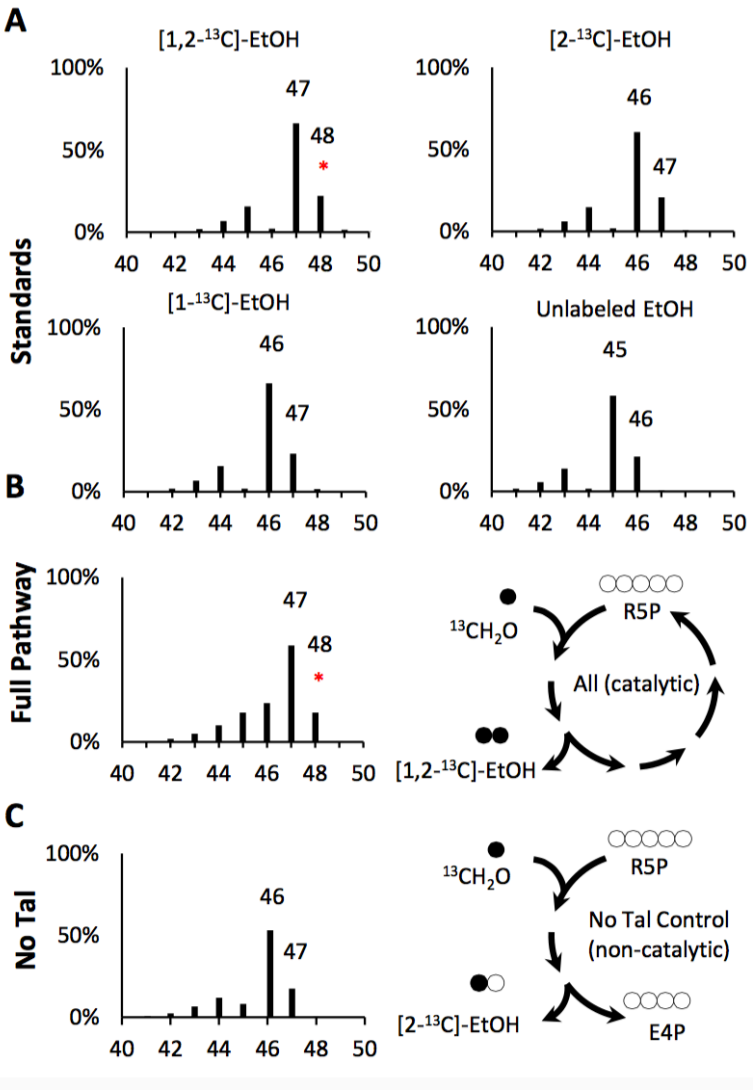

Figure 2-3. ^{13}C tracing from ^{13}C-fromaldehyde and formate to ethanol

(A) The mass spectra of all four ethanol isotope standards including unlabeled ethanol, [1-^{13}C]-ethanol, [2-^{13}C]-ethanol, double-labeled [1,2-^{13}C]-ethanol. All spectra were normalized to the most abundant internal peak. Only double-labeled ethanol has a significant 48 ion (red asterisks). (B) Mass spectrum of ethanol experimentally produced from ^{13}C-formaldehyde, unlabeled formate, and unlabeled R5P using the full MCC pathway with formate dehydrogenase. The assays were analyzed after two hours at room temperature. Formate was oxidized to CO_2 by formate dehydrogenase to provide the necessary NADH to reduce acetyl-CoA to ethanol. (C) The "No Tal" control contained the same conditions as the full pathway except for omitting transaldolase. No 48 ion was detected for the control. m/z, mass to charge ratio; R.A., relative abundance. The in vitro assays in this figure were performed by Dr. Igor W. Bogorad with technical assistance by Albert Lam.

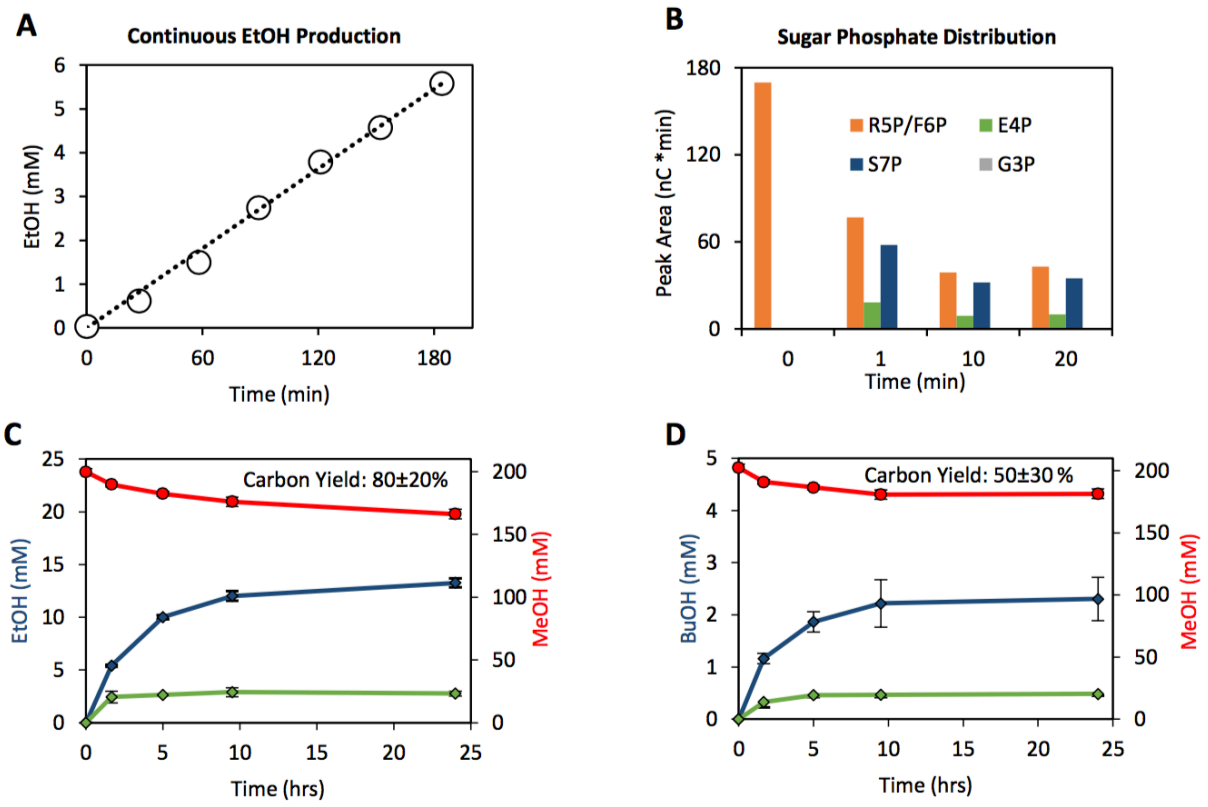

Figure 2-4. Ethanol and 1-butanol production from formaldehyde or methanol using MCC

(A) Steady-state production of ethanol from formaldehyde with MCC using formic acid as electron source. 6 mM formaldehyde, 10 mM formate, and 0.5 mM R5P were added at the 0-, 1-, and 2-h points. This was performed by Dr. Igor W. Bogorad with technical assistance by Albert Lam. (B) Sugar phosphate measurement over time using HPIC-PAD for the batch conversion of formaldehyde to acetyl-phosphate. Most of the carbon rearrangement occurred within the first minute. F6P and R5P standards overlap so the combine area is provided in the full assay. This was performed by Dr. Igor W. Bogorad with technical assistance by Albert Lam. (C) Conversion of methanol to ethanol and (D) to 1-butanol over 24 h. Chang-Ting Chen performed the assays demonstrated in (C) and (D). Dr. Tung-Yun Wu performed the large scale protein purifications with assistance by Alicia Schlenz. The productivity drops after five hours, likely due to instability of intermediates. The alcohol production assays were independently run in triplicate. Methanol consumption (for full assay only) is shown in red circles, whereas ethanol and 1-butanol production is shown with diamonds. Blue colors indicate the full MCC pathway, whereas green illustrates the "No Tal" control. Assays were independently run in triplicate (n = 3) with error bars representing SD.

2.8 Supplementary Text

Plasmid construction. Plasmids used in enzyme purification were constructed either on the pQE9 (Qiagen, Hilden, Germany) or pCDF-Duet1 (EMD Chemicals Inc., NJ) vectors which contained a Histidine (His) tag, IPTG-inducible promoter, and high-copy origin of replication. The plasmids are maintained with 100 mg/L ampicillin.

Enzyme purification. Enzymes were expressed in IPTG-inducible plasmids with 6x histidine tags in transformed in E. coli strain XL1-Blue or BL21(DE3). Induction was accomplished with 0.1 mM IPTG. Enzymes were purified using the QIAExpressionist purification procedure for proteins under native conditions. Enzyme concentration was determined by the method of Bradford using a commercial dye (Thermo Fisher Scientific, Waltham, Massachusetts, USA).

***In Vitro* Assays for Each Enzyme.** All assays were conducted at 25 °C unless otherwise stated. Conditions for Hps-Phi assays: In 500 µL reaction contained 50 mM Tris buffer pH 7.5, 5 mM MgCl2, 0.2 mM NADP+, 5 mM R5P, 5 mM formaldehyde, 6.1 µg Pgi, 1.1 µg Zwf, 48 µg Rpi. In Phi assays, 9.6 µg of Hps and 0.0048 µg Phi were used. In Hps assays, 47 µg Phi and 1.9 µg Hps were used. The assays followed the generation of NADPH at 340 nm. The assays were initiated by the addition of R5P.

Conditions for F/Xpk assay: A 550 µL reaction contained 50mM potassium phosphate buffer pH 7.5, 5 mM MgCl2, 0.2 mM NADP+, 1 mM TPP, 0.2 mM ADP, 20 mM glucose, 10 mM F6P, 1.6 µg F/Xpk, 30 µg Ack, 2 Units Glk, 2 Units Zwf. The production of NADPH was followed at 340 nm. Similar assay was done to measure Xpk activity by adding 10 mM R5P as substrate with 10 µg each of Rpi and Rpe.

Conditions for Tal, Tkt, Rpe, Rpi assays: A 550 µL reaction mixture contains 5mM R5P, 50 mM Gly-Gly buffer pH 8.5, 5 mM MgCl2, 1 mM TPP, 0.26 mM NADP+, 0.4 U Zwf, 0.4 U Pgi. For coupling reactions, high enzyme amounts were used: 260 µg Tal, 8 µg Tkt, 14 µg Rpe, and 12 µg Rpi. The tested enzyme in each assay was used at the following levels: 0.5 µg Tal, 0.3 µg Tkt, 0.2 µg Rpe, 0.1 µg Rpi. The production of NADPH was measured at 340 nm.

Conditions for PduP (Bm) assay: A 500 µL reaction contained 50 mM Tris buffer pH 7.5, 5 mM MgCl2, 0.3 mM NADH, 1 mM AcCoA, 25 µg PduP (Bm). The assays followed the consumption of NADH at 340 nm. The assays were initiated by the addition of AcCoA.

Conditions for PduP (Se) assay: A 500 µL reaction contained 50 mM Tris buffer pH 7.5, 5 mM MgCl2, 0.3 mM NADH, 1 mM Butyryl-CoA, 10 µg PduP (Se). The assays followed the consumption of NADH at 340 nm. The assays were initiated by the addition of Butyryl-CoA.

Conditions for Pta assays: A 550 µL reaction contained 50 mM Tris buffer pH 7.5, 0.2 mM NADH, 2 mM acetyl-phosphate, 10 mM coenzyme A, 0.077 µg Pta and 44 µg PduP (Se). The decrease in NADH was followed at 340 nm.

Conditions for Hbd assay: A 550 µL reaction contained 50mM potassium phosphate buffer pH 7.5, 5 mM MgCl2, 0.2 mM NADH, 0.01 µg Hbd, 0.3 mM acetoacetyl-CoA. The decrease in NADH was followed at 340 nm.

Conditions for AtoB assay: A 550 µL reaction contained 50mM potassium phosphate buffer pH 7.5, 5 mM MgCl2, 0.2 mM NADH, 20 µg Hbd, 0.3 µg AtoB, 0.3 mM acetyl-CoA. The decrease in NADH was followed at 340 nm.

Conditions for Mdh assays: A 500 µL reaction contained, 500 mM methanol, 1 mM NAD+, 50mM diglycine buffer pH 8.0, 5 mM MgCl2. The assays followed the generation of NADH at

340 nm. The assays were initiated by the addition of 10-200 µg of alcohol dehydrogenase, depending on the organism.

Conditions for Adh assays: A 500 µL reaction contained 50mM Gly-Gly buffer pH 8.5, 2 mM acetaldehyde, 5mM MgCl2, 1mM NADH, and 0.01 U Adh (Sc). The decrease in NADH was followed at 340 nm.

GC-MS and GC-FID Analysis. All columns and instruments were purchased from Agilent Technologies (Santa Clara, California, USA). GC/MS data were obtained from a 6890/5973 GC/MS. An HP-FFAP column was used to reproducibly quantitate acetic acid. A three-point plus zero-intercept standard curve was generated with R2 = 0.998 up to 5 mM acetic acid and RSD 3.5-7% (N=3, SSD) to ensure reliable quantitation. Acetic acid has a strong mass peak at its molecular weight 60 in GC/MS analysis which is free of surrounding peaks. Thus, 60, 61 & 62 mass peaks were used to quantify the isotopes of acetic acid. An inlet temperature of 250 °C was used. Oven temperature started at 70 °C and held for one minute, followed by a ramp at 20 °C/min and 2 minute hold at 240 °C. Injection of 0.2 µL in splitless mode with constant pressure of 10 psi at the inlet was used.

Analysis of methanol to ethanol and butanol experiments was carried out using a DB-624UI (GC/MS) or DB-FFAP (GC-FID) column. An inlet temperature of 225 °C was used. Oven temperature started at 40 °C for 3 minutes, followed immediately by a ramp 45 °C/min to 235 °C and hold for 3 minutes. Injection of 1 µL with split ratio of 25 in constant pressure mode with 9.52 psi at the inlet was used. For mass scatters of alcohol samples, the GC-MS was used. GC-FID was typically used for quantification of alcohols, though GC-MS also produced reproducible linear standard curves with ethanol and n-butanol.

Sugar Phosphate Analysis. Thermo ICS5000+ with a Coulochem III detector and a CarboPac PA1 guard and analytical column, the flow rate was set at 1.0 mL/min with Buffer A (50 mM NaOH) and Buffer B (50 mM NaOH/500 mM NaAce). The injection volume was 10 μL. The column was equilibrated for 3 hours with 100% A. From 0-25 minutes, Buffer B was linearly increased to 20%, from 25-45 min Buffer B was linearly increased to 75%, from 45-46 min Buffer B was linearly dropped back to 0% and held for another 10 minutes to re-equilibrate the column.

Thermodynamic Profile of MCC. Using the Equilibrator website (http://equilibrator.weizmann.ac.il/), all reactions (Mdh, Hps, Phi, F/Xpk, Tkt, Tal, Rpe, Rpi, Pta, Ato, Hbd, Crt, Ter, PduP, Adh) were set to pH 7.5, ionic strength of 0.2 mM and standard concentrations. For non-standard conditions, a theoretical set of concentrations for all intermediates.

Robustness of MCC by Ensemble Model and Robustness Analysis (EMRA). EMRA is a technique for determining how likely it is that perturbations in enzyme parameters, including enzyme amount, will interrupt the nature of a steady state. A model including the effects of Fpk was used. A reference steady state was chosen to represent MCC operation. A total of 200 paramater sets were generated and perturbations from 0.1-fold to 10-fold for each enzyme were investigated. The robustness of the system at each point for each system was reported and YR,M is the fraction of the 200 parameter sets that are robust at each point.

Predicting ^{13}C-Tracing with Time-Domain Integration. A system modelling the conversion of ^{13}C-formaldehyde and priming amounts of unlabeled R5P to acetic acid was generated in MATLAB. Michaelis-Menten equations modeling the effect of each enzyme were chosen from

based on number of products, substrates and reversibility of each reaction. Parameters for each reaction were chosen at random. V_{max} parameters were chosen uniformly from a 3-fold range while K_m parameters were chosen from a 10-fold range. Phosphoketolase V_{max} parameters were not chosen at random but assigned as and varied over a range. Xpk:Fpk activity was 1:7, as previously reported. The simulation time was chosen to be representative of the in vitro experiment performed. K_{eq} values for reversible reactions were chosen to be realistic, based on thermodynamics.

The effects of carbon labelling were incorporated by charting the locations of labeled ions and assigning a different compound for each different isotope. The saturation of each enzyme was found by calculating the total amount of each compound, while the flux interconverting each isotope was calculated as a fraction of total flux, depending on the abundance of the isotope generating that flux.

Kinetic Analysis. The overall specific productivity (μmol/min/mg total protein) of the pathway production is calculated by a modification of Bar-Even et al. (Bar-Even et al., 2010).

Abbreviations. Enzyme names: Mdh = methanol dehydrogenase; Hps = 3-hexuolse-6-phospate synthase; Phi = phosphohexulose isomerase; Fpk = phosphoketolase (F6P activity); Xpk = phosphoketolase (X5P activity); Tal = transaldolase; Tkt = transketolase; Rpe = D-ribulose-5-phosphate 3-epimerase; Rpi = ribose-5-phosphate isomerase; PduP = acylating aldehyde dehydrogenase; Adh = alcohol dehydrogenase; Glk = glucokinase ; Zwf = glucose-6-phosphate dehydrogenase; Pgi = glucose-6-phosphate isomerase. Compound names: CH2O = formaldehyde; H6P = 3-hexulose-6-phosphate; F6P = fructose-6-phosphate; E4P = erythrose-4- phosphate; S7P

= sedoheptulose-7-phosphate; X5P = xylulose-5-phosphate; R5P = ribose-5- phosphate; Ru5P = ribulose-5-phosphate; AcP = acetyl phosphate; EtOH = ethanol.

2.9 Supplementary figures

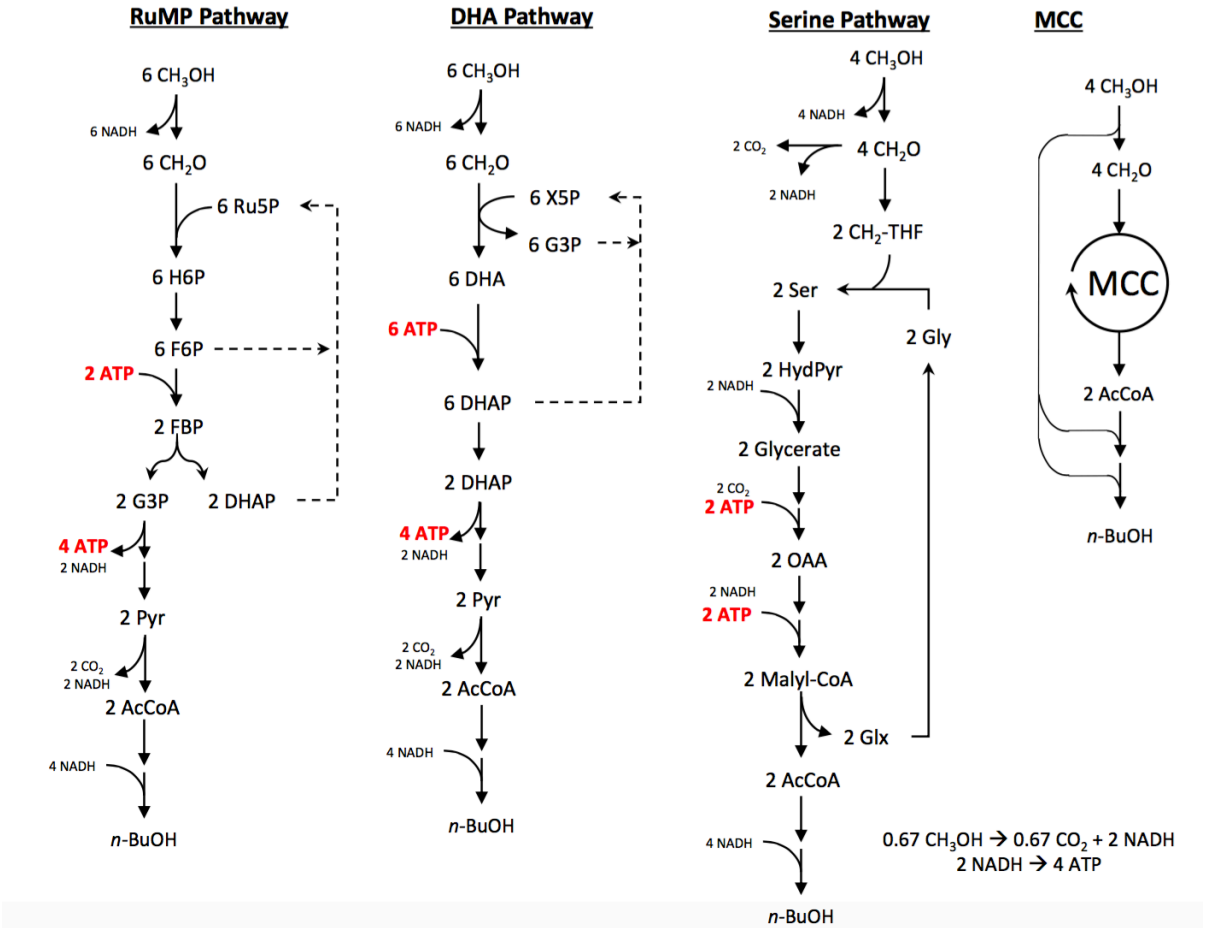

Figure 2-5. Schematic of natural and synthetic pathways for the conversion of methanol to 1-butanol

The RuMP and DHA pathways result in a carbon loss from pyruvate decarboxylation. The Serine pathway requires ATP input which lowers the carbon yield due to oxidative phosphorylation. MCC is the only theoretical route that can achieve stoichiometric conversion with amenable enzymes. This figure was drawn by Dr. Igor W. Bogorad.

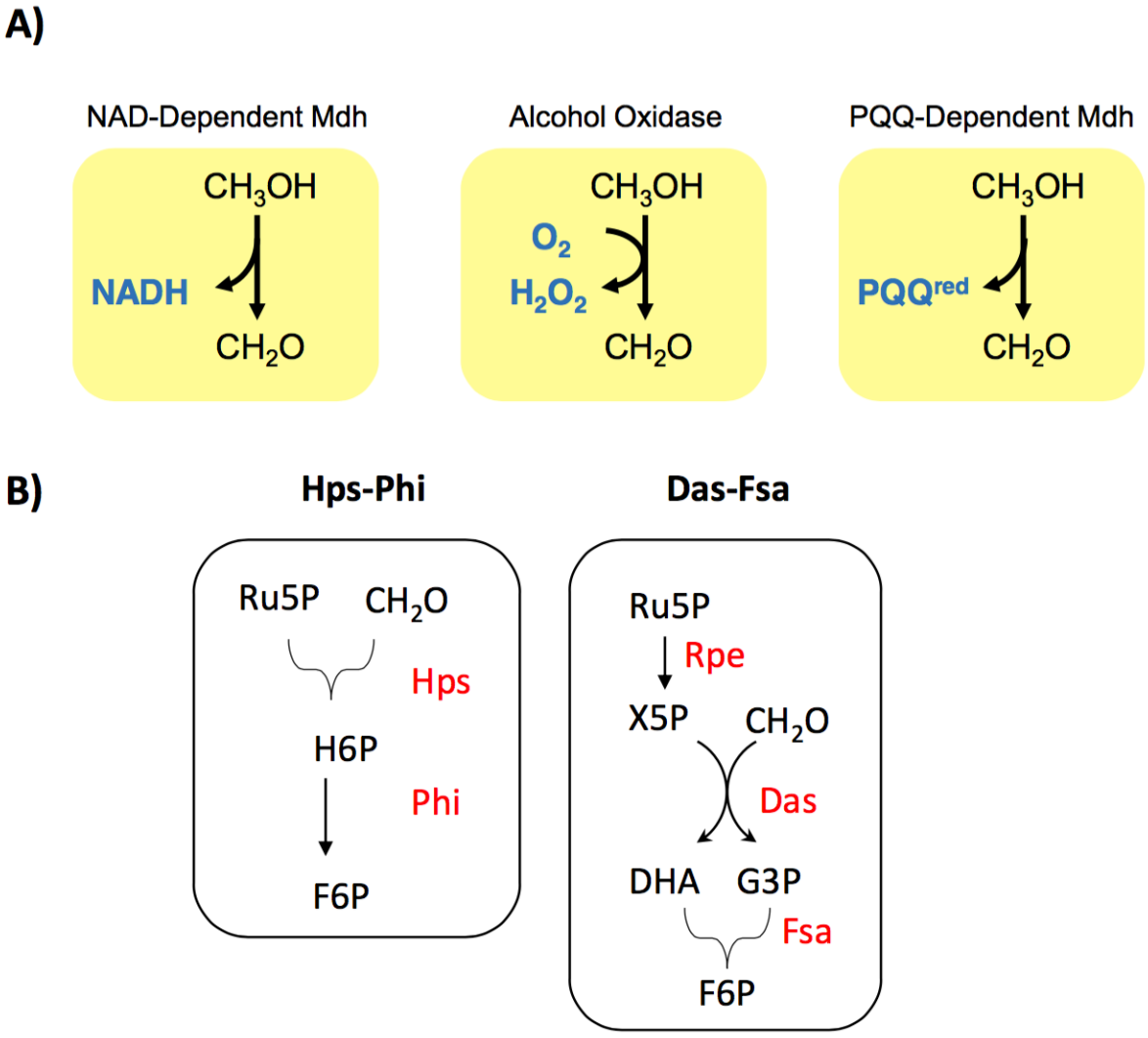

Figure 2-6. Methanol assimilation variations

(A) Three classes of enzymes that oxidize methanol to formaldehyde. Only NAD-Dependent Mdh produces the reduced NADH cofactor for acetyl-CoA reduction. (B) Two equivalent routes for the assimilation of formaldehyde to fructose-6-phosphate. Fsa is a recently discovered enzyme that is not known to participate in any metabolic pathway. The Hps-Phi route was chosen for our cell-free systems since it has better kinetics (significantly lower K_m for substrates). This figure was drawn by Dr. Igor W. Bogorad.

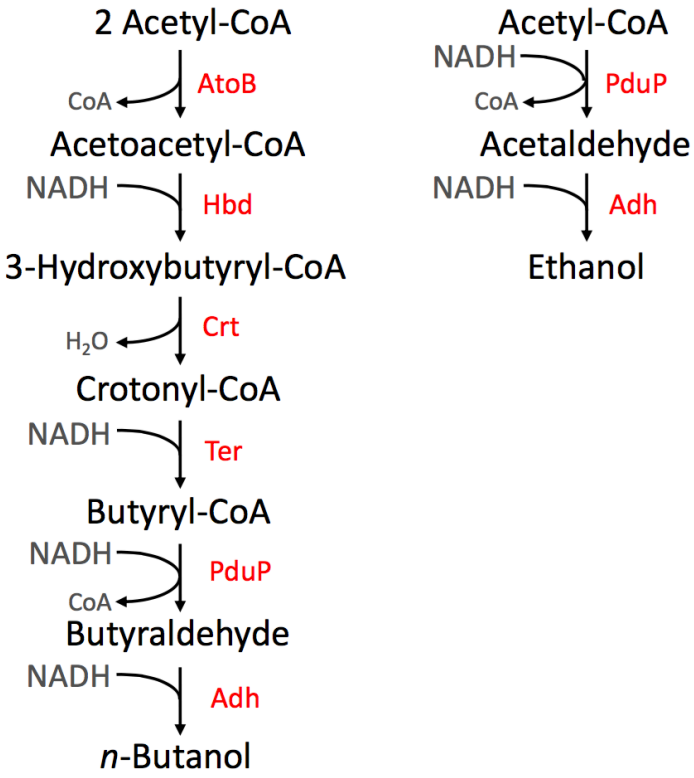

Figure 2-7. Reduction of acetyl-CoA to alcohols

Acetyl-CoA can be reduced with NADH to form 1-butanol or ethanol.

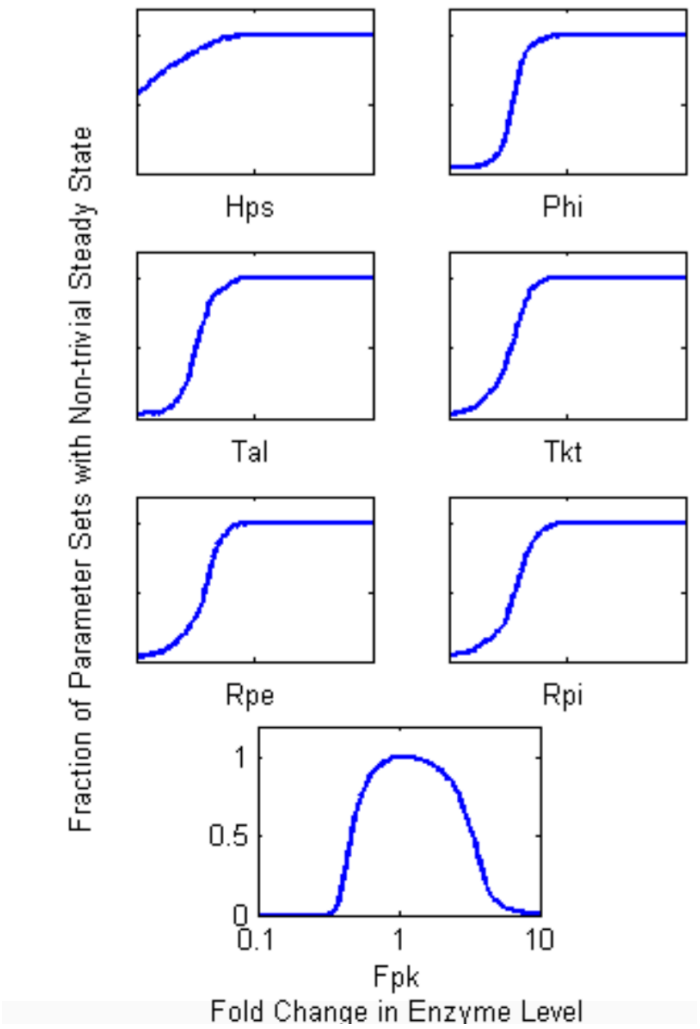

Figure 2-8. MCC simulation using EMRA

The EMRA analysis indicates that for phosphoketolase, very high activity levels will cause the cycle to have a change in the nature of its steady state (bifurcation). Other enzymes cause this only when they are present at low levels. Source files can be included in future submissions. This data was generated by Dr. Matthew K. Theisen.

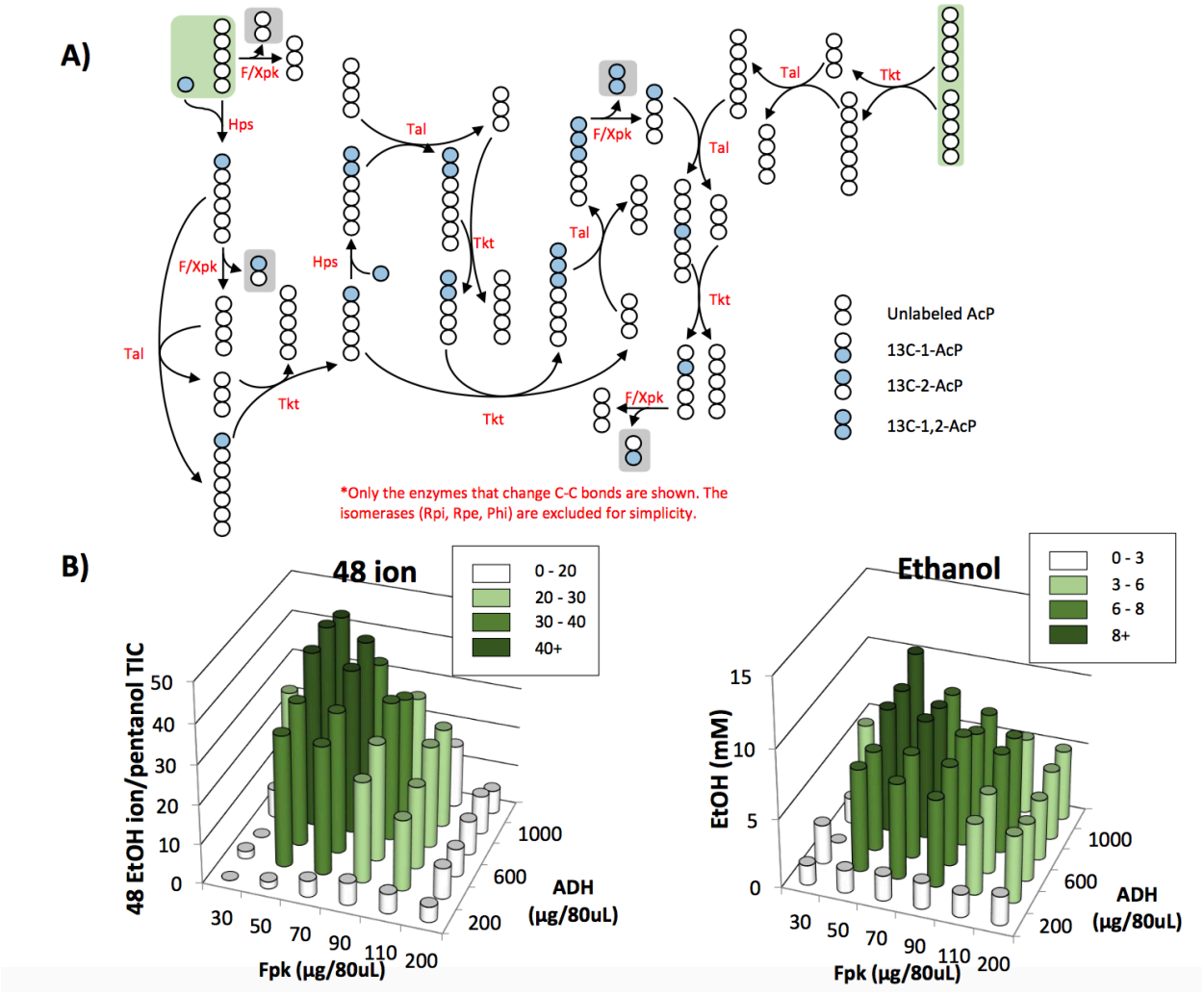

Figure 2-9. Carbon tracing scheme and optimization

(A) Schematic of ^{13}C tracing in MCC. All four isotopes of AcP are predicted if ^{13}C-formaldehyde and unlabeled R5P are used as substrates. This figure was drawn by Dr. Matthew Theisen. (B) Optimization of F/Xpk and Adh levels for increase production of double labeled [1,2-^{13}C]-ethanol using 48 ion and total ethanol amount as outputs. Effect of kinetic trap was observed when F/Xpk is higher than 50 µg/80 µL. This data was performed by Chang-Ting Chen.

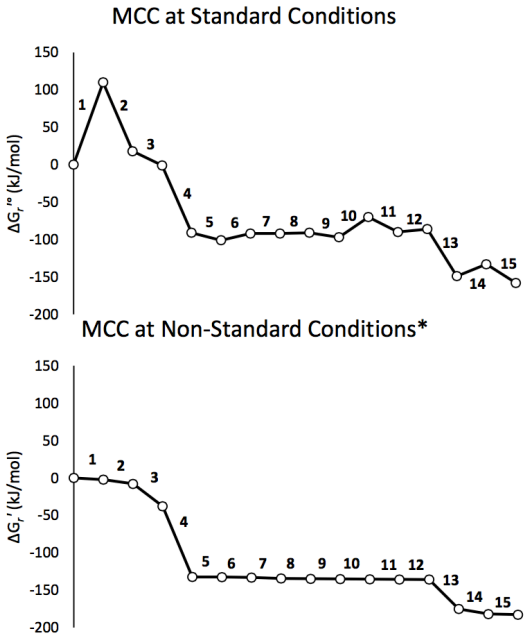

Phase		Name	Standard	Non-Standard
Methanol Oxidation	1	Mdh (x4)	110	-2.4
	2	Hps (x4)	-92	-5.6
	3	Phi (x4)	-19	-30
	4	Fpk (x2)	-90	-94
	5	Tkt (x2)	-10	-0.2
	6	Tal (x2)	9	-0.6
	7	Rpe (x2)	0	-1.2
	8	Rpi (x2)	1	-0.4
Core MCC	9	Pta (x2)	-6	-0.4
	10	Thl	27	-0.2
	11	Hbd	-20	-0.3
	12	Crt	4	-0.2
	13	Ter	-63	-39
AcCoA Reduction	14	PduP	16	-6.7
	15	Adh	-25	-0.9
		Total	**-158**	**-182**

Name	Concentration (mM)	Name	Concentration (mM)
Methanol	200	Ru5P	0.4
Formaldehyde	0.02	X5P	2
H6P	0.2	AcCoA	2
F6P	3	AcAcCoA	0.01
AcP	10	3HB-CoA	0.1
E4P	1	CrotCoA	0.02
S7P	1	ButCoA	0.2
G3P	2	Butyraldehyde	0.5
R5P	1	n-Butanol	50
Phosphate (Pi)	2		

Figure 2-10. Thermodynamics of MCC in the conversion of methanol to 1-butanol

Though the initial oxidation of methanol is thermodynamically difficult, Hps, F/Xpk, and Ter provide a significant driving force for irreversible formation of 1-butanol. *At non-standard conditions, it is possible to choose a set of concentrations so that every reaction has a negative ΔGr'. The reason for the discrepancy between the total ΔG (-158 for standard and -182 for non-standard) is due to a predicted error range from each reaction. This figure was generated by Igor Bogorad. The values for each reaction were taken from the Equilibrator website.

2.10 Supplementary Tables

Table 2-1. Futile ATP burning in RuMP-NOG versus ATP-independent MCC

Name	Reactant	Product	Direction	Enzyme
RuMP	6 CH_2O + 6 Ru5P	6 H6P	→	Hps
	6 H6P	6 F6P	↔	Phi
	F6P + ATP	FBP + ADP	→	Pfk
	FBP	G3P + DHAP	↔	Fba
	DHAP	G3P	↔	Tpi
	2 G3P + 2 F6P	2 X5P + 2 E4P	↔	Tkt
	2 E4P + 2 F6P	2 G3P + 2 S7P	↔	Tal
	2 G3P + 2 S7P	2 R5P + 2 X5P	↔	Tkt
	4 X5P	4 Ru5P	↔	Rpe
	2 R5P	2 Ru5P	↔	Rpi
NOG m3	F6P	AcP + E4P	→	Fpk
	E4P + F6P	G3P + S7P	↔	Tal
	G3P + S7P	R5P + X5P	↔	Tkt
	R5P	Ru5P	↔	Rpi
	Ru5P	X5P	↔	Rpe
	2 X5P	2 AcP + 2 G3P	→	Xpk
	G3P	DHAP	↔	Tpi
	G3P + DHAP	FBP	↔	Fba
	FBP	F6P	→	Fbp
MCC	6 CH_2O + 6 Ru5P	6 H6P	→	Hps
	6 H6P	6 F6P	↔	Phi
	2 G3P + 2 F6P	2 X5P + 2 E4P	↔	Tkt
	3 E4P + 3 F6P	2 G3P + 2 S7P	↔	Tal
	3 G3P + 3 S7P	3 R5P + 3 X5P	↔	Tkt
	3 X5P	3 Ru5P	↔	Rpe
	3 R5P	3 Ru5P	↔	Rpi
	F6P	AcP + E4P	→	Fpk
	2 X5P	2 AcP + 2 G3P	→	Xpk

*In the RuMP-NOG combination, the reactions in orange can be eliminated. The reactions (Pfk and Fbp) in red constitute a futile ATP-burning cycle. By eliminating these unnecessary reactions, MCC reaches stoichiometric conversion of 6 CH_2O to 3 AcP (2 to 1 ratio) without

ATP expenditure. NOGm3 denotes the third mode of NOG (Bogorad et al., 2013) that involves Fpk and two Xpk. A similar results could be obtained using either the first mode (Fpk only) or the second mode (Xpk only).

Table 2-2. Primer sequences

Construct	Primer names	Primer sequences		Template
pQE9 backbone	IWB94	TCTAGAGGCATCAAATAAAACGAAAGGC		—
	IWB005F	TCCCTGAAAATACAGGTTTT		
pQE9-HIS-Fpk	Previous work	—		*B. adolescentis*
pQE9-HIS-Tkt	Previous work	—		*E. coli*
pQE9-HIS-Tal	Previous work	—		*E. coli*
pQE9-HIS-Rpe	Previous work	—		*E. coli*
pQE9-HIS-Rpi	Previous work	—		*E. coli*
pQE9-HIS-Hps(Bs)	IWB415	GATCCGAAAACCTGTATTTTCAGGGAATGGAATTACAGCTTGCATTAGACCTCG		*B. subtilis*
	IWB386	TTATCCTTGGACAATCAGCTGCTTCATTTTTGAAG		
pQE9-HIS-Hps(Bm)	IWB534	GGATCCGAAAACCTGTATTTTCAGGGAATGCAACTACAATTAGCTCTAGATTTGGTAAAC		*B. methanolicus*
	IWB535	GTTTTATTTGATGCCTCTAGATCATAACCCTTGTTTAACTAATTTATTAATTTTTTCAGC		
pQE9-HIS-Hps(Mc)	IWB528	ATCACGGATCCGAAAACCTGTATTTTCAGGGAATGGCAAGACCATTGATTCAGCTCGC		*M. capsulatus*
	IWB529	CGACTGAGCCTTTCGTTTTATTTGATGCCTCTAGATTAGGCGGAAGCGGCGACG		
pQE9-HIS-Phi(Mf)	IWB419	GATCCGAAAACCTGTATTTTCAGGGAATGAATAAATATCAAGAGCTCGTGGTCAACAAGC		*M. flagellatus*
	IWB390	TTATTCAAGATTGGCGTGAATTGCACGC		
pQE9-HIS-PduP(Bm)	IWB469	GGATCCGAAAACCTGTATTTTCAGGGAATGTTACGAGATAAAGATTTGCAATCTATCC		*B. methanolicus*
	IWB470	GCCTTTCGTTTTATTTGATGCCTCTAGATTATTTTGTTAGGGCAGGTTCTTGTTGAGC		
pCDF-Duet1 backbone	T589	AGCCAGGATCCGAATTCGAG		—
	T590	GTGGTGATGATGGTGATGGC		
pCDF -Duet1-HIS-Pta	T983	CAGCAGCCATCACCATCATCACCACGCAGATTTATTTTCAACAGT		*B. subtilis*
	T984	CCGAGCTCGAATTCGGATCCTGGCTTTACAGTGCTTGCGCCGCTG		
pQE9-HIS-Mdh-PB1*	CT051	Flanking region	TCGTAAGTATGCACTTTATTAACATATAGTATCGAATAGT	*B. methanoloicus PB1*
	CT052		AACGGTATAAGTAGCTCCCTCTTTCGG	
	CT032	Mdh gene	CAGCAGCCATCACCATCATCACCACACGCAAAGAAACTTTTTCAT	—
	CT031		CCGAGCTCGAATTCGGATCCTGGCTTTACAGAGCGTTTTTGATGA	
pQE9-HIS-Mdh-MGA3	CT023	CAGCAGCCATCACCATCATCACCACACAACAAACTTTTTCATTCC		*B. methanoloicus MGA3*
	CT022	CCGAGCTCGAATTCGGATCCTGGCTTTACATAGCGTTTTTGATGA		
pQE9-HIS-Mdh-MGA3-S98G	CT021	Fragment 1	GGTGGAGGTGGATCTCACGATACAGCTAAAGC	*B. methanoloicus MGA3*
	CT022		CCGAGCTCGAATTCGGATCCTGGCTTTACATAGCGTTTTTGATGA	
	CT023	Fragment 2	CAGCAGCCATCACCATCATCACCACACAACAAACTTTTTCATTCC	
	CT041		GCTTTAGCTGTATCGTGAGATCCACCTCCACC	

Table 2-3. Kinetic analysis of MCC

Enzyme Reaction	Organism	Enzyme Specific Activity (μmol/min/mg protein)		
		WT Enzymes	Round 1 (1 Enzyme)	Round 2 (3 Enzymes)
Mdh	*B. methanolicus*	0.25	7	15
Hps	*M. capsulatus*	69	69	69
Phi	*M. flagellatus*	147	147	147
Fpk	*B. adolescentis*	0.83	0.83	10
Tal	*E. coli*	60	60	60
Tkt	*E. coli*	100	100	100
Rpe	*E. coli*	257	257	257
Rpi	*E. coli*	937	937	937
Pta	*B. subtilis*	1150	1150	1150
AtoB	*E. coli*	1078	1078	1078
Hbd	*C. acetobutylicum*	147	147	147
Crt	*C. acetobutylicum*	6155	6155	6155
Ter	*T. denticola*	43	43	43
PduP	*S. enterica*	27	27	27
Adh	*S. cerevisiae*	18	18	18
g BuOH/g protein/hr		0.044	2.61	4.94

*Calculations are based on specific activity and pathway stoichiometry. For example, Mdh must react four times to generate one 1-butanol. Targeted enzyme improvement could drastically improve pathway productivity as shown.

3 Characterization and evolution of an activator-independent methanol dehydrogenase from *Cupriavidus necator* N-1

Disclaimer: This chapter was originally published with the same title in *Applied Microbiology and Biotechnology* **100** (2016) 4969-4983.

This publication had equal 1st co-authorship between Dr. Tung-Yun Wu and myself. Chang-Ting and Dr. Wu identified the Mdh2 from *C. necator* N-1. Dr. Wu characterized the WT Mdh2. Chang-Ting performed directed evolution, designed the high-throughput screening (HTS) process, and characterized the resulting enzyme variants. Both 1st-coauthors participated in the manuscript writing. Dr. Robert Damoiseaux provided assistance for automation facility for HTS. Dr. Bogorad implemented Nash assay for Mdh HTS. Jessica Tse-Jin Liu was laboratory technician who assisted with *in vitro* enzyme assays.

3.1 Abstract

Methanol utilization by methylotrophic or non- methylotrophic organisms is the first step toward methanol bioconversion to higher carbon-chain chemicals. Methanol oxidation using NAD-dependent methanol dehydrogenase (Mdh) is of particular interest because it uses NAD+ as the electron carrier. To our knowledge, only a limited number of NAD-dependent Mdhs have been reported. The most studied is the *Bacillus methanolicus* Mdh, which exhibits low enzyme specificity to methanol and is dependent on an endogenous activator protein (ACT). In this work, we characterized and engineered a group III NAD-dependent alcohol dehydrogenase (Mdh2) from *Cupriavidus necator* N-1 (previously designated as *Ralstonia eutropha*). This enzyme is the first NAD-dependent Mdh characterized from a Gram-negative, mesophilic, non-methylotrophic

organism with a significant activity towards methanol. Interestingly, unlike previously reported Mdhs, Mdh2 does not require activation by known activators such as *B. methanolicus* ACT and *Escherichia coli* Nudix hydrolase NudF, or putative native *C. necator* activators in the Nudix family under mesophilic conditions. This enzyme exhibited higher or comparable activity and affinity toward methanol relative to the *B. methanolicus* Mdh with or without ACT in a wide range of temperatures. Furthermore, using directed molecular evolution, we engineered a variant (CT4-1) of Mdh2 that showed a 6-fold higher K_{cat}/K_m for methanol and 10-fold lower K_{cat}/K_m for 1-butanol. Thus, CT4-1 represents an NAD-dependent Mdh with much improved catalytic efficiency and specificity toward methanol compared with the existing NAD-dependent Mdhs with or without ACT activation.

3.2 Introduction

Methanol may become an attractive substrate for bioconversion to chemical commodities due to the abundance of meth- ane. Methanol bioconversions to amino acids using methylotrophic bacteria such as Methylobacterium sp. for L-serine (Hagishita et al., 1996) and *Methylobacillus glycogenes* for L-threonine (Motoyama et al., 1994), L-glutamate (Motoyama et al., 1993), and L-lysine (Motoyama et al., 2001) have been demonstrated. Despite previous successes, many hurdles remain before industrial applications. In particular, genetic tool development and physiological studies of methylotrophic bacteria are needed for further strain engineering (Schrader et al., 2009). An alternative is to enable methanol assimilation or even bestow methylotrophic growth on strains suitable for industrial processing. In principle, synthetic methylotrophy can be achieved by overexpressing heterologous enzymes for methanol oxidation

and engineering a formaldehyde assimilation pathway to produce central metabolites for growth. Methanol oxidation is categorized into three groups of enzymes based on their terminal electron acceptors: (1) Pyrroloquinoline quinone (PQQ)-dependent methanol dehydrogenases (Mdhs), (2) methanol oxidases, and (3) NAD-dependent Mdhs. NAD-dependent Mdhs are within metal-containing group III alcohol dehydrogenases (Adhs), named Mdh when the enzymes present significant methanol activity, such as *Bacillus methanolicus* Mdhs (de Vries et al., 1992). Group III Adhs are structurally unrelated to group I or II Adhs and are highly diverse (Elleuche and Antranikian, 2013). Among the three types of methanol-oxidizing enzymes, NAD-dependent Mdhs are the favorable option for synthetic methylotrophy due to their applicability in both aerobic and anaerobic conditions (Whitaker et al., 2015). Furthermore, electrons derived from methanol oxidation are stored in NADH, which can be used to drive production of target metabolites without sacrificing additional carbons. As such, this type of enzyme was used in a redox balanced methanol condensation cycle (MCC) to achieve conversion of methanol to higher alcohols (Bogorad et al., 2014). In addition, an NAD-dependent Mdh of *B. methanolicus* was introduced in *Escherichia coli* and *Corynebacterium glutamicum* to demonstrate methanol assimilation via the ribulose monophosphate pathway (Jonas E.N. Müller et al., 2015; Witthoff et al., 2015).

To our knowledge, NAD-dependent Mdhs with relatively high activity have only been reported in the Gram-positive, thermophilic methylotroph, B. methanolicus (Arfman et al., 1989; Hektor et al., 2002; Krog et al., 2013), with a few homologs reported from other Gram-positives, both mesophilic and thermophilic bacteria (Ochsner et al., 2014; Sheehan et al., 1988). The existence of NAD-dependent Mdhs in thermophiles is in agreement with the thermodynamic

argument that NAD^+-dependent methanol oxidation is favorable at high temperatures (Whitaker et al., 2015). Their sequences have 45–53 % similarity to the NAD-dependent 1,3-propanediol dehydrogenase of *Klebsiella pneumoniae* (Krog et al., 2013). In contrast to the PQQ-dependent Mdhs which exhibit high methanol specificity (Keltjens et al., 2014), NAD-dependent Mdhs have broad substrate specificities, with optimum activity to 1-propanol or 1-butanol and marginal activity to methanol (Krog et al., 2013; Sheehan et al., 1988).

The methanol activity of Mdhs of *B. methanolicus* can be greatly enhanced by an endogenous activator protein ACT, which contains a conserved motif for hydrolyzing nucleoside diphosphates linked to a moiety X (Nudix) (Arfman et al., 1997, 1991, 1989; Hektor et al., 2002; Kloosterman et al., 2002). This activation effect has been found to be widespread among group III Adhs (Ochsner et al., 2014) and results in both increased K_{cat} and decreased K_m. Notably, this activation is general to all substrates, instead of a specific activation for methanol (Krog et al., 2013; Ochsner et al., 2014). ACT activates Mdh by hydrolytically removing the nicotinamide mononucleotide (NMN) moiety of the Mdh-bound NAD, causing a change in its reaction mechanism from the ping-pong type mechanism to the ternary complex mechanism (Arfman et al., 1997). The ACT-Mdh activation model has been proposed to be a reversible process in which the interaction between ACT and Mdh results in conformational change to position NAD^+ and methanol binding sites closer together, thus enabling direct electron transfer (Kloosterman et al., 2002). However, the detailed mechanism of Mdh activation is still unclear. For the purpose of metabolic engineering, it would be useful to identify an Mdh with high activity under mesophilic or thermophilic conditions without the need for ACT.

In this work, we characterized a putative Mdh encoded by mdh2 in the genome of a non-methylotrophic bacteria *Cupriavidus necator* N-1. We showed that Mdh2 was an active NAD-dependent Mdh without the need for ACT. Mdh2 is the first group III Adh identified in Gram-negative, mesophilic bacteria that possesses significant methanol activity. Using directed evolution, we further improved the Mdh activity and specificity for methanol.

3.3 Materials and methods

Reagents

All chemicals were purchased from Sigma-Aldrich or Fisher Scientific unless otherwise specified. KOD Xtreme DNA polymerases were purchased from EMD Biosciences (San Diego, CA, USA). Phusion Hot Start II High-Fidelity DNA polymerases were purchased from Thermo Scientific (Waltham, MA, USA). DpnI enzymes were purchased from New England Biolabs (Ipswich, MA, USA).

Strains and plasmids

The complete plasmids and primers list used in this work is shown in Table 3-1. E. coli XL-1 blue was used as the cloning strain to propagate all plasmids. *C. necator* N-1 strain (ATCC43291) was purchased from ATCC (Manassas, VA, USA) and the genomic DNA was extracted by Qiagen (Valencia, CA, USA) DNeasy Blood & Tissue Kit.

PCR amplif ication and cloning

The annotated mdh1 (CNE_2c07940) and mdh2 (CNE_2c13570) genes from *C. necator* N-1 genome were found from Uniprot protein data base (The Uniprot Consortium 2015). The inserted mdh1 gene on plasmid pCT23 was amplified from *C. necator* N-1 genomic DNA using

primers CT74 and CT75 (Table 3-1). The inserted mdh2 gene on plasmid pCT20 was amplified from *C. necator* N-1 genomic DNA using primers CT64 and CT65 (Table 3-1). The inserted nudF gene on plasmid pTW195 was amplified from E. coli MG1655 (ATCC700926) genomic DNA using primers T1478 and T1479 (Table 3-1). The inserts encoding the putative Nudix genes were amplified from C. necator N-1 genomic DNA to create pMS4 (CNE_BB1p03180, primers MS14 and MS15), pMS5 (CNE_1c08460, primers MS16 and MS17), pMS12 (CNE_1c14320, primers MS33 and MS34), pMS13 (CNE_1c04760, primers MS35 and MS36), and pMS14 (CNE_1c10080, primers MS37 and MS38). The insert adhA (Cgl2807) gene of plasmid pTW113 was amplified from Corynebacterium glutamicum (ATCC 13032D-5) by T1151 and T1152 (Table 3-1). The backbones of pTW195, pCT20, pCT23, pTW113, and all pMS plasmids were amplified from a modified plasmid pZE12-luc (Lutz and Bujard 1997), pIB4, of which a lacI repressor was included using primers T989 and T990. For plasmid pQE9-Act(Bm), the insert act gene was amplified from *B. methanolicus* PB1 genomic DNA using primers IWB445 and IWB446, whereas vector backbone was amplified from pQE9 acquired from Qiagen using primers IWB094 and IWB141. Polymerase chain reactions (PCRs) were conducted using Phusion Hot Start II High- Fidelity or KOD Xtreme DNA Polymerases, followed with DpnI digestion. The DNA products were purified by Zymo DNA clean & concentrator kit (Zymo Research, Irvine, CA, USA). The purified backbone and insert were assembled in a 10 μL reaction using isothermal DNA assembly method (Gibson et al., 2009) at 50 °C for 20 min. Five microliters of the reaction mixture was transformed in 50 μL Zymo Z-competent XL-1 blue competent cell (Zymo research) and plated on LB agar plates containing

the appropriate antibiotic. Positive transformants were verified by colony PCR and Sanger sequencing.

Protein purification and SDS-PAGE

The Mdh1 and Mdh2 were synthesized from plasmids pCT20 (Mdh2) and pCT23 (Mdh1) with N-terminal His-tag in E. coli strain XL-1 blue. The XL-1 blue strains were cultured 16–20 h aerobically at 37 °C in Luria-Bertani (LB) media supplemented with appropriate antibiotics. The next day, 1 % of overnight culture was inoculated into LB medium with antibiotics and cultured at 37 °C for 2 to 3 h until OD600 was around 0.4–0.8, followed by the addition of 0.1 mM isopropyl-β-D- thiogalactopyranoside (IPTG) induction at room temperature (22–25 °C) for 16 to 20 h. Cells were harvested by centrifu- gation at 4 °C and either used directly or stored in −80 °C for later protein purification. The purification was conducted with Ni-NTA column using glycylglycine based buffers at room temperature. Protein concentration was measured by Coomassie Plus Assay (Thermo Scientific) at OD_{595}. The purified proteins were analyzed on 12 % Mini-PROTEAN TGX gel (Bio-rad, Hercules, CA, USA) and the gel was stained with SimplyBlue SafeStain (Life Technologies, Carlsbad, CA, USA).

Enzyme assays

Mdh activity assays were carried out in a 200-µL assay mixture containing 100 mM sodium bicarbonate buffer (pH 9.5), 30µg of Mdh, 5mM of Mg^{2+}, 3mM NAD^{+}, and 800mM of methanol at 30 °C. For C2-C4 alcohol affinity assays, 10 mM ethanol with 1 µg Mdh, 5 mM 1-propanol with 0.5 µg Mdh, and 100 mM 1-butanol with 0.5 µg Mdh were used instead. For pH assays, buffers pH 6 (2-(N-morpholino)ethanesulfonic acid), pH 7 (potassium phosphate), pH 8.5 (glycylglycine), pH 9.5 (sodium bicarbonate), and pH 10.5 (sodium bicarbonate) were used with

the same recipe of Mdh activity assay stated above. For thermal stability assays, the reaction mixture (use sodium bicarbonate pH 9.5) containing everything except the initiating substrate (methanol) was pre-incubated at temperatures ranging from 25 to 60 °C in a Bio-rad PCR machine for 10 min before initiating the assay at 30 °C. For temperature activity profile assays, the reaction mixture (use sodium bicarbonate pH 9.5) containing all the components except the enzyme and methanol was pre-incubated at assay temperature for 5 min before starting the assay. All assays were initiated by adding methanol. One microgram of purified his-tagged ACT or NudF was used to test Mdh activation. It should be noted that NAD^+ needs to be added before mixing with Mdh because significant inhibition will be otherwise observed. The activity was defined by the reduction rate of NAD^+ at OD340 using Bio-Tek Eon microplate spectrophotometer. One unit (U) of Mdh activity was defined as the amount of enzyme that converts 1 μmol of substrate into product per minute. The Km values and Vmax of Mdh were calculated by Prism 6 (GraphPad Software, La Jolla, CA, USA).

High throughput screening (HTS): Nash reaction-based screening

Cells were grown overnight in LB medium supplemented with 20 mM $MgCl_2$, 0.1 mM IPTG, and appropriate antibiotics. Nash reagent was prepared by dissolving 5 M ammonium acetate and 50 mM acetylacetone in M9 buffer. Before the assay, cell density was determined by OD_{595}. The assay was started by mixing 100 μL of overnight cell culture, 80 μL Nash reagent, and 20 μL 5 M methanol in 96-well plate (#3370, Corning, Corning, NY, USA). After 3 h of incubation in 37 °C shaker (250 rpm), the reaction mixture was centrifuged at 3500× rpm (Allegra X14-R centrifuge, rotor SX4750, Beckman Coulter, Brea, CA, USA) for 10 min. One hundred microliters of supernatant was transferred to a fresh 96-well plate, from which OD_{405}

measurement was taken. All the OD measurements were accomplished on Victor 3V plate reader (Perkin Elmer, Waltham, MA, USA). For the quantification of the Nash reaction and cell density, we substituted OD_{595} and OD_{405} for OD_{600} and OD_{412}, respectively.

High throughput screening (HTS): library construction and procedure

The random mutagenesis libraries for HTS were constructed by GeneMorph II EZClone mutagenesis kit (Agilent, Santa Clara, CA, USA) following manufacturer's protocol. In short, 10 ng of parent Mdh DNA was used as the template for primers CT64 and CT65 for error-prone PCR. The error- prone PCR was carried out for 30 thermal cycles and resulted in an average error rate of 2 nt/kb. The error-prone PCR prod- uct was gel-purified (Zymoclean gel DNA recovery kit, Zymo Research) and assembled to a backbone based on pCT20. The assembled library was transformed to the E. coli strain DH10B (Life Technologies) by electroporation and plated on Bioassay QTrays (Molecular Devices, Sunnyvale, CA, USA) containing 200 mL LB agar (1.5 % w/vol) with appro- priate antibiotics. From the Bioassay QTrays, single colonies were picked by a QBot colony picker (Molecular Devices) and inoculated into 96-well low profile plates (X6023, Molecular Devices) containing 150 μL of LB supplemented with 15 % (v/v) glycerol, 1 % (w/vol) glucose, and appropriate antibiotics. As positive control, 96 colonies containing the wild-type Mdh or parent Mdh were picked into a single 96- well plate and processed together with other plates. Similarly, colonies containing E. coli transketolase (Tkt) was used as the negative control. The plates were covered with a lid and grown overnight in a 37 °C the incubator. Subsequently, plates were used to re-inoculate a fresh 96-well plate (#3370, Corning) filled with 200 μL LB supplemented with 20 mM MgCl2, 0.1 mM IPTG, and appropriate antibiotics. The new plate was sealed with aluminum sealing film (#6569, Corning)

and incubated in 37 °C shaker (250 rpm), while the old plate was kept in −80 °C as stock. After about 16 h of growth, the culture plates were transferred to the BenchCel 4R system with Vprep Velocity11 liquid handler (Agilent) using a 96 LT head. The cells were gently re- suspended and 100 µL of the samples was aliquoted to a fresh 96-well plate (#3370, Corning). Cell density was assessed by OD595 at this point. After the measurement, Mdh variants were assessed by the Nash reaction in a 96-well format at 405 nm using the Victor 3V plate reader (Perkin Elmer) as above.

Site-saturation mutagenesis

The site-saturation mutagenesis on Mdh2 A169 site was constructed by Quikchange II site-directed mutagenesis kit (Agilent) with primers CT291 and CT292. The de- generate codons on the primers generate all possible amino acid substitutions. The library was transformed to E. coli DH10β strain and single colonies containing all 19 amino acid substitution variants were isolated for further analysis.

Mdh2 sequence analysis

The Mdh2 amino acid sequence was uploaded to SWISS-MODEL web server (http://swissmodel.expasy.org/) (Guex et al., 2009), which performed the structure analysis and generated a 2D plot to present Mdh2 homologs of existing protein structure repository. The Mdh2 and its homologs were aligned using T-coffee (http://www.tcoffee.org/Projects/tcoffee/) (Notredame et al., 2000) and visualized by ESPript 3.0 web server (ESPript - http://espript.ibcp.fr) (Robert and Gouet, 2014).

3.4 Results

3.4.1 Expression, purification, and characterization of *C. necator* N-1 Mdh2

To determine whether the two putative Mdhs in *C. necator* N- 1, encoded by mdh1 and mdh2 genes (gene names designated as in UniProt), exhibit catalytic activity towards methanol, these genes were cloned and expressed from the His-tag plasmids pCT20 (Mdh2) and pCT23 (Mdh1) in E. coli XL-1, and the Mdh1 and Mdh2 proteins were purified. SDS-PAGE analysis showed both the purified Mdh1 and Mdh2 were detected with molecular masses of approximately 40 kDa, which is close to the predicted sizes 38.8 and 40.7 kDa for Mdh1 and Mdh2, respectively (Figure 3-8). To test whether Mdh1 or Mdh2 shows the desired activity, we performed the methanol dehydrogenase activity assay by monitoring $NAD(P)^+$ reduction. Mdh1 methanol-linked oxidation was not observed when using either NAD^+ or $NADP^+$ as the electron acceptor (data not shown). However, Mdh2 showed significant specific activity 0.32 U/mg (Table 3-3) when NAD^+ was used as the electron acceptor, whereas no methanol oxidation activity was detected when $NADP^+$ was used. The K_m values of Mdh2 for methanol and NAD^+ were 132 and 0.93 mM, respectively. The specific activity and K_m values of Mdh2 at 30 °C without ACT were comparable to the ACT activated *B. methanolicus* Mdhs at 45 °C (Krog et al., 2013). Examination of the catalytic activity of Mdh2 to C1-C4 alcohols showed that Mdh2 exhibits broad substrate specificity, with highest specificity towards 1-propanol and low affinity to methanol, similar to previously reported Mdhs (Table 3-3) (Krog et al., 2013).

3.4.2 Effect of pH, temperature, and ions on Mdh2

Further characterization was conducted using methanol as a substrate to investigate the effect of pH, temperature, and different metal ions on Mdh2. As shown in Figure 3-1a, the Mdh2

was active from pH 6 to 10.5, with its optimum at pH 9.5. The thermal stability assay revealed that Mdh2 enzyme was inactivated (Figure 3-1b) when incubating for 10 min at temperatures higher than its physiological growth condition (30 °C). In particularly, 13 % of activity remained after pre-incubation at 55 °C (Figure 3-1b) and the activity was abolished at 60 °C. To detect the enzyme sensitivity to various metal ions and EDTA, we performed the assay in the presence of these additives. Figure 3-2 shows that the activity of Mdh2 was activated by the addition of 1 mM Ni^{2+} and was strongly inhibited by 0.1 mM of Cu^{2+} or Zn^{2+}.

3.4.3 Insensitivity of Mdh2 to ACT

Activation of type III Adhs by the activator protein ACT or its homolog Nudix hydrolase is common, and may even be general for all enzymes in this class (Ochsner et al., 2014). The activation results in drastic improvement in V_{max} and K_m. For instance, six Mdhs of *B. methanolicus* PB1 and MGA3 can be strongly activated by ACT (Krog et al. 2013) at their physiological temperature, 45 °C. To test if Mdh2 from *C. necator* N- 1 can be activated by ACT, we cloned and purified a his-tagged thermophilic ACT from *B. methanolicus* PB1 and its mesophilic homolog Nudix hydrolase NudF from *E. coli* (Ochsner et al. 2014). The ACT and NudF were used to activate Mdh2 at various temperatures from 25 to 65 °C. Since *B. methanolicus* PB1 ACT is a thermophilic enzyme, the *E. coli* NudF was used to ensure the activator protein was active under mesophilic temperatures. Mdh3 of *B. methanolicus* MGA3, which was previously shown to be activated by ACT (Krog et al. 2013), served as a positive control. Interestingly, Mdh2 was largely insensitive to ACT and NudF between 25 and 40 °C (Figure 3-3a). The activity of Mdh2 was mildly increased by ACT or NudF at 55 °C and 60 °C

where it reached the optimum specific activity at 55 °C with 70 % improvement. In contrast, Mdh3 was significantly activated when assay temperature was above 42 °C. At its optimum temperature 60 °C, the specific activity improved more than 15-fold to 0.35 U/mg (Figure 3-3b).

To verify if Mdh2 is insensitive to the Nudix proteins from *B. methanolicus* and *E. coli*, we first varied the activator concentration by 10-fold (up to 50 μg/mL). No activation effect was observed under the conditions tested (Figure 3-4a). In addition, K_m and K_{cat} for methanol and NAD^+ remained unchanged in the presence of *B. methanolicus* ACT or *E. coli* NudF at 30 °C (Table 3-4). Next, we investigated if Mdh2 can only be activated by unknown native activators in *C. necator*. Mdh2 activity was assayed using purified Mdh2 incubated with *C. necator* N-1 crude extracts at concentrations 50 and 150 μg/mL. However, no activity improvement was observed (Figure 3-4b). To investigate this possibility further, we found five Nudix family proteins annotated in *the C. necator* N-1 genome: two hydrolase family proteins (coded by CNE_BB1p03180, CNE_1c08460) and three pyrophosphatases (code by CNE_1c14320, CNE_1c04760, CNE_1c10080). We also used BLAST analysis to identify *B. methanolicus* ACT or *E. coli* NudF homologs in *C. necator* N-1 and obtained no additional possibilities. We individually his-tag cloned and expressed these five putative Nudix genes and purified the proteins using *E. coli* for the activation tests. Consistent with crude extract results, none of these putative Nudix proteins can activate Mdh2 (Figure 3-4b).

3.4.4 Development of automatic high throughput screening (HTS) for Mdh evlution

Mdh2 exhibited significant methanol activity without activator protein in mesophilic conditions, this enzyme represents a promising choice for engineering synthetic methylotrophy. However, the activity and substrate specificity remain low for methanol (Table 3-2). To solve

this problem, we sought to engineer Mdh2 for better performance. An NAD^+ binding site mutation S97G of *B. methanolicus* C1 Mdh had been shown to increase methanol oxidation activity significantly (Hektor et al. 2002). However, the mutation of the corresponding residue (S106G) on Mdh2 did not show methanol oxidation activity (data not shown). Another group modified *B. stearothermophilus* Adh, which has methanol oxidation activity, to become hydrogel forming enzyme by outfitting it with cross-linking domains (Kim et al. 2013). Although the modification remarkably increased the *in vitro* methanol oxidation activity, the feasibility of applying hydrogel-forming enzymes in metabolic engineering needs to be further investigated.

To engineer Mdh, we developed an automatic HTS strategy based on automatic liquid handling, colony picking, incubation, and whole cell assay without lysis. Nash reaction (Nash 1953) allows Mdh assay without cell lysis, which detects formaldehyde produced from methanol oxidation by reacting with acetylacetone and ammonium acetate. The reaction product, diacetyldihydrolutidine, exhibits yellow color (Figure 3-5a) and can be quantified by absorbance at 405 nm. Since formaldehyde is able to diffuse through the cell membrane, Nash reaction-based screening does not require cell lysis. This greatly simplified the screening procedure and bypassed the background interference in cell crude extracts.

The scale of the screening was enhanced with utilizing automated colony picker and liquid handler as described in the material and methods. After integrating all equipment into the work flow, the initial design was capable to screen 6000 colonies in a single round using 384-well plates to carry the samples. The readout of Nash reaction was normalized to cell density (OD_{595}). Although the process successfully displayed Mdh activity in colorimetric reading, no improved Mdh was obtained from the first few testing rounds due to high false positive rate. The

setback prompted us to inspect the screening accuracy of the initial design. Zhang et al. had developed a standard measure to evaluate and validate the quality of HTS assays (Zhang et al., 1990). The so-called Z′- factor is a statistical characteristic of any given assay with the value between 0 and 1. The Z′-factor was calculated from the positive control and negative control of an assay: a value larger than 0.5 indicates a large separation between the populations of the measured signals and the assay will be considered as high quality. To evaluate our HTS system, strains containing wild-type Mdh2 or Tkt was tested as positive and negative controls, respectively. Three hundred eighty-four single colonies of each control were picked and assayed by Nash reaction. The resulting Z′-factor was 0.23 (Figure 3-5b), suggesting the low quality of the initial HTS design.

While revisiting the details of the process, we noticed that the small well dimension of 384-well plates might be constraining mixing during Nash reaction even with shaking. To test the hypothesis that the inaccuracy of the system originated from mixing during Nash reaction, 96-well plates were used to replace 384-well plate in the HTS process. After adjusting the process according to the new plate, the Z′-factor improved to 0.76 (Figure 3-5b). This Z′ indicated that the HTS system was suitable for screening for Mdh mutants of high activity and was properly validated. The optimized HTS process is shown in Figure 3-5c.

3.4.5 Directed evolution of Mdh2

We started the Mdh evolution with error-prone PCR-generated library using the wild-type mdh2 from *C. necator* N-1 as the template. The first round of screening generated 8 possible positive variants with 50 % or higher activity improvement based on Nash reaction out of 2000 variants screened. These variants were sequenced and tested by NADH-based assay for

crude extract activity to eliminate the false positives. Variants CT1-1 and CT1-2 displayed the highest improved activity based on the crude extract assay and were selected for purifi- cation and further characterization. Purified variant CT1-2 showed a 5-fold decrease in K_m, while CT1-1 improved marginally in K_m and K_{cat} (Table 3-4). However, K_{cat} of CT1-2 decreased by almost 50 % compared to the wild-type.

In the second round of screening, CT1-2 was used as the parent to generate another error-prone PCR library. Seven possible positive variants with at least 70 % activity improvement by Nash reaction were obtained from total of 2000 screened. After confirmation by sequencing and crude extract activity assay, only variant CT2-1 was selected for characterization. Variant CT2-1 restored wild-type K_{cat} while maintain- ing the K_m improvement (Table 3-4). In addition to the mutation A169V that originated from the previous screen, CT2-1 included another mutation, A26V. To determine the effect of A26V, we introduced this mutation in the wild-type mdh2 and determined its effect after purification. Interestingly, the mutation A26V alone demolished Mdh activity (Table 3-4), suggesting a synergistic effect of mutation A26V and A169V in enzyme function.

After these rounds of HTS, a chimeric variant CT4-1 was created by recombining three mutations found so far (A169V, A31V, and A26V). The K_m value of methanol was further lowered to 21.6 mM and K_{cat} remained unchanged (Table 3-4). Variant CT4-1 represented the best performing variant from the series of engineering with about 6-fold higher K_{cat}/ K_m ratio towards methanol compared to the wild-type.

3.4.6 Substrate specificity of the evolved Mdh2

To characterize the kinetic parameters of Mdh variants toward longer chain alcohols, 1-butanol was chosen as an example to measure K_m and K_{cat}. Results indicates that K_m values for 1-butanol were increased by 10-fold or higher (Table 3-4) for variants CT1-2, CT2-1, and CT4-1. The increased K_m towards n-butanol was concomitant with the decrease of K_m towards methanol. The best variant, CT4-1, displayed the most significant 19-fold decrease in K_{cat}/K_m towards 1-butanol among all variants. To further investigate substrate preferences on other higher alcohols, the specific activities towards ethanol and propanol were measured at the concentrations that saturate wild-type Mdh2 activity (Figure 3-6a). Consistent with the n-bu- tanol data, variants CT1-2, CT2-1, and CT4-1 showed 5- to 10-fold lowered specific activity towards ethanol and 6- to 8- fold lowered for propanol. As summarized in Figure 3-6b, CT4-1 significantly improved its methanol over C2 to C4 alcohol activity ratio compares to wild-type.

3.4.7 Sequence analysis

The Mdh2 amino acid sequence was uploaded to SWISS-MODEL server (Guex et al., 2009) to predict a hypothetical model based on structural information in the database. The server returned a plot of sequence similarity as shown in Figure 3-7a. The most structurally similar enzymes were K. pneumoniae 1,3-propanediol dehydrogenase (1,3-PDH) and Zymomonas mobilis ZM4 alcohol dehydrogenase 2 (Adh2) with 55 and 54 % sequence identities, respectively. Both en- zymes were categorized as group III metal-dependent dehydrogenases and contained Fe^{2+} in their catalytic centers (Marçal et al., 2009; Moon et al., 2011). Notably, Mdh2 also has 55 % sequence identity to *B. methanolicus* MGA3 Mdh, which also belongs to group III

dehydrogenases. The structure of group III dehydrogenases can be divided into N-terminal domain and C-terminal domains, which are responsible for $NAD(P)^+$ and metal ion binding, respectively. The metal ion coordination motif composed mainly of two to three histidine residues (Carpenter et al., 1998; Marçal et al., 2009; Montella et al., 2005; Moon et al., 2011; Ruzheinikov et al., 2001). In *K. pneumoniae* 1,3-PDH and *Z. mobilis* ZM4 Adh2, there were three histidine and one aspartic acid. These four amino acid residues were conserved in all of the enzymes aligned (Figure 3-7b), corresponding to D201, H205, H270, and H284 in Mdh2. On the other hand, the NAD-binding motif ($GGGSX_2DX_2K$) was also observed in the alignment (Figure 3-7b) (Wierenga et al., 1986). Taken together, the similarity of both amino acid sequences and functional domains indicated that Mdh2 belongs to group III metal-dependent dehydrogenases. Previously, NAD-dependent Adhs from *Lysinibacillus sphaericus* C3-41, *Lysinibacillus fusiformis* ZC1, and *Desulfitobacterium hafniense* Y51 were identified with methanol oxidation activity (Müller et al. 2015). Alignment with other Mdhs revealed that these methanol-oxidizing dehydrogenases shared the common NAD-binding domain and metal coordination motif (Fig. 7b).

Among the mutations acquired during Mdh2 evolution, A169V contributed significantly to the K_m decrease in methanol. The same mutation also greatly reduced the activity toward C2-C4 aliphatic alcohols. *Z. mobilis* Adh2 is one of the most structurally similar enzymes to Mdh2 and its binding pocket had been predicted (Moon et al. 2011). Residue A169 is one of the predicted binding pocket residues, which were conserved between *Z. mobilis* Adh2 and Mdh2 (Figure 3-7b). Therefore, we hypothesized that the change of alanine to bulkier valine reduces the binding space and subsequently hinders larger substrate binding. To test this hypothesis and

explore the best possible amino acid substitution at A169, a site-saturation mutagenesis library of A169 was constructed. The specific activities of all 19 variants were measured by Nash reaction (Figure 3-9), six best variants were selected for characterization. Although three of the variants with bulkier side chains (A169V, A169I, A169C) showed lower K_m for methanol, the others displayed the opposite (Table 3-5). Presumably, the K_m improvement is determined by both size and functional groups in the amino acid side chain. In agreement with this note, extremely large (F, W, Y) or small (G) amino acids at A169 showed no activity (Figure 3-9). Interestingly, A169P displayed higher K_{cat} as well as K_m (Table 3-5). Although protein structure characterization would be required to define the role of residue A169, the results here showed that A169 is crucial to Mdh2 activity and substrate preference.

3.5 Discussion

NAD-dependent methanol oxidation presents a principal step in utilizing methanol as a substrate for microbial production of chemicals. Mdhs reported heretofore from *B. methanolicus* (Krog et al. 2013) and a few additional homologs (Ochsner et al. 2014) require ACT and thermophilic conditions at 50 °C to activate methanol oxidation activity. A recent report (Müller et al. 2015) also presents challenges in activation of recombinant *B. methanolicus* Mdh in *E. coli* under mesophillic conditions. Despite previously reported as being NAD-dependent, type I Adhs from human liver, horse liver, yeast, and *C. glutamicum*, and *Bacillus stearothermophilus* which exhibited moderate enzymatic activity toward methanol without the requirement for activation (Kotrbova-Kozak et al., 2007; Mani et al., 1970; Sheehan et al., 1988), successful attempts of methanol assimilation were only reported using Mdhs from *B. methanolicus* (Müller et al. 2015;

Witthoff et al. 2015). Unfortunately, unlike PQQ-dependent Mdhs, NAD-dependent Mdhs exhibit broad substrate specificity and only show moderate activity towards methanol. In this work, we characterized and engineered a NAD-dependent methanol dehydrogenase, Mdh2, from a non-methylotrophic bacteria *C. necator* N-1 in the recombinant host *E. coli*. Mdh2 represents the first identified group III Adh in Gram-negative, mesophilic organism to exhibit significant activity towards methanol. Wild-type Mdh2 exhibits methanol oxidation activity 0.32 U/mg and K_m value 132 mM at 30 °C, and is insensitive to activation under mesophilic temperatures. After protein evolution using HTS, the best variant CT4-1 retained methanol oxidation activity with remarkable K_m values 21.6 and 120 mM for methanol and 1-butanol, respectively.

It should be noted that during HTS of Mdh2, a high meth- anol concentration (500 mM) was used that presumably favored variants with higher K_{cat}. Interestingly, the results showed that the HTS process was capable of identifying variants with improvement in either K_m (CT1-2 in round 1 showed lower K_m than wild-type, Table 3-4) or K_{cat} (CT2-1 in round 2 showed higher K_{cat} than CT1-2, Table 3-4). Although the methanol concentration (500 mM) used in the screening was higher than the K_m of Mdh2, the intracellular methanol concentration might be much lower because of diffusion limitation. Since the cells were not lysed in the Nash assay used in HTS, we have shown that the activity was not saturated even at 500 mM (data not shown), suggesting a possible diffusion limitation into the cell. Under non-saturating methanol concentrations, methanol oxidation rate will be a function of both K_{cat} and K_m. Therefore, improvement in either K_{cat} or K_m could be identified. The best variant CT4-1 has three mutations (A26V, A31V, A169V). It is intriguing that A26V or A31V individually showed no or

even a negative effect on K_m or K_{cat}, while together with mutation A169V they significantly improved K_m. Since the crystal structure of Mdh2 has not been solved, it remains unclear how mutations A26V or A31V alter the function of Mdh2. Alignment of Mdh2 with other type III NAD-dependent Adhs (Figure 3-7b) also provides very limited insight about the function of A26 and A31 since they are not conserved among the Adhs. Structural studies about Mdh2 will be required to uncover the functions of A26 and A31.

To our knowledge, CT4-1 is the best NAD-dependent, activator-independent Mdh with respect to methanol specificity. It was previously reported that AdhA from *Corynebacterium glutamicum* R exhibits appealing K_m and V_{max} values towards methanol (Kotrbova-Kozak et al. 2007). We cloned this enzyme with a his-tag, expressed and purified the protein from *E. coli*. In our hands, the K_m (97 mM) and V_{max} (0.29 U/mg) (Table 3-6) are significantly different from the reported values (K_m = 3 mM, V_{max} = 0.7 U/mg) (Kotrbova-Kozak et al. 2007) and comparable to the wild-type Mdh2. The difference could possibly be attributed to difference in assay conditions (NAD^+ concentration, buffer, additional metal ions) or unknown reasons. Regardless, under the same enzyme assay condition, CT4-1 has 4.4-fold higher catalytic efficiency than AdhA, mainly owing to the K_m difference. As such, it is suitable for metabolic engineering of organisms for in vivo or in vitro applications. A previous study (Ochsner et al. 2014) suggested that group III Adh activation by ACT homolog Nudix hydrolases represents a common mechanism. However, Mdh2 does not require activation.

Structural analysis and sequence alignment confirmed that Mdh2 belongs to group III Adh, by the high structural similarities to the 1,3-PDH of *K. pneumoniae* and Adh2 of *Z. mobilis*

ZM4, in addition to a putative NAD^+ binding motif and metal binding resides. Notably, the two most similar enzymes, *Z. mobilis* Adh2 and *K. pneumoniae* 1,3-PDH, do not have methanol oxidation activity. Similarly, *C. necator* N-1 cannot grow on methanol as a carbon source (data not shown), suggesting that the methanol oxidation may be a gratuitous activity in Mdh2. Discovery of *C. necator* N-1 Mdh2 opens up the possibility of searching for useful NAD-dependent Mdhs for synthetic methylotrophy from Gram-negative, mesophilic organisms. General perception of Mdhs in Gram-negative, mesophilic methyltrophs are mostly PQQ-dependent enzymes localized in periplasm. In contrast, NAD-dependent Mdhs are localized in bacterial cytoplasm (Keltjens et al. 2014). Despite the fact that *C. necator* N-1 possesses an active Mdh, this organism cannot utilize methanol as a carbon source. It remains unclear the physiological role of mdh2 in *C. necator* N-1. A possible explanation can be found in recent study on a non-methylotrophic, Gram-positive bacteria *C. glutamicum* which possesses a AdhA for methanol oxidation to CO_2, where methanol served as an auxiliary carbon source for energy generation, of which four essential enzymes alcohol dehydrogenase, acetaldehyde dehydrogenase, mycothiol-dependent formaldehyde dehydrogenase, and formate dehydrogenase are involved (Witthoff et al., 2013). More detailed characterizations on physiological growth conditions and genome analysis for *C. necator* N-1 are necessary to unveil the role of mdh2.

3.6 Figures

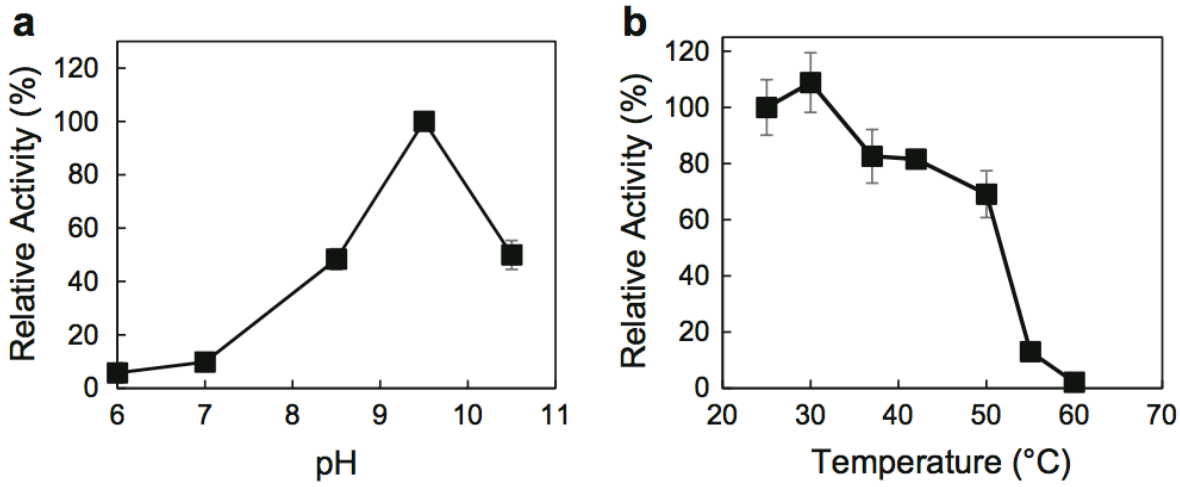

Figure 3-1. Effect of activator at different temperatures with a Mdh2 of C. necator N-1; b Mdh3 of B. methanolicus MGA3.

Assays were performed using 800 mM methanol and 3 mM NAD^+ as substrates at 30 °C and pH 9.5. ACT(BM) indicates the ACT of B. methanolicus (thermophilic ACT) and NudF(EC) indicates the ACT homolog NudF of E. coli (mesophilic ACT). N-1, C. necator N-1. MGA3, B. methanolicus MGA3. BM, B. methanolicus. EC, E. coli. The data shown were from triplicate experiments

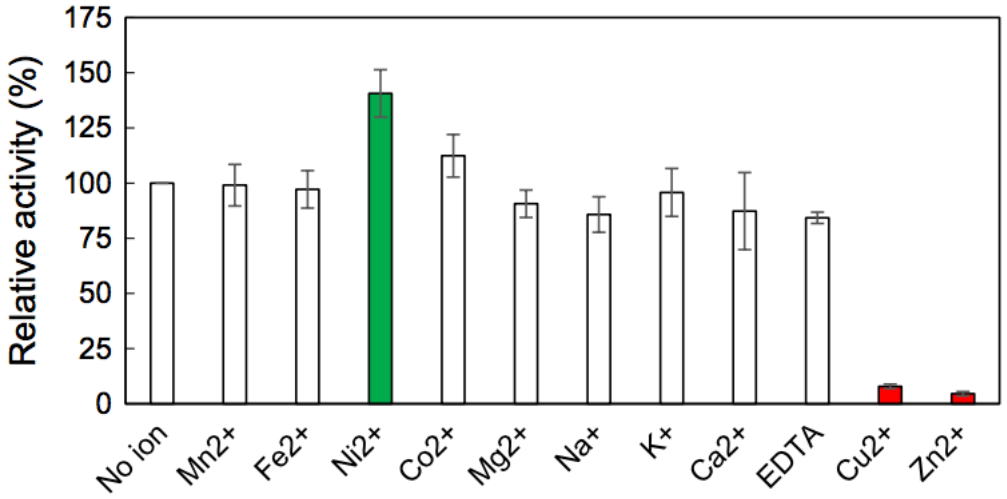

Figure 3-2. Effect of ions and chelator to Mdh2.

Experiments were performed by incubating enzyme with 1 mM ions (0.1 mM for Cu^{2+} and Zn^{2+}) or EDTA for 3 min, then using 800 mM methanol and 3 mM NAD^{+} as substrates at 30 °C and pH 9.5. The highlighted green color indicates significant activity increase and red color indicates significant activity decrease. The data shown were from triplicate experiments

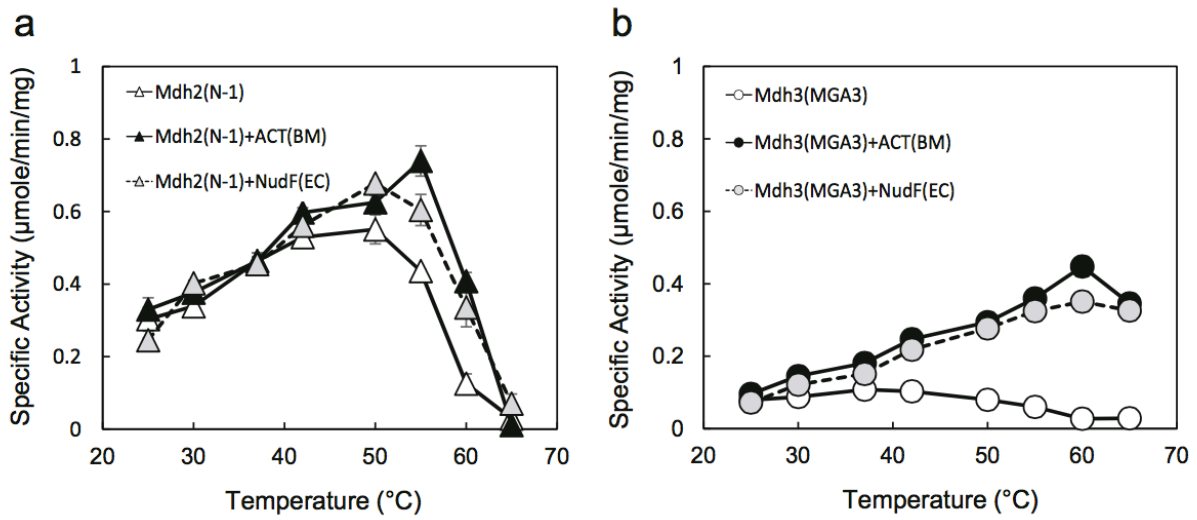

Figure 3-3. Effect of activator at different temperatures with a Mdh2 of C. necator N-1; b Mdh3 of B. methanolicus MGA3.

Assays were performed using 800 mM methanol and 3 mM NAD^+ as substrates at 30 °C and pH 9.5. ACT(BM) indicates the ACT of *B. methanolicus* (thermophilic ACT) and NudF(EC) indicates the ACT homolog NudF of *E. coli* (mesophilic ACT). N-1, *C. necator* N-1. MGA3, *B. methanolicus* MGA3. BM, *B. methanolicus*. EC, *E. coli*. The data shown were from triplicate experiments

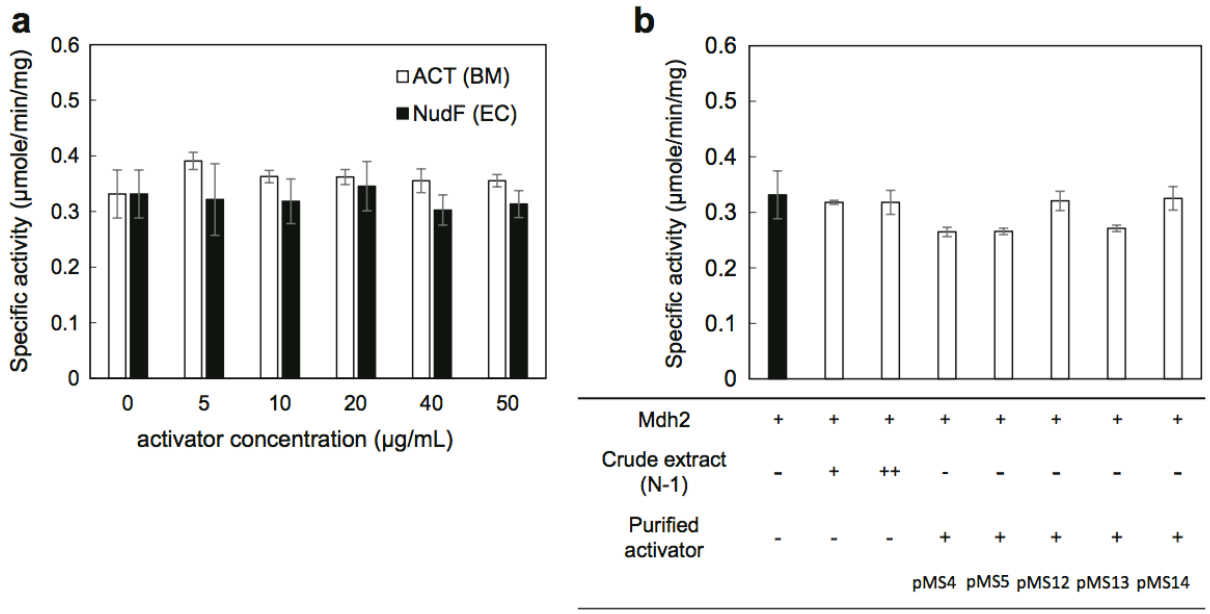

Figure 3-4. Mdh2 insensitivity to activation effect. a Effect of different activator concentrations to Mdh2 activity. b Effect of putative activator proteins of C. necator N-1.

ACT(BM) indicates the ACT of *B. methanolicus* (thermophilic ACT) and NudF(EC) indicates the ACT homolog NudF of *E. coli* (mesophilic ACT). Mdh2 activity was measured in the presence of crude extract (50 (+) or 150 (++) µg/mL) or 5 µg/mL purified activator using standard Mdh assay at 30 °C and pH 9.5. pMS4 (CNE_BB1p03180 of *C. necator* N-1), pMS5 (CNE_ 1c08460 *C. necator* N-1), pMS12 (CNE_1c14320 *C. necator* N-1), pMS13 (CNE_1c04760 *C. necator* N-1), pMS14 (CNE_1c10080 *C. necator* N-1). "+" sign indicates addition of protein in the assay. The data shown were from triplicate experiments

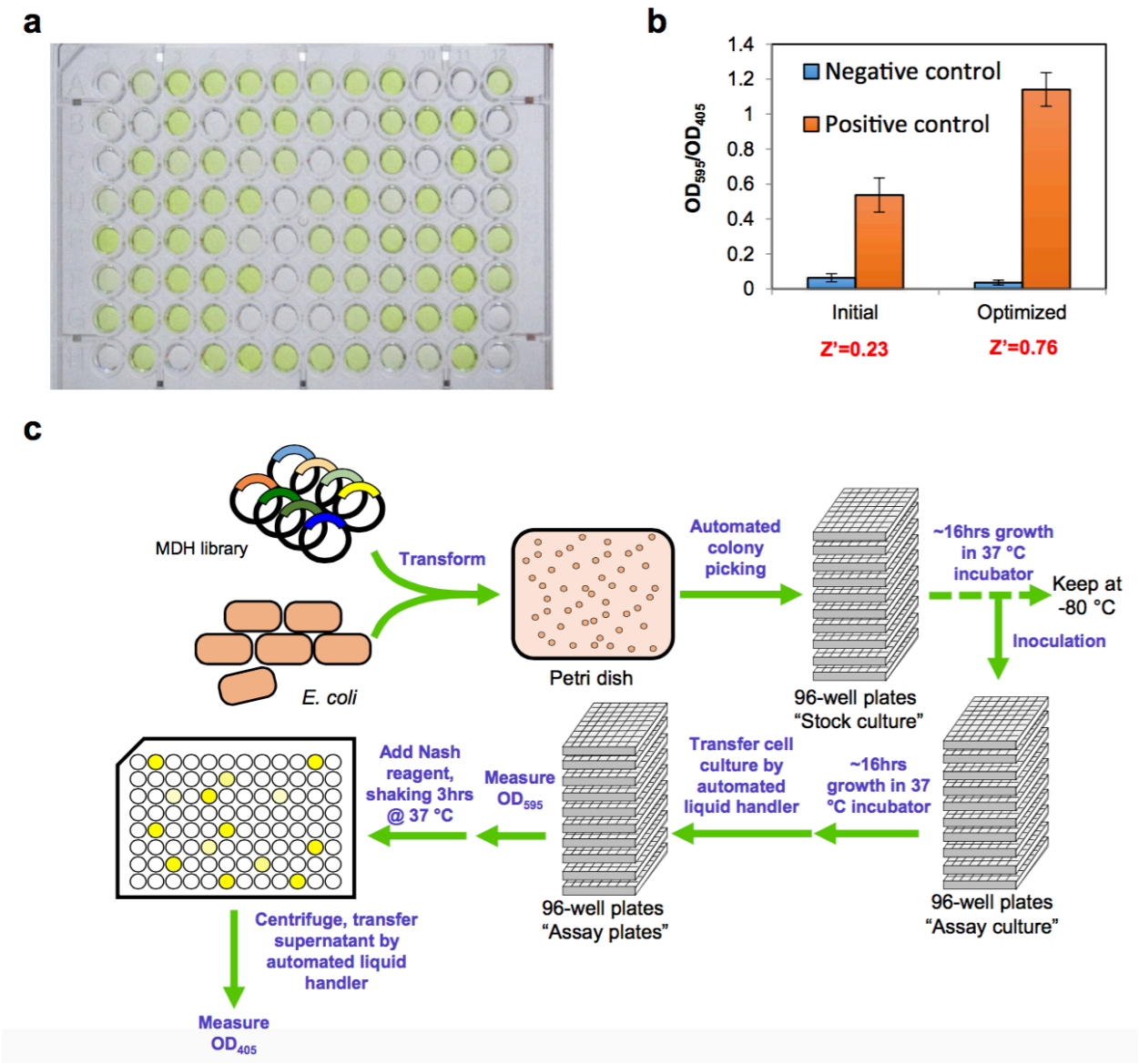

Figure 3-5. Development of HTS for Mdh.

a. Utilizing the colorimetric Nash reaction to measure Mdh activity. The yellow color indicates reaction product diacetyldihydrolutidine and can be quantified by OD405. b. Optimization of HTS process by showing improved Z′-factor. Wild- type Mdh2 was used as the positive control and *E. coli* transketolase was used as the negative control. c. Schematic diagram of Mdh HTS process

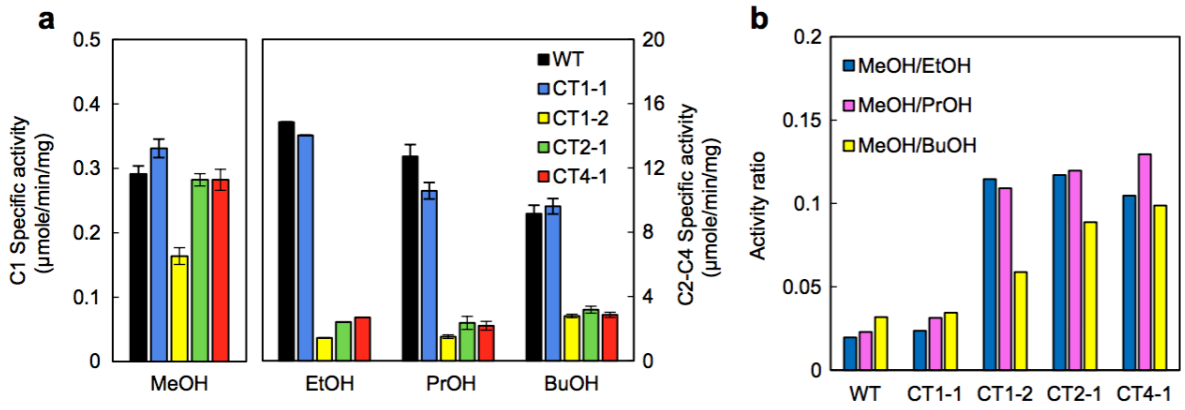

Figure 3-6. C1 to C4 alcohol specificity of Mdh2 and its engineered variants.

Alcohol concentrations used in the activity assays: MeOH, 800 mM; EtOH, 10 mM; PrOH, 5 mM; BuOH, 100 mM. b Activity ratio of methanol over longer chain alcohols (C2 to C4). WT, Mdh2; CT1-1, A31V; CT1-2, A169V; CT2-1, A26V, A169V; CT4-1, A26V, A31V, A169V. NAD^+ 3 mM and alcohol concentrations saturate activity of wild-type Mdh2 were chosen for assay conditions and the assays were performed at 30 °C and pH 9.5. The data shown were from triplicate experiments

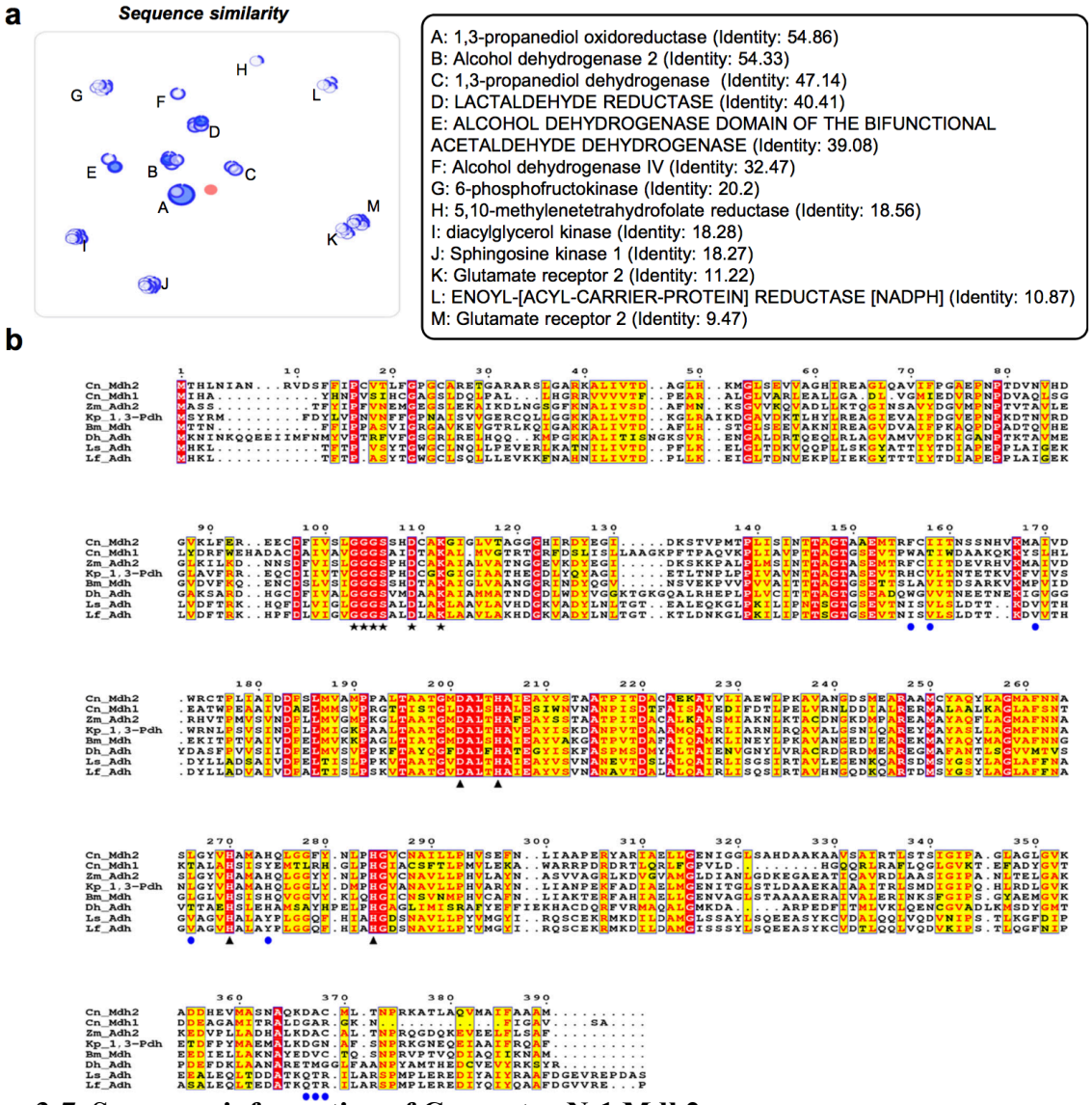

Figure 3-7. Sequence information of C. necator N-1 Mdh2.

(a) Sequence similarity predicted by SWISS-MODEL protein structure homology modeling. Mdh2 was shown as red circle in the middle, each template enzyme was shown as a blue circle which clusters with a group of similar enzymes. The distance between two template enzymes is proportional to the sequence identity. (b) Sequence alignment of group III alcohol dehydrogenases/methanol dehydrogenase and recently identified methanol-oxidizing Adhs. Cn, *C. necator* N-1; Zm, *Z. mobilis* ZM4; Kp, *K. pneumoniae*; Bm, *B. methanolicus* MGA3; Ls, *L. sphaericus* C3-41; Lf, *L. fusiformis* ZC1; Dh, *D. hafniense* Y51. Amino acid residues that are highly conserved are enclosed by blue boxed and highlighted in yellow. Identical residues are highlighted in red background. The NAD^+ binding motif and metal coordination domain are

annotated by black stars and triangles, respectively. Predicted residues of substrate binding based on Zm_Adh2 are indicated by blue circles

3.7 Tables

Table 3-1. List of plasmids and primers used in this study.

Plasmids	Genotype	Reference
pZE12-luc	AmpR ; ColE1 ori ; PLlacO-1:: luc(PP)	(Lutz and Bujard, 1997)
pIB4	AmpR ; ColE1 ori ; PLlacO-1:: fbp(EC)-fxpk(BA), with lacI	(Bogorad et al., 2013)
pCT20	AmpR; Derivative of pIB4 with mdh2 (C. necator N-1)	This Study
pCT23	AmpR; Derivative of pIB4 with mdh1 (C. necator N-1)	This Study
pCT20_10C12	AmpR; Derivative of pIB4 with mdh2 (A31V)	This Study
pCT20_4D8	AmpR; Derivative of pIB4 with mdh2 (A169V)	This Study
pCT20_15E9	AmpR; Derivative of pIB4 with mdh2 (A26V, A169V)	This Study
pTW212	AmpR; Derivative of pIB4 with mdh2 (A26V)	This Study
pCT20_S1	AmpR; Derivative of pIB4 with mdh2 (A26V, A31V, A169V)	This Study
pCT20_A169I	AmpR; Derivative of pIB4 with mdh2 (A169I)	This Study
pCT20_A169L	AmpR; Derivative of pIB4 with mdh2 (A169L)	This Study
pCT20_A169M	AmpR; Derivative of pIB4 with mdh2 (A169M)	This Study
pCT20_A169P	AmpR; Derivative of pIB4 with mdh2 (A169P)	This Study
pCT20_A169C	AmpR; Derivative of pIB4 with mdh2 (A169C)	This Study
pQE9-Act(Bm)	AmpR; Derivative of pIB4 with act (B. methanolicus PB1)	This Study
pTW113	AmpR; Derivative of pIB4 with adhA (C. glutamicum 534)	This Study
pTW195	AmpR; Derivative of pIB4 with nudF (E.coli MG1655)	This Study, (Ochsner et al., 2014)
pMS4	AmpR; Derivative of pIB4 with CNE_BB1p03180 (C. necator N-1)	This Study
pMS5	AmpR; Derivative of pIB4 with CNE_1c08460 (C. necator N-1)	This Study
pMS12	AmpR; Derivative of pIB4 with CNE_1c14320 (C. necator N-1)	This Study
pMS13	AmpR; Derivative of pIB4 with CNE_1c04760 (C. necator N-1)	This Study
pMS14	AmpR; Derivative of pIB4 with CNE_1c10080 (C. necator N-1)	This Study
Primer name	Sequence 5'->3'	
T989	TCTAGAGGCATCAAATAAAACGAAA	

T990	TCCCTGAAAATACAGGTTTTCGGAT
T1151	atccgaaaacctgtattttcagggaATGACCACTGCTGCACCCCA
T1152	tttcgttttatttgatgcctctagaTTAGAAACGAATCGCCACAC
T1478	ATCCGAAAACCTGTATTTTCAGGGAATGCTTAAGCCAGAC AACCT
T1479	TTTCGTTTTATTTGATGCCTCTAGATTATGCCCACTCATTTT TTA
IWB094	TCTAGAGGCATCAAATAAAACGAAAGGC
IWB141	TCCCTGAAAATACAGGTTTTCGGATCCGTGATGGTGATGG TGATGCGATCC
IWB445	TCCGAAAACCTGTATTTTCAGGGAATGGGAAAATTATTTG AGGAAAAAACAATTAAAAC
IWB446	GCCTTTCGTTTTATTTGATGCCTCTAGATCATTTATGTTTGA GAGCCTCTTGAAGCTGC
CT64	GGATCCGAAAACCTGTATTTTCAGGGAATGACCCACCTGA ACATCGCTA
CT65	GAGCCTTTCGTTTTATTTGATGCCTCTAGATTACATCGCCG CAGCGAAGATTGCC
CT74	CGGATCCGAAAACCTGTATTTTCAGGGAATGATCCATGCC TACCACAACC
CT75	CCTTTCGTTTTATTTGATGCCTCTAGACTAGGCAGACACGG CGCCGATAAA
CT291	CGAGCAATCATGTGAAGATGNNKATCGTCGACTGGCGTTG CAC
CT292	GTGCAACGCCAGTCGACGATMNNCATCTTCACATGATTGC TCG
MS14	aaaacctgtattttcagggaGAAGTTTATCAAAAGCACTCACATG
MS15	ttttatttgatgcctctagaTCAACGATCAGGCAAGACTCTTTCA
MS16	aaaacctgtattttcagggaCGTCCTGCTTTCGATCCCGAATCCC
MS17	ttttatttgatgcctctagaTCAGGCCGCCAGCAGGTGGTAAAGA
MS33	aaaacctgtattttcagggaATGAAATTCTGCTCGAACTGTGGTC
MS34	ttttatttgatgcctctagaTCAGGGCGTGACCGTGGCCCGGCTG
MS35	aaaacctgtattttcagggaATGTCCTACAAGATCCCGGAATCCG
MS36	ttttatttgatgcctctagaTCATGGCTGCGCTCCGTACACCGCC
MS37	aaaacctgtattttcagggaATGACCGACAAGATCCAACGCGGCA
MS38	ttttatttgatgcctctagaCTATATGGCGTAATGCGGCAGCGGC

Table 3-2. Substrate specificity to C1 - C4 alcohols and kinetic constants of recombinant Mdh2 *in vitro*

Substrate	K_m (mM)	K_{cat} (s^{-1})	K_{cat}/K_m (M^{-1} s^{-1})	V_{max} (U/mg)	V_{max} [a] (U/mg) (MGA3 Mdh3, 45 °C)
Methanol	132.1±15.4	0.22±0.01	1.6	0.32	0.07
Ethanol	0.77±0.1	11.1±0.3	14483	16	1.3
Propanol	0.54±0.1	9.6±0.2	17759	14.2	2.8
n-butanol	7.2±1	6.5±0.2	906	9.6	2.6
NAD^+	0.93±0.079	0.24±0.005	258	0.36	-
$NADP^+$	N.D.	N.D.	N.D.	N.D.	-

The values shown indicate mean ± standard deviation. Triplicate experiments were performed. Mdh assays to determine K_m for different alcohols were performed using various alcohol concentrations and 3 mM NAD^+ as substrates at 30 °C and pH 9.5. To determine kinetic parameters of NAD^+, 800 mM of methanol was used and the rest of conditions remained unchanged.

[a] The V_{max} values of *B. methanolicus* MGA3 Mdh3 were obtained from published data (Krog et al., 2013).

Table 3-3. Effect of activator proteins on kinetic parameters of recombinant Mdh2 *in vitro*

Substrate	Activator protein	K_m (mM)	K_{cat} (s^{-1})	K_{cat}/K_m (M^{-1} s^{-1})	V_{max} (U/mg)
Methanol	-	132.1±15.4	0.22±0.01	1.6	0.32
Methanol	*B. methanolicus* ACT	100.7±16.1	0.22±0.01	2.2	0.33
Methanol	*E. coli* NudF	122.1±18.2	0.23±0.01	1.9	0.35
NAD^+	-	0.93±0.079	0.24±0.005	258	0.36
NAD^+	*B. methanolicus* ACT	0.93±0.11	0.20±0.006	215	0.30
NAD^+	*E. coli* NudF	1.3±0.33	0.21±0.02	162	0.31

The values shown indicate mean ± standard deviation. Triplicate experiments were performed. Mdh assays to determine K_m were performed using various methanol concentrations and 3 mM NAD^+ as substrates at 30 °C and pH 9.5. To determine kinetic parameters of NAD^+, 800 mM of methanol was used with various NAD^+ concentrations.

Table 3-4. Kinetic Parameters of engineered Mdh2 variants to methanol and n-butanol, using NADH as cofactor.

Mdh2 variant	Library	Mutations	Nash activity	Methanol			*n*-Butanol		
				K_m (mM)	K_{cat} (s^{-1})	K_{cat}/K_m (M^{-1} s^{-1})	K_m (mM)	K_{cat} (s^{-1})	K_{cat}/K_m (M^{-1} s^{-1})
WT	–	–	1.00	132 ± 15.4	0.22 ± 0.01	1.6	7.2 ± 2.1	6.5 ± 0.1	903
CT1-1	Round 1	A31V	1.45	129 ± 11.9	0.25 ± 0.01	1.9	11.3 ± 1.3	7.2 ± 0.2	637
CT1-2	Round 1	A169V	1.47	26.9 ± 2.7	0.13 ± 0.003	4.8	66.5 ± 11.8	3.3 ± .0.1	50
CT2-1	Round 2	A26V, A169V	2.96	30.7 ± 3.6	0.21 ± 0.01	6.8	75.9 ± 1.1	5.0 ± 0.2	66
CT2-2	–	A26V	ND	ND	ND	ND	ND	ND	ND
CT4-1	Recombination	A26V, A31V, A169V	3.46	21.6 ± 1.5	0.20 ± 0.01	9.3	120 ± 17.9	5.7 ± 0.4	48

Table 3-5. Effect of A169 replacement to Mdh2 methanol specificity

Mdh2 variant	K_m (mM)	K_{cat} (S^{-1})	K_{cat}/K_m ($M^{-1}S^{-1}$)	K_{cat}/K_m Fold change
WT	132±15.4	0.22±0.01	1.6	-
A169V	26.9±2.65	0.13±0.003	4.8	3
A169I	68.9±9.0	0.064±0.002	0.93	0.58
A169L	201±31.5	0.093±0.004	0.46	0.29
A169M	203±25.5	0.073±0.002	0.36	0.23
A169P	303±34.9	0.41±0.014	1.4	0.88
A169C	46.0±3.34	0.16±0.003	3.5	2.2

Table 3-6. Comparison of methanol activity on reported mesophilic alcohol dehydrogenase from *Corynebacterium glutamicum*

Mdh/Adh	K_m (mM)	Vmax (U/mg)	K_{cat} (S^{-1})	K_{cat}/K_m ($M^{-1}S^{-1}$)
Mdh2 (*C. necator* N-1)	132±15.4	0.32	0.22±0.01	1.6
CT4-1 (*C. necator* N-1)	21.6±1.5	0.29	0.20±0.01	9.3
AdhA (*C. glutamicum*)	97±9.8	0.29	0.20±0.01	2.1

3.8 Supplementary

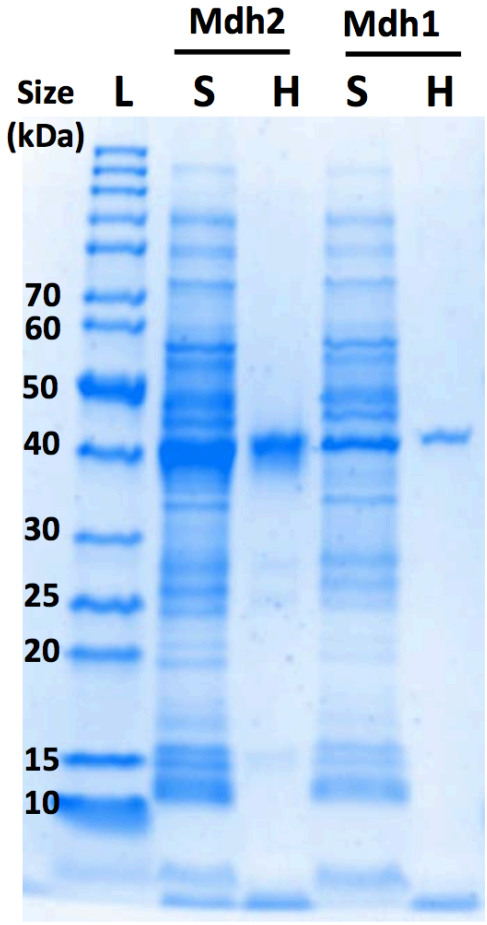

Figure 3-8. SDS-PAGE analysis to show expression of Mdh1 and Mdh2.

L: PageRuler ladder (Thermo Scientific), S: Soluble fraction protein, H: His-tagged purified protein

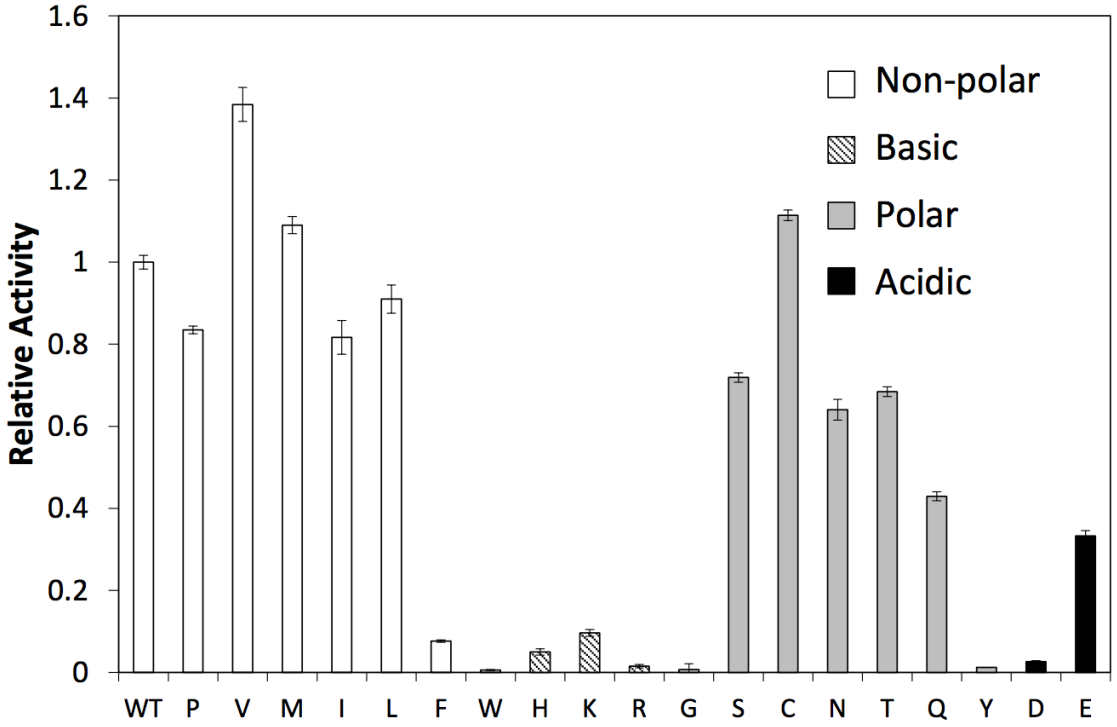

Figure 3-9. Relative activity of A169 variants measured by Nash assay

4. Synthetic methanol auxotrophy of *Escherichia coli* for methanol dependent growth and production

Disclaimer: This chapter contains unpublished material which is confidential. Dr. Igor Bogorad developed the idea of methanol auxotrophy, constructed *ΔrpiAB* and *Δrpe* strains, and achieved methanol dependent growth using *Δrpe* strains. Yu-Hsiao Chen evolved *ΔrpiAB* strains to realize methanol dependent growth. Chang-Ting Chen characterized the phenotype of methanol dependent growth, the genotype of evolved *ΔrpiAB* strains, demonstrated ethanol and 1-butanol production in both *ΔrpiAB* and *Δrpe* strains, carried out growth based selection for an engineered strain that grows on lower methanol, and wrote this chapter. Dr. Tung-Yun Wu processed the next-generation sequencing data of evolved *ΔrpiAB* strains.

4.1 Abstract

Methanol is a potentially attractive substrate for bioproduction of chemicals because of the abundance of natural gas and biogas. To utilize methanol, engineering an industrially-relevant organism, such as *Escherichia coli* for production of chemicals from methanol is one of the promising approaches. Although previous work has demonstrated limited methanol conversion to cell mass or products by *E. coli*, methanol utilization is not coupled to growth, thus not possible to evolve the strain for further methanol utilization. Here we altered pentose metabolism in *E. coli* to couple methanol uptake with growth. By deleting essential genes in the pentose phosphate pathway and expressing heterologous enzymes from the ribulose-monophosphate (RuMP) pathway, we constructed a strain that cannot grow on xylose or ribose minimal media unless methanol is utilized, creating a phenotype termed “synthetic methanol auxotrophy”. This strain allowed us to optimize expression of the RuMP enzymes and evolve for

faster methanol-dependent growth. Our best strains were able to utilize methanol for growth to an OD_{600} of 4.0 in 30 hrs with methanol and xylose co-assimilation at a molar ratio of about 1:1. The methanol auxotrophic strain was further engineered to produce ethanol or 1-butanol to final titers of 4.6 g/L and 2.0 g/L, respectively. ^{13}C tracing showed that 40% and 71% of ethanol and 1-butanol produced has labeled carbon derived from methanol, respectively. We further demonstrated the utility of this strain as a selection platform to significantly decrease required methanol concentration for growth. Lowering required methanol concentration for growth reduces the residual methanol substrate in the cell culture, which is beneficial for downstream processing. The "synthetic methanol auxotrophy" represents a platform for engineering methanol utilization.

4.2 Significance statement

Methanol utilization has become increasingly important, as natural gas production sharply increased in the past decade. Biological utilization of methanol has been limited to methylotrophs, which are relatively difficult to manipulate for industrial production. Here we engineered an *E. coli* strain to create a phenotype called "synthetic methanol auxotrophy". This strain does not grow on xylose or ribose, unless methanol is consumed. The coupling between methanol assimilation and growth allows the cell to evolve for better methanol utilization. We demonstrated that the strain consumes approximately equal molar of methanol and xylose, and can produce ethanol or 1-butanol. The synthetic methanol auxotrophy provides a unique approach for methanol conversion and opens new possibilities of further engineering towards synthetic methylotrophy.

4.3 Introduction

Methanol is an intermediate in methane utilization, and thus is potentially an abundant feedstock derived from natural gas or anaerobic digest. Methanol is highly reduced and can provide three "H_2" equivalents per carbon. As such, it is desirable to explore possibilities of utilizing methanol in microbial production of chemicals and fuel (James M Clomburg et al., 2017; Conrado and Gonzalez, 2014; Haynes and Gonzalez, 2014). While natural methylotrophs can utilize methanol, the genetic tools for engineering these organisms are not as mature as those for *E. coli* (Bennett et al., 2018; Zhang et al., 2017). Thus, it will be advantageous if a readily editable organism such as *E. coli* can be engineered to utilize methanol for production and growth.

There are at least three pathways that allow organisms to grow on methanol: the ribulose-monophosphate (RuMP) pathway, the xylulose monophosphate (XuMP) pathway, and the serine pathway (Zhang et al., 2017). These pathways all assume a cyclic configuration to assimilate methanol and generate an output while recycling intermediate metabolites. All these pathways assimilate methanol via first oxidation to formaldehyde, which must be quickly consumed by an acceptor metabolite, such as ribulose-5-phosphate (Ru5P) in the RuMP pathway. The RuMP pathway shares many enzymes with the pentose phosphate pathway (PPP), and is our choice for integrating with *E. coli* metabolism. The only three unique enzymes are methanol dehydrogenase (Mdh) which oxidizes methanol to formaldehyde, 3-hexulose-6-phosphate synthase (Hps), which ligates formaldehyde with Ru5P to form hexulose 6-phosphate (H6P), and 6-phospho-3-hexuloisomerase (Phi), which isomerizes H6P to fructose 6-phosphate (F6P).

There are several challenges in engineering methanol assimilation into *E. coli*. First, oxidation of methanol to formaldehyde requires the thermodynamically unfavorable NAD-linked reaction catalyzed by the NAD-dependent methanol dehydrogenase (MDH), pyrroloquinoline quinone (PQQ)-dependent MDH, or oxygen-dependent methanol oxidase. The latter two cannot recycle electrons easily (Whitaker et al., 2015; Zhang et al., 2017). Second, formaldehyde is extremely reactive and spontaneously reacts with proteins, causing nonspecific cell damage (Gonzalez et al., 2006). Once methanol is oxidized, the formaldehyde produced must be rapidly consumed by reacting with acceptor metabolite to prevent toxicity. As such, regeneration of the acceptor metabolite must be efficient. Third, since methanol is a non-native and somewhat toxic substrate for *E. coli*, modification of cell regulation might be required for the strains to adapt to methanol uptake.

Methanol incorporation to biomass has been demonstrated in *E. coli* (Bennett et al., 2017; Gonzalez et al., 2017; Jonas E.N. Müller et al., 2015; Whitaker et al., 2016), as well as *Saccharomyces cerevisiae* (Dai et al., 2017), *Corynebacterium glutamicum* (Leßmeier et al., 2015; Witthoff et al., 2015), and *Pseudomonas putida* (Koopman et al., 2009). For *E. coli*, overexpression of RuMP enzymes such as Mdh, Hps, and Phi for methanol assimilation has been widely explored (Bennett et al., 2017; Gonzalez et al., 2017; Jonas E.N. Müller et al., 2015; Price et al., 2016; Whitaker et al., 2016). Recently, several new strategies to improve methanol utilization had been reported (Bennett et al., 2017; Gonzalez et al., 2017). Phosphoglucose isomerase (Pgi) deficient *E. coli* was demonstrated with enhanced methanol con-utilization with glucose (Bennett et al., 2017). Deletion of leucine-responsive regulatory protein was shown to promote methanol incorporation to biomass when provided with yeast extract (Gonzalez et al.,

2017). However, none of the engineered strains mentioned required methanol to grow. Thus, adaptive evolution could not be applied to accelerate the progress in methanol assimilation.

Here, we designed a methanol assimilating *E. coli* strain that couples methanol uptake to growth with pentose co-substrate (Figure 4-1). The strain cannot grow on xylose or ribose minimal media unless methanol is being incorporated. The created phenotype is termed "synthetic methanol auxotrophy". This strain enables the use of evolutionary strategies for methanol metabolism.

4.4 Results

4.4.1 Design of synthetic methanol auxotrophy

Our design goal was to engineer a strain that cannot grow on a simple co-substrate unless methanol is assimilated (Figure 4-1). There should be no detectable growth on the co-substrate alone when methanol is absent. When considering possible co-substrates, we chose precursors of Ru5P to maximize the carbon flux for formaldehyde fixation. Among the possible candidates, D-ribose and D-xylose are both natural substrates for *E. coli* and require only a few enzymatic reactions to produce Ru5P. Theoretically, disrupting any reaction in the non-oxidative part of PPP would abolish the cell's ability to grow on ribose or xylose as a sole carbon source. We focused on Δ*rpe* (coding for ribulose-phosphate 3-epimerase) and Δ*rpiAB* (coding for ribose-5-phosphate isomerase A and B) mutants for constructing synthetic methanol auxotrophy. The Δ*rpe* and Δ*rpiAB* strains cannot grow on ribose and xylose minimal medium, respectively. In principle, the growth deficiency of the Δ*rpe* or Δ*rpiAB* strains can be rescued if the first three steps of the RuMP pathway catalyzed by Mdh, Hps and Phi were introduced, forming an

alternative route for F6P synthesis (Figure 4-1). In this strategy, we essentially convert pentose and methanol into a hexose equivalent.

Although transketolase (Tkt) and transaldolase (Tal) deletion mutants can theoretically be used to construct the methanol auxotrophy strain, there were drawbacks in using these strains. The Tal deficient strain was reported to grow on xylose as sole carbon source using a sedoheptulose-1,7-bisphosphate dependent pathway (Nakahigashi et al., 2009). The Tkt deficient strain cannot use xylose or ribose as sole carbon source, but it cannot synthesize aromatic amino acids (Zhao and Winkler, 1994) due to inability of producing erythrose 4-phosphate.

4.4.2 Development of synthetic methanol auxotroph using Δ*rpe*

We first used the IB405 (*Δrpe*) strain to develop synthetic methanol auxotrophy since it can grow on both glucose and ribose plus xylose (Figure 4-2A). An ideal candidate should be able to grow on glucose since it is an indication of growth phenotype when F6P is produced from methanol assimilation. Growth on ribose plus xylose confirmed the functionality of PPP except for the intended knock-out. Consistent with previous results in the literature (Long et al., 2016; Lyngstadaas et al., 1998), the growth rates in both conditions are significantly slower then that of a wild-type strain. It was suggested that altered level of pentose phosphates caused growth repression by changing the regulation of metabolic enzyme(s) (Lyngstadaas et al., 1998).

To construct the synthetic methanol auxotrophy strain, heterologous expression of Mdh, Hps and Phi is required. We initially designed a plasmid pCTI2 with various expression level of the three enzymes by using synthetic ribosomal binding sites (RBS) as described (Salis et al., 2010). We reasoned that Mdh has the lowest activity among the three enzymes, therefore

required higher expression level to match the other two enzymes. Therefore, the RBS of Mdh was designed to have highest predicted translation initiation rate among the three genes (Table 4-1). Although transformation of pCTI2 to IB405 resulted in methanol dependent growth, it took around 100 hrs to reach OD of 0.7 (Figure 4-2B). The result urged us to further optimize the strain. One of the main challenges in implementing a non-native pathway, such as methanol assimilation, is optimizing the expression of heterologous enzymes. Since a cell has limited resource for protein production, refining of protein expression levels might be required. In our case, Mdh expression needs to be sufficient to support growth. However, if the expression ratio of Mdh to Hps/Phi was too high, accumulation of formaldehyde will lead to cell toxicity. Here we used a plasmid-based system to quickly test various genetic constructs. Mdh, Hps, and Phi were constructed under a single operon, in which the protein expression level of each genes were modulate by alternating the RBS using the RBS Library Calculator described previously (Salis et al., 2010) (Figure 4-2C). The methanol auxotrophy strain itself can serve as a platform to select for the genetic constructs that render better methanol dependent growth.

After transformation of the plasmid library to the Δ*rpiAB* strain, our test showed that the isolated colonies demonstrated diverse expression level of Mdh, Hps, and Phi (Figure 4-8) and methanol dependent growth phenotype (Figure 4-2D). The result highlighted the substantial impact that enzyme expression could have on methanol-dependent growth. With the encouraging preliminary result, we further investigate the whole plasmid library to seek for the best strain we can obtain. The Δ*rpe* strain containing the plasmid library was grown in MOPS minimal medium with ribose and methanol for 48 hours before being passed into fresh medium. The fast growing variants in the library would theoretically be enriched during methanol-dependent growth. After

4 passages, individual colonies from the final culture were isolated on a MOPS agar plate with methanol and ribose for further growth test. The colony with the fastest growth rate was renamed as IB958 and its plasmid named pIB208. Notably, the predicted translation initiation rate of Hps is higher than Mdh on plasmid pIB208 (Table 4-1). The result signified the importance of coordination between formaldehyde production and assimilation for better growth. With optimized ribose and methanol concentration, the IB958 strain was able to grow to OD_{600} of 4.0 in 29 hours with a specific growth rate of 0.18 (h^{-1}) (Figure 4-2E). However, the Δ*rpe* (IB958) strain overall consumed 38 mM of ribose but only 21 mM of methanol. Theoretically, methanol and pentose consumption should be equimolar (Figure 4-1B). The result indicated an alternative metabolic pathway in the Δ*rpe* methanol auxotrophy might exist that enables ribose metabolism without methanol. Indeed, we observed that the Δ*rpe* strain was able to grow solely on ribose after 29 hours (Figure 4-2E). The suppressor mutant was not found in earlier experiments possibly due to lower ribose concentration.

Previously, a bypass pathway involved deoxyribonucleosides that produced G3P and acetaldehyde from R5P was predicted (Nakahigashi et al., 2009). However, elimination of key genes *deoB* or *deoC* did not affect the growth on ribose (data not shown). We also examined two genes, *sgcE* and *alsE*, that might encode proteins carrying Rpe function (Kim et al., 1997; Nakahigashi et al., 2009) Although individual knock-outs of these two genes did not prevent ribose growth, extended lag phase or decreased probability of developing loophole indicated the contribution of these gene to the loophole pathway (Figure 4-9). Intriguingly, combination of Δ*sgcE* and Δ*alsE* seemed to enhance the loophole growth (Figure 4-9). Further characterization will be required to uncover the underlying pathway(s) of the ribose growing phenotype.

4.4.3 Evolution of Δ*rpiAB* strain allows for a more stringent synthetic methanol auxotrophy strain

The loophole phenotype of the Δ*rpe* (IB958) strain urged us to explore possibility of developing synthetic methanol auxotrophy in the Δ*rpiAB* strain. However, the Δ*rpiAB* strain had no growth in both glucose or ribose plus xylose during our test (Figure 4-2A), implying a fundamental deficiency in pentose utilization, glycolysis, or other pathways. Intriguingly, it has been reported that *rpiAB* mutant is possible to grow on ribose plus xylose (Sørensen and Hove-Jensen, 1996). Therefore, we hypothesized that unexpected genome mutation during strain construction might be responsible and can be resolved by adaptive evolution.

The initial *ΔrpiAB* (IB730) strain was grown in Terrific broth (TB) medium with ribose and xylose, followed by passages (0.1% inoculation) of the culture in a MOPS based medium supplemented with low levels of amino acids, vitamins, and nucleotides (Hi-Def Azure, HDA media). After the 11th passage, the supplements in MOPS medium were eliminated and the culture were evolved for another 9 passages. An isolate from the 20th passage (CFC 65) was able to reach an OD_{600} of 1.7 in 24 hours with xylose and ribose (Figure 4-3A). CFC65 was then transformed with the Mdh-Hps-Phi plasmid pIB208 to create strain CFC68, as we hypothesize that the same optimized methanol assimilation plasmid used for *Δrpe* strain would be compatible with the *ΔrpiAB* strain. However, initial attempts to demonstrate methanol dependent growth with xylose proved unsuccessful. Thus we once again gradually adapt the CFC68 for methanol dependent growth. Similar to the previous workflow, we grew the strain initially in the HDA medium with methanol and xylose and gradually eliminate the supplements. After another 35

passages, the evolved strain (CFC133) was finally able to grow on methanol and xylose as sole carbon sources without any amino acid supplements (Figure 4-3B). Importantly, no growth was observed when methanol was omitted during the course of evolution and characterization (Figure 4-3).

Further characterization of CFC133 showed a saturation OD of 4.0 with specific growth rate of 0.19 (h^{-1}) (Figure 4-3C). The Δ*rpi* (CFC133) strain overall consumed 38 mM of xylose and 43 mM of methanol (Figure 4-3C), which is very close to the theoretical equimolar consumption. The results implied that most of the methanol consumed was assimilated, since xylose alone cannot be utilized. The exceeding amount of methanol may be attributed to methanol dissimilation through formaldehyde detoxification pathways (Gonzalez et al., 2006).

The loophole issues in the Δ*rpe* strain also urged us to carry out an extensive test of the Δ*rpiAB* strain. Fortunately, growth of Δ*rpiAB* strain on xylose only was never observed in multiple individual experiments of 30 days or longer cultivation (data not shown). We hypothesize that Δ*rpiAB* is more robust because it utilizes xylose, which is less involved in *E. coli* metabolism. Xylose is incorporated to central metabolism by converting to X5P by *xylA* and *xylB*. X5P is only being utilized in the pentose phosphate pathway, hence there is little chance to develop loopholes. On the other hand, R5P derived from ribose is involved in the pivotal 5-phospho-α-D-ribose 1-diphosphate (PRPP) biosynthesis (Hove-Jensen et al., 2017, 2003), thus providing E. coli more possibilities to bypass the requirement of assimilating methanol.

To our knowledge, this CFC133 is the first strain that demonstrates growth fully dependent on methanol in minimal media without supplementing any rich nutrients such as LB or yeast extract.

4.4.4 Conversion of methanol to ethanol and 1-butanol

To this point, we have established two designs of methanol auxotrophy strains. The Δ*rpiAB* strain is more stringent in substrate utilization. It has the advantage to assimilate xylose together with methanol. Xylose is one of the most abundant sugars in cellulosic biomass, co-utilization with methanol can potentially "upgrade" the production by providing extra carbon and reducing power. The Δ*rpe* strain was found to have a loophole to enable growth solely using ribose when cultured for a longer time frame. Although such deficiency eventually prevents the Δ*rpe* strain from being a good platform for metabolic evolution of methanol utilization, certain level of methanol can still be assimilated during growth on methanol plus ribose (Figure 4-2E).

To demonstrate the utility of methanol auxotroph strain for methanol conversion to chemical products, we aimed to produce higher alcohols such as ethanol and 1-butanol. These are desired products since they are more energy dense compared to methanol and can be used as chemical precursors and fuels. The ethanol production pathway was constructed by plasmid-based expression of pyruvate decarboxylase (Pdc) and alcohol dehydrogenase (AdhB) from *Zymomonas* (Figure 4-4A) as described previously (Ohta et al., 1991). Here we used ^{13}C-methanol to trace the carbon derived from methanol was used with either ribose or xylose. After 3 hours of fermentation, the Δ*rpiAB* strain yielded 4.6 g/L (100 mM) of ethanol (Figure 4-4B) from methanol and xylose. The control strain (wild-type BL21(DE3) with the same plasmids) only showed 2.8 g/L (61mM) of ethanol produced, representing a 64% of titer increase when the synthetic methanol auxotrophy was implemented for methanol conversion. The Δ*rpe* strain ethanol production using methanol and ribose showed a similar trend. The titer was enhanced by

37% when comparing the auxotrophy strain (90 mM, 4.1 g/L) to the control strain (66 mM, 3.0 g/L) (Figure 4-4D).

Both ethanol production using sCT745 and sCT760 showed significant M+1 labeling product in the mass spectra (Figure 4-4C and E). Increment of labeling product (either M+1 or M+2) was observed when comparing the BL21 strain to sCT745 (1.9% to 42.7%) or sCT760 (6% to 31.1%) auxotrophy strain (Figure 4-4F). The result demonstrated high level of methanol incorporation to the product. Notably, the theoretical product labeling should be 50% if pyruvate was only synthesized from ^{13}C methanol and non-labeled xylose through EMP glycolysis ((Figure 4-4A). The lower labeling percentage in the Δ*rpiAB* auxotrophy strain is expected due to extra non-labeled G3P generated during carbon rearrangement in the PPP, while in the Δ*rpe* auxotrophy strain it could be attributed to the unknown loophole pathway that bypasses incorporation of methanol.

Methanol consumption was also enhanced by 11-fold and 5-fold for the Δ*rpiAB* and Δ*rpe* strain (Figure 4-4G) when compared to BL21 strain, respectively. The extra carbon from methanol assimilation (70.5 mM for Δ*rpiAB*, 38.2 mM for Δ*rpe*) accounts for 89% and 78% of the increased ethanol titer in the Δ*rpiAB* and Δ*rpe* strains (39.5 mM for Δ*rpiAB*, 24.4 mM for Δ*rpe*), respectively. It implied that the titer improvement is not only due to the utilization of methanol as a source of carbon, but possibly also a source of reducing power to enhance overall production of reduced product. The results indicated that the synthetic methanol auxotrophy engineering strategy effectively increase production titer by enabling more efficient methanol utilization.

The encouraging result of ethanol production urged us to expand the production to 1-butanol. Heterologous genes for 1-butanol production (*atoB*, *hbd*, *crt*, *ter*, and *pduP*), as described previously (Lan et al., 2013; Shen et al., 2011), was expressed using plasmid-based construct. With the Δ*rpiAB* auxotrophy strain, we demonstrated 150 mM (2.0 g/L) of 1-butanol when 87 mM of methanol and 100 mM of xylose was consumed (Figure 4-4H). Since PduP also has activity towards acetyl-CoA, a significant amount (1.5 g/L) of ethanol was produced as byproduct. Similar to the results in ethanol production, significant M+1 and M+2 mass isotopomer of 1-butanol was observed in the mass spectra (Figure 4-4I). Close to the expectation, M+1 mass isotopomer accounts for 52% of the product 1-butanol while M+2 molecules took up 20%.

In both cases of ethanol and 1-butanol production using the Δ*rpiAB* strain, equimolar consumption of methanol and xylose was observed. The substrate utilization pattern was consistent with that of methanol-dependent growth (Figure 4-3C). It again served as an evidence to show that most of the methanol consumed was assimilated.

4.4.5 Engineering Δ*rpiAB* for lower methanol requirement

One of the drawbacks that we noticed from the growth of current methanol auxotrophy strain was the high amount of methanol required. The CFC133 strain grows fast with 250 mM of methanol, but only consume about 40 mM. The unused methanol increases the cost of substrate and downstream separation for industrial applications. Therefore, it would be ideal to further improve the auxotrophy strain to utilize lower methanol concentration.

With the success in enriching plasmids that renders higher growth performance in the Δ*rpe* strain, we reasoned that the same strategy can be applied for the Δ*rpiAB* strain. We aimed to further engineer the CFC133 Δ*rpiAB* strain to grow on 50 mM of methanol since the amount is close to the total methanol consumption when higher (250 mM) methanol was used (Figure 4-3C) and also represents a limit condition of which the current strain cannot grow (Figure 4-5B). A random mutagenesis library was created that covered the whole Mdh, Hps, and Phi operon (Figure 4-5A) except for the coding region of Phi. The isomerase enzyme was left out since it already has high activity. We hypothesized that such a large library would be necessary since a dramatic growth phenotype change we are seeking might require synergistic altered enzyme kinetics, expression, etc.

The library was transformed to Δ*rpiAB* strain sCT497 (CFC133 cured plasmid pIB208). After 17 passages of growth with xylose and 50 mM methanol, a strain that can grow on this low methanol concentration was obtained and its plasmid pCT239 was isolated. The plasmid pCT239 was considered the main contribution for the lower-methanol (50 mM) growth phenotype since the growth phenotype was transferable when transforming pCT239 back to the original background strain sCT497. The engineered plasmid enabled methanol dependent growth to a saturation OD of 4.48 with specific growth rate of 0.88 (h^{-1}), while the parental plasmid pIB208 did not result in any growth under 50 mM methanol (Figure 4-5B). Although the strain showed a slower growth rate when compared to CFC133 with higher methanol concentration, it still represented a substantial progress in engineering desired growth phenotype. Further improvement on growth rate can possibly be achieved by adaptive evolution as demonstrated in earlier results (Figure 4-3).

Plasmid pCT239 was identified with mutations on the promoter and the coding region of Mdh and Hps (Figure 4-6A). Crude extract assay shows that Mdh, Hps, and Phi activities in the strain with pCT239 are all higher than the strain with pIB208 (Figure 4-6C). However, the mutation on promoter did not showed significant effect on protein expression level with or without inducer when using GFP as a readout (Figure 4-6B). Characterization of kinetic parameters of Mdh and Hps showed that the mutations did not promote enzyme activity or affinity (Table 4-2). Further experiments such as investigation on transcription level or protein stability will be required to explain the phenomena.

4.5 Discussion

Methanol utilization is challenging since the substrate is not natively accepted by *E. coli*. Existing methanol assimilation pathways involve highly toxic formaldehyde as intermediate (James M Clomburg et al., 2017). Overexpressing RuMP enzymes proved to have limited methanol assimilation and cannot support *E. coli* to grow on methanol alone (Jonas E.N. Müller et al., 2015; Whitaker et al., 2016). Indeed, it is an intriguing question why *E. coli* cannot grow on methanol as sole carbon source after expressing all the essential enzymes in the RuMP pathway. In addition to kinetically unfavorable enzymes like NAD-dependent Mdh, the underlying hurdles might be related to the fundamental difference of cell metabolism between *E. coli* and methanotrophs. Intensive work to systematically compare the physiology of these organisms might be required to guide further engineering strategies.

In this paper, we implement a novel strategy called “synthetic methanol auxotrophy” that demonstrated an *E. coli* strain that depends on methanol to grow for the first time. The Δ*rpe*

strain allowed an easier case for developing the synthetic methanol auxotroph, but the resulting strain showed a loophole that prevented it from further utilization as a platform for growth based selection. On the other hand, the Δ*rpiAB* strain took more effort to reach methanol auxotrophy, but gave a more stringent methanol-dependent growth. During adaptive evolution in ribose and xylose, the mutation on *tkt* might play a key role for the growth phenotype change. After knocking out *rpiAB*, three amino acids of the *tktA* gene were found truncated, starting from position 606 (Figure 4-10). As evolution process continues, we found out the Δ*rpiAB* strain that successfully grew on ribose and xylose contained TktA with a valine residue recovered among the three deleted amino acids and the new TktA demonstrated higher activity in crude extract (Figure 4-10). This may have explained the poor initial growth of Δ*rpiAB* strain on ribose and xylose, as Tkt is required to convert the substrates into F6P for growth. Despite the identification of the tktA mutation, there was still no apparent clue on how Δ*rpiAB* strain acquired the ability to grown on methanol and xylose. Thus, we stretched further to obtain the whole genome sequence of the evolved variants (Table 4-3). The most significant change in the genome of CFC133 was two large genome deletions. One of the two deleted regions included the entire *frm* operon, which is responsible for formaldehyde detoxification (Gonzalez et al., 2006). Deletion of formaldehyde detoxification had been shown to assist methanol assimilation in previous report (Jonas E.N. Müller et al., 2015). Indeed, the growth phenotype was abolished when the deleted region was restored (Figure 4-7). Another mutation that contributed significantly to the methanol dependent growth phenotype was *cyaA*. Our result showed that when the mutation on the *cyaA* gene was reverted to wild-type sequence, the phenotype of methanol dependent growth cannot be observed (Figure 4-7). Since *cyaA* encodes an enzyme that catalyze the production of important

regulator molecule cyclic AMP, further experiments to investigate the regulation target that benefits methanol assimilation will be required to decipher the meaning of *cyaA* mutation.

There are several advantages of this strain. First, the strain enabled metabolic evolution approach to increase methanol utilization. Due to the complexity of this topic, metabolic evolution allowed us to bypass incremental rational metabolic pathway design. Indeed, the growth-based selection has been successfully applied in many other cases of metabolic flux enhancement (Baek et al., 2016; Jantama et al., 2008; Jiang et al., 2013; Yomano et al., 2008; Zhu et al., 2014). And the outcome of the evolution sometimes attributed to counter-intuitive results that might not be easily predicted by rational design (Zhang et al., 2009). Second, the methanol auxotroph strain can serve as a platform to screen for a methanol assimilation module (e.g. Mdh, Hps, Phi) with higher performance (Figure 4-2, Figure 4-5). The growth related readout provides more direct evaluation of enzyme functionality for methanol assimilation than *in vitro* assays. The methanol auxotroph strain can also be eventually engineer to methanol only growth or production. Since the Δ*rpiAB* strain was forced to evolve for higher activity of PPP to produce nucleotides precursor (Figure 4-1), a complete RuMP cycle can be achieved by restoration of Rpi function in the evolved Δ*rpiAB* auxotrophy strain.

The methanol auxotroph strain has been a significant step toward methanol utilization. We demonstrated the high level of methanol incorporation to fermentation product and significantly enhanced methanol consumption rate. In addition, the strain can be used to upgrade production titer when using xylose as fermentation substrate, which is one of the most abundant sugars in nature. The novel design set forth many new possibilities in methanol utilization and engineering synthetic methylotrophy.

4.6 Materials and methods

Chemicals and Reagents

All reagents were purchased from Sigma-Aldrich (St. Louis, Missouri, USA) unless otherwise stated. ^{13}C methanol was obtained from Cambridge Isotope Laboratories (Tewksbury, Massachusetts, USA). The following enzymes were also purchased from Sigma-Aldrich: hexokinase (*S. cerevisiae*), phosphoglucose isomerase (*S. cerevisiae*), glucose-6-phosphate dehydrogenase (*S. cerevisiae*).

Strains and growth conditions

The Δ*rpiAB* and Δ*rpe* strains described in this research was constructed based on *E. coli* BL21(DE3) strain using P1 transduction (Thomason et al., 2007) with Keio collection (Baba et al., 2006). All of the cloning work was done in *E. coli* XL-1 blue. See Table 4-4 for a complete list of strains used in this study. All bacterial culture was kept at 37 °C, 250 rpm orbital shaker unless otherwise stated. MOPS minimal medium is composed of 40 mM MOPS, 4 mM tricine, 0.01 mM FeSO4, 9.5 mM NH_4Cl, 0.276 mM K_2SO_4, 0.5 μM $CaCl_2$, 0.525 mM $MgCl_2$, 50 mM NaCl, 2.92E-7 mM $(NH_4)_2MoO_4$, 4.0E-5 mM H_3BO_3, 3.02E-6 mM $CoCl_2$, 9.62E-7 mM $CuSO_4$, 8.08E-6 mM $MnCl_2$, 9.74E-7 mM ZnSO4, and 1.32 mM K_2PO_4. For all growth tests in MOPS minimal medium, seed cultures for inoculation were grown in Terrific Broth (TB) medium for 16 hrs. 0.1 mM IPTG for induction of protein expression was added when necessary. For antibiotics, final concentration of 100 mg/L carbenicillin or 30 mg/L kanamycin were used when appropriate. Notably, we experience huge variation of lag phase (1 – 3 days) when passing the Δ*rpiAB* auxotrophy strain directly from rich medium culture to minimal medium for growth on methanol

and xylose. This could be a result of dramatic change of growth condition and the stress caused by expressing the methanol assimilation enzyme in high level. Therefore, an intermediate state that buffers the transition was implemented for characterization of methanol-dependent growth and substrate consumption of strains IB958 and CFC133. The seed cultures were washed twice with equal volume of MOPS minimal medium before inoculation (1%) to 3 ml MOPS minimal medium containing 50 mM ribose/xylose and 250 mM methanol with 0.05 % casamino acids in Vacutainer glass tubes from BD (Franklin Lakes, NJ, USA). The casamino acids were found to shorten the lag phase when the cells are transitioned from growth in rich medium to minimal medium and enabled repeatable growth for the medium transition. The resulting cultures with casamino acids typically reaches OD_{600} ~1.5 in 16 hrs. For the growth and substrate consumption characterization, the "transition" cultures were then washed twice with MOPS medium and inoculated into 3 mL of identical growth medium but without casamino acids to initial OD of 0.1 in Vacutainer glass tubes from BD (Franklin Lakes, NJ, USA). During growth characterization experiment, 300 μL of culture samples were then taken at each desired time point for methanol, xylose, or ribose quantification using HPLC. OD_{600} was monitored by Spectronic 200 (Thermo Scientific) with cultures in BD vacutainer glass tubes (#366430, BD, NJ, USA).

Ethanol and 1-butanol Production

Engineered strains were cultured in TB medium with appropriate antibiotics for 4 h before adding 0.1 mM IPTG. The strains were grown for another 12 to 18 h. 500 ul of the cultures were inoculated into 120 mL Hi-Def Azure (HDA) medium (Teknova, CA, USA) supplemented with 0.1 mM IPTG, 50 mM ribose/xylose, and 250 mM methanol until OD was about 1 (approximately 24 to 40 h). Appropriate amount of cells were pelleted and washed twice with 30

mL of MOPS minimal medium. The washed pellets were resuspended in 850 ul of MOPS medium, 100 ul of 2M ribose/xylose, and 50 ul of 10 M ^{13}C methanol to make1 ml concentrated cultures of OD 100. Samples were taken at desired time points and supernatants were isolated for analysis. Ethanol and 1-butanol were measured by GCMS, ^{13}C-labeling was determined by measured mass isotopomer with correction for nature isotope abundance as described (Fernandez et al., 1996). Methanol, xylose, ribose and organic acids byproducts were quantified by HPLC.

Analytical methods

An Agilent 1100 HPLC was used for measurement of organic acids, sugars (ribose and xylose), and methanol using an Aminex HPX-87H column (Bio-Rad). 30 mM of sulfuric acid was used as mobile phase at a flow rate of 0.6 mL/min and run for 30 minutes. A 6890/5973 GC-MS (Agilent Technologies) was used for quantification of ethanol and 1-butanol. An initial temperature of 40 °C was held for 2 mins, before ramping at 10°C/min to 60 °C followed by ramping at 100°C/min to 240 °C with a final two minute hold. We used a DB-FFAP column (Agilent Technologies 123-3232, 0.32 mm x 30 m x 0.25 μm), with constant pressure of 0.487 bar.

Δ*rpiAB* directed evolution for substrate adaption

All cell strains were passed to the next generation when OD_{600} exceeded 1.2, and inoculated initially at 0.05. The unevolved Δ*rpiAB* strain CFC64 was first inoculated in Terrific Broth (TB Sigma) with 7 mM ribose and 7 mM xylose. Cells grew to saturation in two days and were then passed to two different media, Hi Def azure medium (HDA, Teknova), and MOPS EZ Rich Defined Medium (Teknova), both with 100 mM ribose and 100 mM xylose. From Generation 2 to Generation 10, cells were passed from HDA to HAD. Cultures were also passed to MOPS

media with same amount of ribose and xylose to test for growth (result presented in Figure 4-3). Since Generation 5, ribose and xylose concentrations were reduced to 40 mM. Starting from Generation 11, cells were passed from MOPS media to MOPS media. At Generation 20, a single colony strain was isolated and renamed as CFC65. The plasmid pIB208 was then transformed, and the strain was renamed as CFC68. Colonies were picked and grown in TB with 7 mM ribose and 7 mM xylose. The strain was then inocluated into MOPS minimal medium with 200 mM methanol, 20 mM xylose, 0.1 mM IPTG, 1x of MEM amino acid (Sigma). Cells were also grown without MEM amino acid as a growth control. MEM amino acid was reduced to 0.5x, 0.25x, 0.125x, 0x at Generation 30, 32, 37, 45 subsequently.

Plasmid construction

Plasmids and primers used in the current research were listed in Table 4-5. DNA fragments for plasmid construction were generated by PCR using Phire Hot Start II DNA polymerase (Thermo Scientific). All plasmids were assembled by Gibson Assembly Master Mix (New England Biolabs) as described by manufacturer's protocol.

Genome sequencing

Whole genome sequencing of strain CFC65 and CFC133 was performed by GENEWIZ (South Plainfield, NJ, USA) using Illumina MiSeq platform.

Enzyme assay

Key enzymes in the pentose phosphate pathway (Tkt, Tal, Rpe, Rpi) were purified from overexpressing strains. Cells were inoculated in 3 mL LB from frozen glycerol stock and grown overnight at 37 °C. The following day, 200 mL LB was inoculated with 1% of overnight culture and grown at 37 °C until optical density was between 0.4 and 0.6, at which a final concentration

of 0.1mM IPTG was added. The culture was grown at room temperature overnight, harvested by centrifuge and broken by sonification. After centrifuging for 1 hour at 18000 rpm and 4 °C, protein solution was vacuum filtered before performing IMAC protein purification with Profinia (Biorad). Final concentrations of purified enzymes are: Tkt at 2.0 μg/μL, Tal at 13.0 μg/μL, Rpe at 5.0 μg/μL, and Rpi at 28.7 μg/μL. Commercial phosphoglucose isomerase and glucose-6-phosphate dehydrogenase were obtained from Sigma-Aldrich. Crude extracts from BL21, IB730, CFC65, CFC68, and CFC133 strains were collected. Cells were inoculated in 5 mL LB from frozen glycerol stock and grown overnight at 37 °C with 5000x of 0.5 M IPTG. The following day, cells were harvested by centrifuge and cell pellets were re-suspended in Diglycine Cell Lysis Buffer for sonication. After centrifuging for 30 min at 15000 rpm at 4 °C, solution supernatant was separated and normalized to a concentration of 3.2 μg/μL. Assays were carried out in 100 mM phosphate buffer (pH 7.0) with 20 mM NADP+, 100 mM thiamine pyrophosphate, and 100 mM MgCl2. Tkt, Tal, and Rpe enzyme activity were tested by addition of the substrate, ribose-5-phosphate.

4.7 Acknowledgements

This work was supported by the REMOTE program of the Advanced Research Projects Agency-Energy (ARPAE-E) (Award DE-AR0000430). This material was based upon research performed in a renovated collaborator by the National Science Foundation under Grant No. 0963183, which is an award funded under the American Recovery and Reinvestment Act of 2009 (ARRA).

4.8 Figures

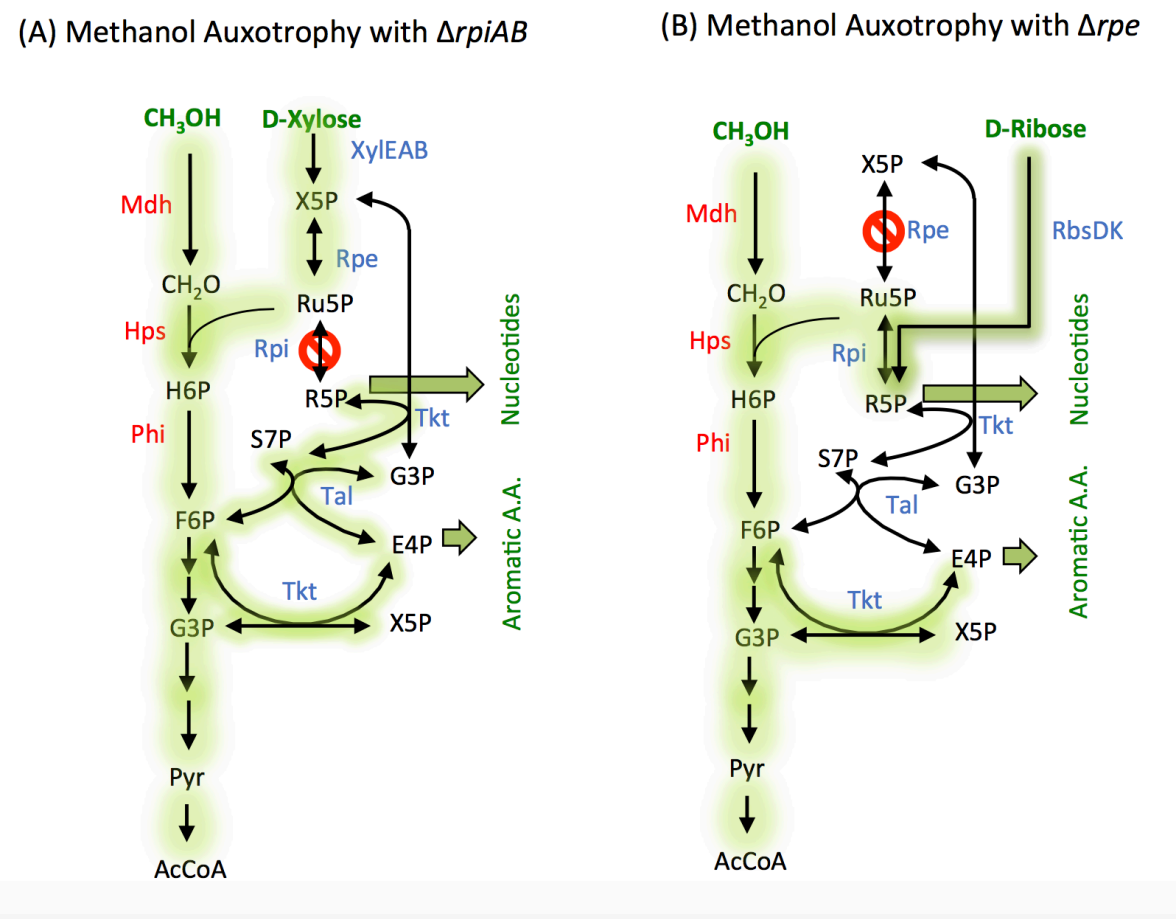

Figure 4-1. Schematic diagram of synthetic methanol auxotrophy with (A) Δ*rpiAB* or (B) Δ*rpe* strain.

The arrows with a slash denotes eliminated reaction. XylE, D-xylose/proton symporter; XylA, xylose isomerase; XylB, xylulokinase; RbsD, D-ribose pyranase; RbsK, ribokinase; Rpe, ribulose-phosphate 3-epimerase; Rpi, ribose-5-phosphate isomerase; Tkt, transketolase; Tal, transaldolase; Mdh, methanol dehydrogenase; Hps, 3-hexulose-6-phosphate synthase; Phi, phosphohexuloisomerase. X5P, xylulose 5-phosphate; R5P, ribose 5-phosphate; Ru5P, ribulose 5-phosphate; S7P, sedoheptulose 7-phosphate; G3P, glyceraldehyde 3-phosphate; E4P, erythrose 4-phosphate; F6P, fructose 6-phosphate; H6P, hexulose 6-phosphate; PEP, phosphoenolpyruvate; Pyr, pyruvate; AcCoA, acetyl-CoA; Cit, citric acid; α-KG, α-ketoglutaric acid; Suc, succinate; OAA, oxaloacetate. Chang-Ting Chen prepared the figure.

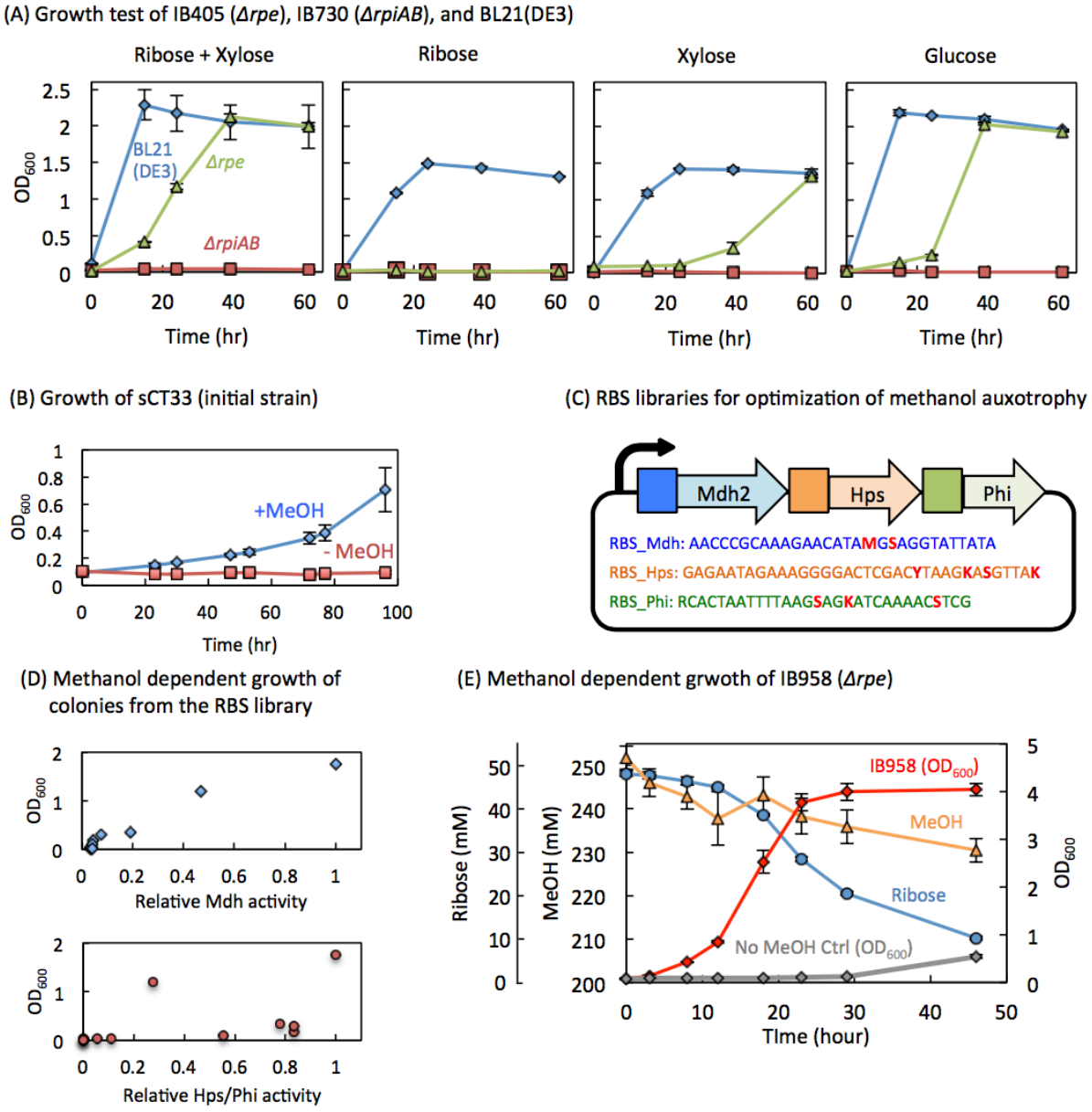

Figure 4-2. Construction and optimization of methanol auxotrophy in IB405 (BL21(DE3) *Δrpe)*.

(A) Growth phenotype of IB730 (*ΔrpiAB)* and IB405(*Δrpe*) was compared to the parental strain BL21(DE3) with 7 mM of ribose, xylose, glucose, or ribose plus xylose (7 mM each). (B) IB405 was transformed with pCTI2 (strain sCT33) for initial trial of methanol dependent growth. (C) RBS libraries of Mdh, Hps, and Phi for further optimization of methanol assimilation. Each RBS contains 16 diverse expression levels across four orders of magnitude. Degenerate bases: M = A,

C; S = C, G; Y = C, T; K = G, T. The RBS library was transformed to IB405 from where (D) 11 colonies were randomly isolated for characterization of methanol dependent growth and Mdh, Hps/Phi activity. OD_{600} was recorded after 48 hrs. (E) Characterization of strain IB958 selected from the library. After transformation of RBS library to strain IB405, 4 passages of methanol dependent growth enrichment (grow for 48 hrs before passing) were carried out. The fastest growing strain IB958 was identified by isolating single colonies from the resulting culture on agar (1.5%) plate with MOPS minimal medium plus 7 mM ribose and 200 mM methanol, followed by repeating liquid medium growth to select for the fastest growing variant. Strains were grown in MOPS minimal medium supplemented 250 mM methanol and 50 mM ribose (growth characterization of sCT33 and IB958) or 200 mM methanol and 7 mM ribose (all other experiments) at initial OD = 0.05 – 0.1. Cultures were kept at 37 °C, 250 rpm orbital shaker with 0.1 mM IPTG induction. Error bars represents the standard deviation (n = 3). Chang-Ting Chen prepared the figure and conducted all the experiments except for the data shown in panel (D), which is done by Dr. Igor W. Bogorad.

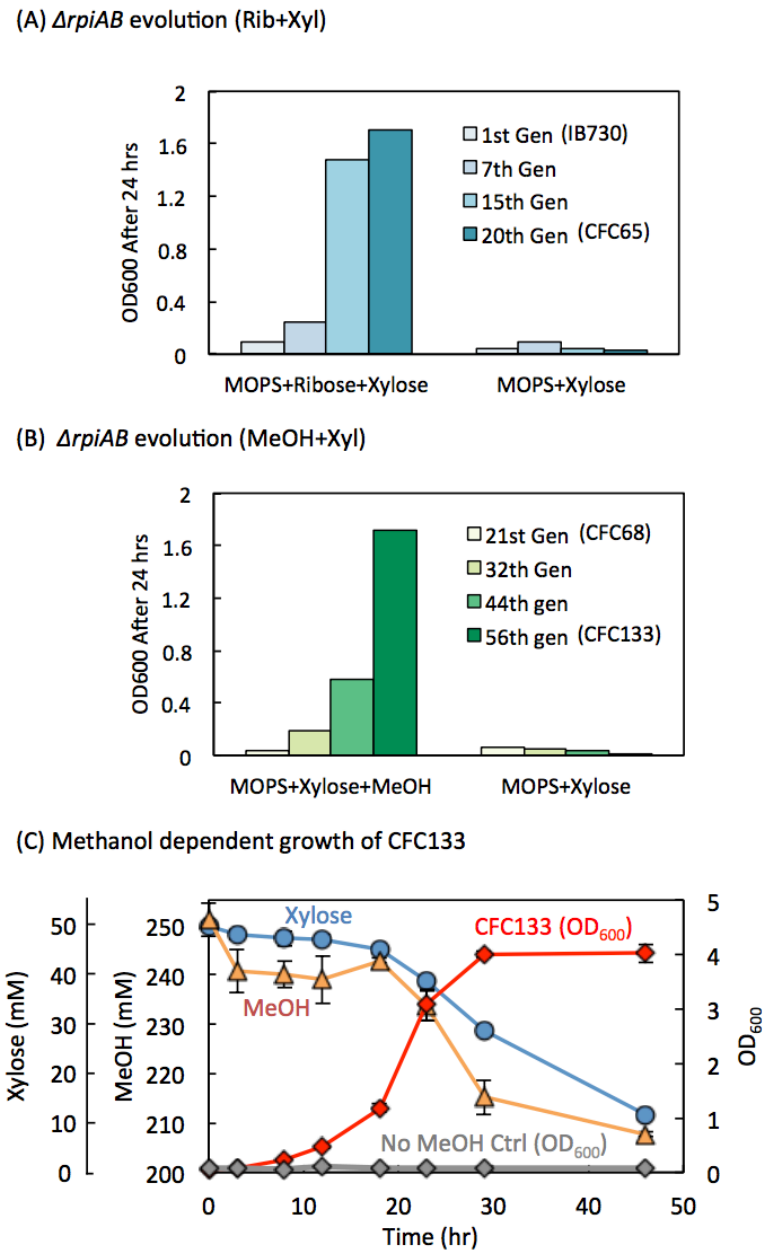

Figure 4-3. Evolution of IB730 (*ΔrpiAB*) strain and characterization of methanol dependent growth of evolved strain CFC133.

(A) Adaptive evolution of the initial IB730 strain for growth with ribose and xylose. The initial *ΔrpiAB* (IB730) strain was grown in Terrific broth (TB) medium with 7 mM each of ribose and xylose, followed by passages (0.1% inoculation) of the culture in the Hi-Def Azure media (HDA media, a MOPS based medium supplemented with low levels of amino acids, vitamins, and

nucleotides). After the 11th passage, the HDA media was replaced by MOPS minimal medium and the culture was evolved for another 9 passages before strain CFC65 was isolated from the 20^{th} passage. (B) Adaptive evolution for methanol dependent growth with xylose. CFC65 was transformed with plasmid pIB208 for overexpression of Mdh, Hps, and Phi. Similar to the previous workflow, the CFC68 strain was grown initially in the HDA media with 200 mM methanol and 7mM D-xylose before switching to MOPS minimal medium. After 35 passages, the evolved strain CFC133 was finally able to grow on methanol and xylose as sole carbon sources without any amino acid supplements. (C) Characterization of methanol dependent growth and substrate consumption of CFC133 in MOPS minimal medium supplemented with 50 mM xylose and 250 mM methanol. Error bars represents the standard deviation (n = 3). Freddy Yu-Hsiao Chen conducted the experiment for Figure (A) and (B) and prepared these two figures. Chang-Ting Chen conducted experiment shown in Figure (C) and prepared the figure.

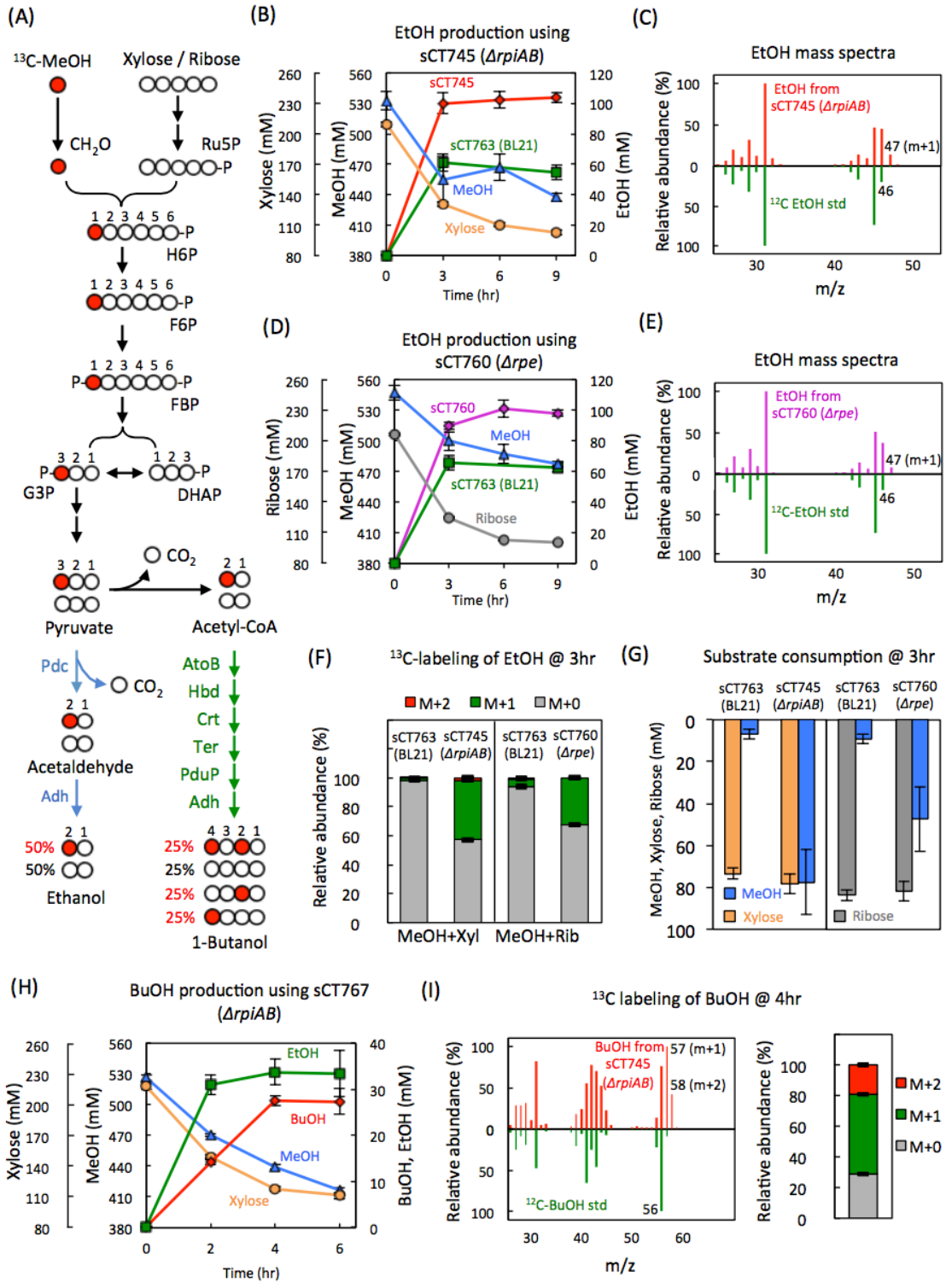

Figure 4-4. Ethanol and 1-butanol production using methanol auxotrophy strains.

For all production experiments, strains were grown in HDA medium for ~24 hrs until OD_{600} reaches 2. Cells were then washed twice with MOPS minimal medium before being concentrated to OD_{600} ~100 in the same medium. The concentrated cells were kept in BD Vacutainer glass tube with stoppers to prevent methanol evaporation. 550 mM methanol and 200 mM ribose or xylose (final concentration) were added to start the production. Ethanol production strains sCT745 (*ΔrpiAB*), sCT760 (*Δrpe*), and sCT763(BL21(DE3)) carried pIB208 (Mdh, Hps, Phi) and pTW244 (Pdc, AdhB). 1-Butanol production strain sCT767 (*ΔrpiAB*) carried pIB208 and pTW242 (AtoB, Crt, Hbd, Ter, PduP). (A) Carbon labeling of ethanol and 1-butanol derived from ^{13}C-methanol with co-utilization of xylose or ribose in the methanol auxotorphy strains. (B) Ethanol production of sCT745 (*ΔrpiAB*) and sCT763(BL21(DE3)) using methanol and xylose. (C) Mass spectra of ethanol produced by sCT745 (3 hr sample). (D) Ethanol production of sCT760 (*Δrpe*) and sCT763(BL21(DE3)) using methanol and ribose. (E) Mass spectra of ethanol produced by sCT760 (3 hr sample). (F) Mass isotopomer abundance of ethanol derived from ^{13}C methanol (3 hr samlpe) (G) Methanol and xylose or ribose consumption during ethanol production (H) 1-Butanol production of sCT767 (*ΔrpiAB*) using methanol and xylose. Ethanol was a primary byproduct due to promiscuity of PduP to convert acetyl-CoA to acetaldehyde. (I) Mass spectra and mass isotopomer abundance of 1-butanol produced by sCT767 (4 hr sample). Relative abundance of mass isotopomers were calculated as described before (Fernandez et al., 1996). All spectra were normalized to the most abundant internal peak. Error bars represents the standard deviation (n = 3). Chang-Ting Chen prepared conducted the experiment and prepared the figure.

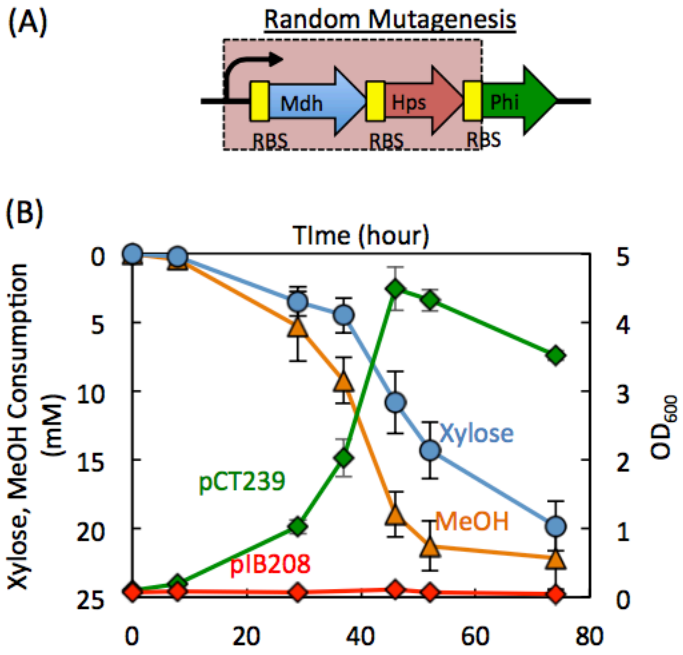

Figure 4-5 Engineering synthetic methanol auxotrophy strain that grows on lower methanol concentration.

(A) Random mutagenesis library was created and transformed to the *ΔrpiAB* strain CFC133 for plasmid enrichment under 50 mM methanol. The target mutagenesis area (dashed rectangular) included promoter, coding sequences of Mdh and Hps, and RBS of Mdh, Hps, Phi. A strain carrying plasmid pCT239 that allows for growth under 50 mM methanol was isolated after 17 passages. (B) Plasmid pCT239 was purified and transformed to *ΔrpiAB* strain CFC133 for characterization of methanol dependent growth under 50 mM methanol. The parental plasmid pIB208 did not enable any growth in the CFC133 strain. Error bars represents the standard deviation (n = 3). Chang-Ting Chen prepared conducted the experiment and prepared the figure.

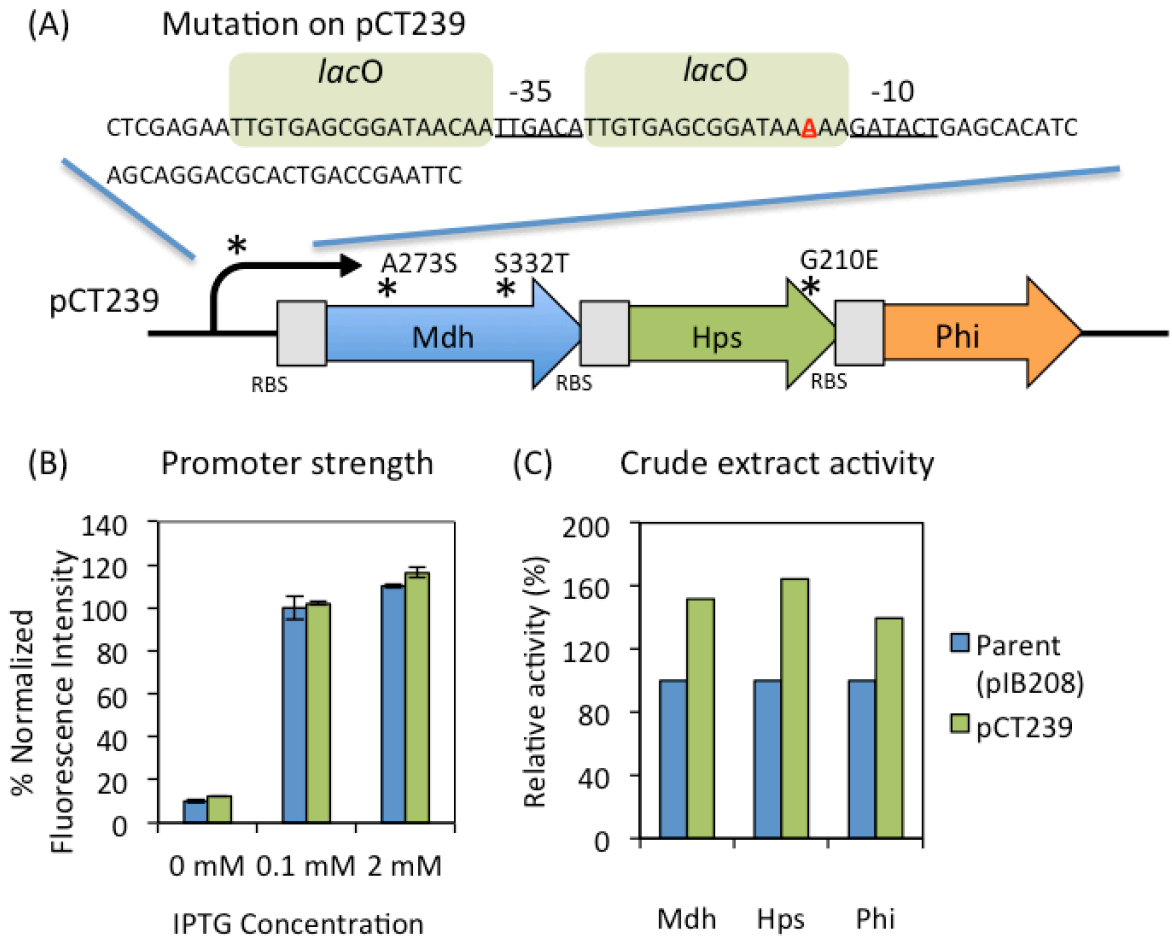

Figure 4-6 Characterization of plasmid pCT239 that enables lower methanol growth.

(A) Mutations characterized from pCT239 when compared to parent plasmid (B) Promoter strength was compared by replacing the Mdh, Hps, and Phi genes with GFP and measure fluorescence intensity with excitation wavelength 488 nm and emmision wavelength 516 nm. (C) Strain sCT497 carrying pIB208 or pCT239 were cultured in TB with 0.1mM IPTG before measuring crude extract activity of Mdh, Hps, and Phi. Error bars represents the standard deviation (n = 3). Chang-Ting Chen prepared conducted the experiment and prepared the figure.

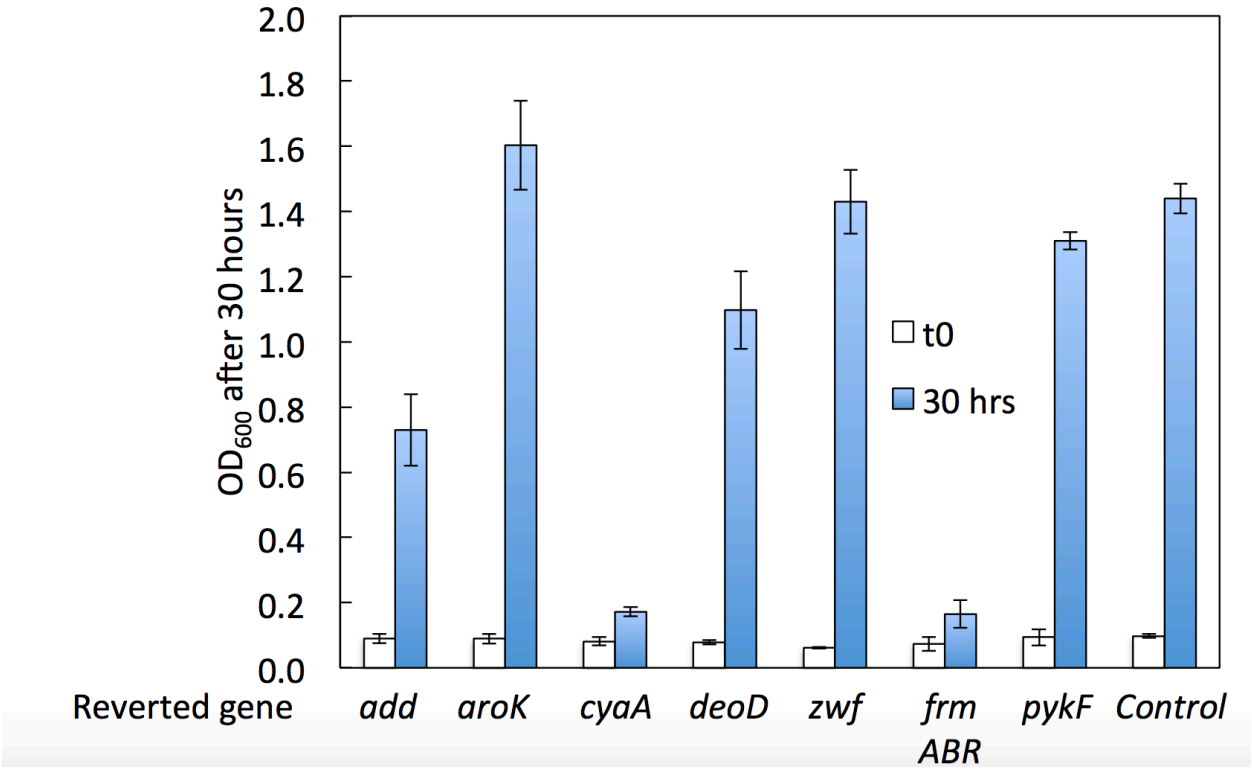

Figure 4-7 Characterization of key mutations for methanol and xylose gorwing phenotype of CFC133 (*ΔrpiAB*) strain.

The mutated genes characterized in strain CFC133 (see Table 4-3) were restored to their wild-type sequence one by one to test their contribution to the growth phenotype. For the *frmABR* restored strain, genome editing based on P1 transduction was applied (Thomason et al., 2007). A strain from the Keio collection (Baba et al., 2006) containing *yaiL* knockout with selection marker was used as source strain from which the *frmABR* region was moved to CFC133 strain to recover the truncation. The rest of the strains with restored genes were constructed by recombineering method described previously (Datsenko and Wanner, 2000). Chang-Ting Chen prepared conducted the experiment and prepared the figure.

4.9 Tables

Table 4-1. Prediction of translation initiation rate of plasmids used for methanol dependent growth using RBS calculator.

RBS calculator is described previously (Salis et al., 2010).

	Translation initiation rate (10^3 au)		
Plasmid	Mdh	Hps	Phi
pCTI2	82.3	5.70	2.4
pIB208	21.4	83.4	0.2

Table 4-2. Characterization of enzymes on pCT239

Plasmid	Parent (CT4-1)	Mdh-pCT239	Hps (*B. methanolicus*)	Hps-pCT239
V_{max} (U/mg)	0.21	0.21	5.48	2.11
K_m	21.6 mM MeOH	27.5 mM MeOH	0.97 mM R5P 0.82 mM CH_2O	0.99 mM R5P 0.84 mM CH_2O

Table 4-3. Point mutation, Indel and genome truncation list in IB730, CFC68 and CFC133 relative to their parental strains.

	Codon Change	Non-coding Region	Indel Codon Change	Large Genome Truncation Location
IB730 (Compared to WT BL21)	None	0	*tktA* (2816_2824_delACTGCACGC) (amino acid: 606_608_delTAR)	*ΔrpiA* *ΔrpiB*
CFC65 (Compared to IB730)	*tktA* (T606V)	8	Capsid component B (149_150_ins AACACAGTGTTATGACA) [Frameshift] *tktA* (2819_2824_delGCACGC) (amino acid: 607_608_delAR) *cyaA* (1373_1377_delCGGGC) [Early Stop Codon]	-
CFC133 (Relative to CFC65)	*insB-9* (M90L) *add* (L157*) *zwf* (Q433*)	6	Capsid component B (150_151_insA) [Frameshift] *clpA* (273_274_insA) [Early Stop Codon] pykF (1384_1385_insTAACACC) [Early Stop Codon] *aroK* (510_delC) [Stop Codon Extended] cyaA (1442_1443_insATCAGCC) [Early Stop Codon] deoD (679-680_insATCA) [Frameshift]	347601-350255 The operon *frmB-frmA-frmR* and *yaiO* was deleted 771473-788064 Capsid component B & C was partially deleted

Table 4-4. Strain list

Name	Genotype	Description	Reference
BL21(DE3)	*E. coli* str. B F^{-} *ompT gal dcm lon* $hsdS_B(r_B^- m_B^-)$ λ(DE3 [*lacI lacUV5-T7p07 ind1 sam7 nin5*]) $[malB^+]_{K-12}(\lambda^S)$	Wild-type	
IB405	BL21(DE3) Δ*rpe*::*kan*	Synthetic methanol auxotrophy strain with Rpe deletion	This study
sCT33	IB405 containing pCTI2	Initial construct of methanol auxotrophy with slow methanol dependent growth	This study
IB958	IB405 containing pIB208	Fast growing methanol auxotrophy strain enriched from Mdh-Hps-Phi library	This study
IB730	BL21(DE3) Δ*rpiA*::*FRT* Δ*rpiB*::*kan*	Initial strain for constructing synthetic methanol auxotrophy strain with Rpi deletion. Cannot grow on ribose plus xylose or methanol plus xylose	This study
CFC65	IB730 evolved in ribose and xylose	Grows in xylose plus ribose	This study
CFC68	CFC65 containing pIB208	Barely grow on methanol and xylose with trace amino acids supplement	This study
CFC133	Containing plasmid pIB208	CFC68 evolved in methanol and xylose. Grows in methanol plus xylose	This study
CFC134	CFC133 Δ*rpiB*::*FRT*	Kanamycin selection marker removed	This study
sCT497	See CFC133	CFC133 strain with plasmid pIB208 removed	This study
sCT745	CFC133 containing pTW244	Ethanol producing strain	This study
sCT760	IB958 containing pTW244	Ethanol producing strain	This study
sCT767	CFC134 containing pTW242	1-Butanol producing strain	This study

Table 4-5. Plasmid list.

mdh2$_{CT4-1}$ and *mdh2*$_{CT2-1}$ indicates engineered variants CT4-1 and CT2-1 of Mdh2 from *Cupriavidus necator* (Wu et al., 2016). BM, *Bacillus methanolicus*; MF, *Methylobacillus flagellates*; EC, *Escherichia coli*; CA, *Clostridium acetobutylicum*; TD, *Treponema denticola*; SE, *Salmonella enterica*; ZM, *Zymomonas mobilis*.

Name	Description	Reference
pIB208	P_L*lac*O_1::*mdh2*$_{CT4-1}$-*hps*$_{BM}$-*phi*$_{MF}$ colE *ori* Carb^r	This study
pCTI2	P_L*lac*O_1::*mdh2*$_{CT2-1}$-*hps*$_{BM}$-*phi*$_{MF}$ colE *ori* Carb^r	This study
pTW242	P_L*lac*O_1::*atoB*$_{EC}$-*crt*$_{CA}$-*hbd*$_{CA}$-*ter*$_{TD}$, P_{trc}::*pduP*$_{SE}$ p15A *ori* Kan^r	This study
pTW244	P_L*lac*O_1::*pdc*$_{ZM}$-*adhB*$_{ZM}$ CDF *ori* Spec^r	This study
pCT239	P_L*lac*O_1*::*mdh2*$_{CT4-1}$**-*hps*$_{BM}$***-*phi*$_{MF}$ colE *ori* Carb^r	This study

* With a C to A mutation within the promoter sequence:
CTCGAGAATTGTGAGCGGATAACAATTGACATTGTGAGCGGATAA**A**AAGATACTGAGCACATCAGCA
GGACGCACTGACCGAATTC

** Mutation A273S, S332T

*** Mutation G210E

4.10 Supplementary figures

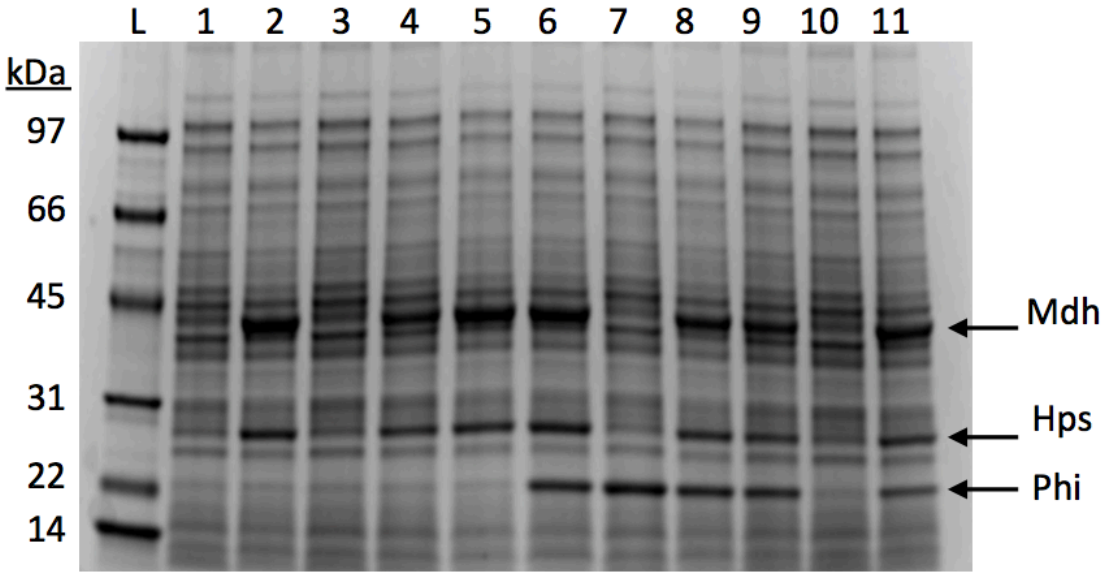

Figure 4-8 SDS-PAGE of crude extracts from isolated colonies of the Mdh, Hps, and Phi library in strain IB405.

L, protein ladder; number 1 – 11 indicates distinctive colonies.

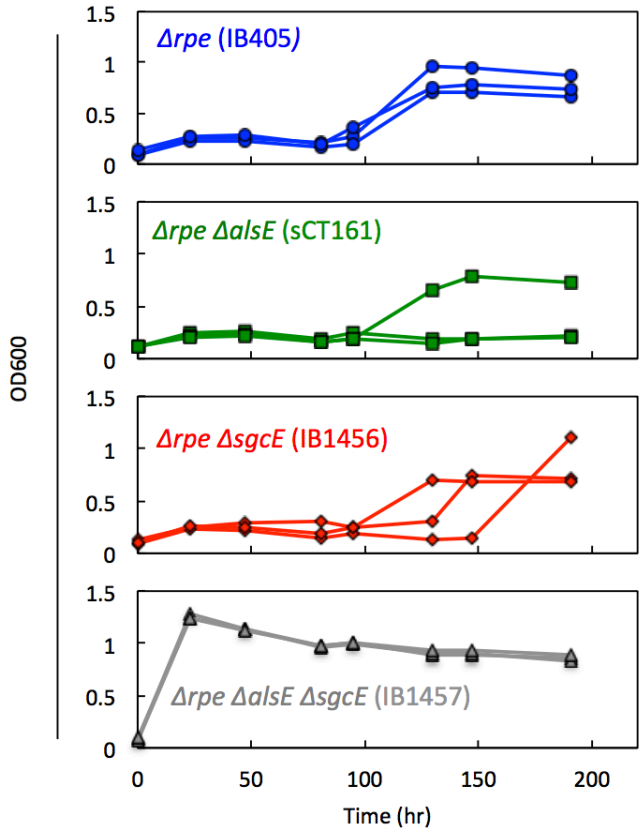

Figure 4-9 Growth test of Δ*rpe* strains with additional deletion of *alsE* and/or *sgcE*.

Strains were grown in TB with appropriate antibiotics for ~16 hrs before washed twice with MOPS minimal medium and ionculate (initial OD 0.05 -0.1) to MOPS minimal medium with 7 mM ribose. Chang-Ting Chen prepared conducted the experiment and prepared the figure.

(A)

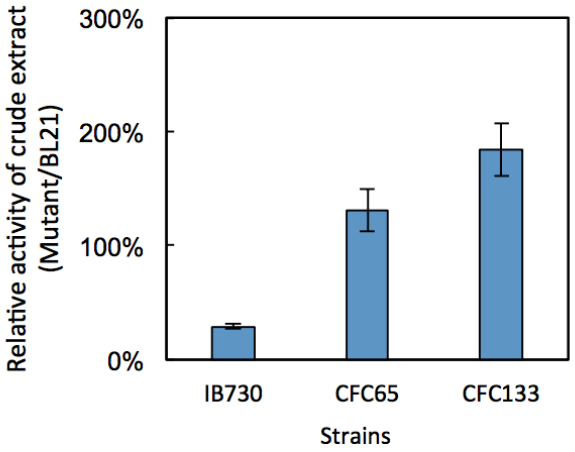

(B)

Strains	Mutation details	Amino acid sequence of tktA starting from site V605
BL21		VTARVAV
IB730	3 codons trimmed	VV---AV
CFC65	1 mutated, 2 codons trimmed	VV--VAV
CFC133		

Figure 4-10 Characterization of mutations and resulting activity of *tktA* in Δ*rpiAB* strains. Freddy Yu-Hsiao Chen conducted the experiment and prepared the figure.

5. References

Anthony, C., Zatman, L.J., 1967. The microbial oxidation of methanol. Purification and properties of the alcohol dehydrogenase of Pseudomonas sp. M27. Biochem. J. 104, 953–9.

Arfman, N., Hektor, H.J., Bystrykh, L. V, Govorukhina, N.I., Dijkhuizen, L., Frank, J., 1997. Properties of an NAD(H)-containing methanol dehydrogenase and its activator protein from Bacillus methanolicus. Eur. J. Biochem. 244, 426–433. doi:10.1111/j.1432-1033.1997.00426.x

Arfman, N., Van Beeumen, J., De Vries, G.E., Harder, W., Dijkhuizen, L., 1991. Purification and characterization of an activator protein for methanol dehydrogenase from thermotolerant Bacillus spp. J. Biol. Chem. 266, 3955–60.

Arfman, N., Watling, E.M., Clement, W., van Oosterwijk, R.J., de Vries, G.E., Harder, W., Attwood, M.M., Dijkhuizen, L., 1989. Methanol metabolism in thermotolerant methylotrophic Bacillus strains involving a novel catabolic NAD-dependent methanol dehydrogenase as a key enzyme. Arch. Microbiol. 152, 280–288. doi:10.1007/BF00409664

Baba, T., Ara, T., Hasegawa, M., Takai, Y., Okumura, Y., Baba, M., Datsenko, K.A., Tomita, M., Wanner, B.L., Mori, H., 2006. Construction of Escherichia coli K-12 in-frame, single-gene knockout mutants: The Keio collection. Mol. Syst. Biol. 2. doi:10.1038/msb4100050

Baek, S.H., Kwon, E.Y., Kim, Y.H., Hahn, J.S., 2016. Metabolic engineering and adaptive evolution for efficient production of D-lactic acid in Saccharomyces cerevisiae. Appl. Microbiol. Biotechnol. 100, 2737–2748. doi:10.1007/s00253-015-7174-0

Bar-Even, A., Noor, E., Lewis, N.E., Milo, R., 2010. Design and analysis of synthetic carbon fixation pathways. Proc. Natl. Acad. Sci. U. S. A. 107, 8889–94. doi:10.1073/pnas.0907176107

Bennett, R.K., Gonzalez, J.E., Whitaker, W.B., Antoniewicz, M.R., 2017. Expression of heterologous non-oxidative pentose phosphate pathway from Bacillus methanolicus and phosphoglucose isomerase deletion improves methanol assimilation and metabolite production by a synthetic Escherichia coli methylotroph. Metab. Eng. 45, 75–85. doi:10.1016/j.ymben.2017.11.016

Bennett, R.K., Steinberg, L.M., Chen, W., Papoutsakis, E.T., 2018. Engineering the bioconversion of methane and methanol to fuels and chemicals in native and synthetic methylotrophs. Curr. Opin. Biotechnol. 50, 81–93. doi:10.1016/j.copbio.2017.11.010

Bjørgen, M., Joensen, F., Spangsberg Holm, M., Olsbye, U., Lillerud, K.P., Svelle, S., 2008. Methanol to gasoline over zeolite H-ZSM-5: Improved catalyst performance by treatment with NaOH. Appl. Catal. A Gen. 345, 43–50. doi:10.1016/j.apcata.2008.04.020

Bogorad, I.W., Chen, C.-T., Theisen, M.K., Wu, T.-Y., Schlenz, A.R., Lam, A.T., Liao, J.C., 2014. Building carbon–carbon bonds using a biocatalytic methanol condensation cycle. Proc. Natl. Acad. Sci. 111, 15928–15933. doi:10.1073/pnas.1413470111

Bogorad, I.W., Lin, T.-S., Liao, J.C., 2013. Synthetic non-oxidative glycolysis enables complete carbon conservation. Nature 502, 693–7. doi:10.1038/nature12575

Caballero, A., Pérez, P.J., 2013. Methane as raw material in synthetic chemistry: the final frontier. Chem. Soc. Rev. 42, 8809. doi:10.1039/c3cs60120j

Carpenter, E.P., Hawkins, A.R., Frost, J.W., Brown, K.A., 1998. Structure of dehydroquinate synthase reveals an active site capable of multistep catalysis. Nature 394, 299–302. doi:10.1038/28431

Chang, C.D., 1983. Hydrocarbons from Methanol. Catal. Rev. 25, 1–118. doi:10.1080/01614948308078874

Clomburg, J.M., Crumbley, A.M., Gonzalez, R., 2017. Industrial biomanufacturing: The future of chemical production. Science (80-.). 355, aag0804. doi:10.1126/science.aag0804

Clomburg, J.M., Crumbley, A.M., Gonzalez, R., 2017. Industrial biomanufacturing: The future of chemical production. Science (80-.). 355, aag0804. doi:10.1126/science.aag0804

Conrado, R.J., Gonzalez, R., 2014. Envisioning the bioconversion of methane to liquid fuels. Science (80-.). doi:10.1126/science.1246929

Dai, Z., Gu, H., Zhang, S., Xin, F., Zhang, W., Dong, W., Ma, J., Jia, H., Jiang, M., 2017. Bioresource Technology Metabolic construction strategies for direct methanol utilization in Saccharomyces cerevisiae. Bioresour. Technol. 245, 1407–1412. doi:10.1016/j.biortech.2017.05.100

Datsenko, K.A., Wanner, B.L., 2000. One-step inactivation of chromosomal genes in Escherichia coli K-12 using PCR products. Proc. Natl. Acad. Sci. U. S. A. 97, 6640–6645. doi:10.1073/pnas.120163297

de Vries, G.E., Arfman, N., Terpstra, P., Dijkhuizenl, L., 1992. Cloning , Expression , and Sequence Analysis of the Bacillus methanolicus Cl Methanol Dehydrogenase Gene. J.

Bacteriol. 174, 5346–5353.

Elleuche, S., Antranikian, G., 2013. Bacterial group III alcohol dehydrogenases - function, evolution and biotechnological applications. OA Alcohol 1, 1–6. doi:10.13172/2053-0285-1-1-489

Fernandez, F.A., Des Rosiers, C., Previs, S.F., David, F., Brunengraber, H., 1996. Correction of 13C Mass Isotopomer Distributions. J. mass Spectrom. 31, 255–262.

Fox, J.R., Pesa, F.A., Curatolo, B.S., 1984. Formation of Higher Alcohols from Methanol Metal Acetylides in the Presence of metal acetylides. J. Catal. 90, 127–138.

Gibson, D.G., Young, L., Chuang, R.Y., Venter, J.C., Hutchison, C.A., Smith, H.O., 2009. Enzymatic assembly of DNA molecules up to several hundred kilobases. Nat. Methods 6, 343–345. doi:10.1038/nmeth.1318

Gonzalez, C.F., Proudfoot, M., Brown, G., Korniyenko, Y., Mori, H., Savchenko, A. V., Yakunin, A.F., 2006. Molecular basis of formaldehyde detoxification: Characterization of two S-formylglutathione hydrolases from Escherichia coli, FrmB and YeiG. J. Biol. Chem. 281, 14514–14522. doi:10.1074/jbc.M600996200

Gonzalez, J.E., Bennett, R.K., Papoutsakis, E.T., Antoniewicz, M.R., 2017. Methanol assimilation in Escherichia coli is improved by co-utilization of threonine and deletion of leucine-responsive regulatory protein. Metab. Eng. 45, 67–74. doi:10.1016/j.ymben.2017.11.015

Groussac, E., Ortiz, M., Francñois, J., 2000. Improved protocols for quantitative determination of

metabolites from biological samples using high performance ionic-exchange chromatography with conductimetric and pulsed amperometric detection. Enzyme Microb. Technol. 26, 715–723. doi:10.1016/S0141-0229(00)00163-0

Guex, N., Peitsch, M.C., Schwede, T., 2009. Automated comparative protein structure modeling with SWISS-MODEL and Swiss-PdbViewer: A historical perspective. Electrophoresis 30, 162–173. doi:10.1002/elps.200900140

Hagishita, T., Yoshida, T., Izumi, Y., Mitsunaga, T., 1996. Efficient L-serine Production from methanol and glycine by resting cells of Methylobacterium sp. Strain MN43. Chem. Pharm. Bull. 14, 369–375. doi:10.1248/cpb.37.3229

Haynes, C.A., Gonzalez, R., 2014. Rethinking biological activation of methane and conversion to liquid fuels. Nat. Chem. Biol. 10, 331–339. doi:10.1038/nchembio.1509

Hektor, H.J., Kloosterman, H., Dijkhuizen, L., 2002. Identification of a magnesium-dependent NAD(P)(H)-binding domain in the nicotinoprotein methanol dehydrogenase from Bacillus methanolicus. J. Biol. Chem. 277, 46966–46973. doi:10.1074/jbc.M207547200

Hove-Jensen, B., Andersen, K.R., Kilstrup, M., Martinussen, J., Switzer, R.L., Willemoës, M., 2017. Phosphoribosyl Diphosphate (PRPP): Biosynthesis, Enzymology, Utilization, and Metabolic Significance. Microbiol. Mol. Biol. Rev. 81, e00040-16. doi:10.1128/MMBR.00040-16

Hove-Jensen, B., Rosenkrantz, T.J., Haldimann, A., Wanner, B.L., 2003. Escherichia coli phnN, encoding ribose 1,5-bisphosphokinase activity (phosphoribosyl diphosphate forming): Dual role in phosphonate degradation and NAD biosynthesis pathways. J. Bacteriol. 185, 2793–

2801. doi:10.1128/JB.185.9.2793-2801.2003

Ivanova, E.G., FEDOROV, D.N., DORONINA, N. V, TROTSENKO, Y.A., 2006. Production of vitamin B 12 in aerobic methylotrophic bacteria. Microbiology 75, 494–496. doi:10.1134/S0026261706040217

Jantama, K., Haupt, M.J., Svoronos, S.A., Zhang, X., Moore, J.C., Shanmugam, K.T., Ingram, L.O., 2008. Combining metabolic engineering and metabolic evolution to develop nonrecombinant strains of Escherichia coli C that produce succinate and malate. Biotechnol. Bioeng. 99, 1140–1153. doi:10.1002/bit.21694

Jiang, L.Y., Chen, S.G., Zhang, Y.Y., Liu, J.Z., 2013. Metabolic evolution of Corynebacterium glutamicum for increased production of L-ornithine. BMC Biotechnol. 13. doi:10.1186/1472-6750-13-47

Jones, J.H., 2000. The Cativa(tm) Process for the Manufacture of Acetic Acid. Platin. Met. Rev. 44, 94–105.

Keltjens, J.T., Pol, A., Reimann, J., Op den Camp, H.J.M., 2014. PQQ-dependent methanol dehydrogenases: Rare-earth elements make a difference. Appl. Microbiol. Biotechnol. 98, 6163–6183. doi:10.1007/s00253-014-5766-8

Kessler, D., Herth, W., Knappe, J., 1992. Ultrastructure and pyruvate formate-lyase radical quenching property of the multienzymic AdhE protein of Escherichia coli. J. Biol. Chem. 267, 18073–18079.

Kien, C.L., Chang, D.H., Murray, R.D., Ailabouni, A., Kepner, J., 1990. Measurement of Stable

Isotopic Enrichment of Underivatized Acetate by Gas Chromatography/Mass Spectrometry : Application to in vivo Estimation of Acetate Production. Biomed. Environ. Mass Spectrom. 19, 554–558.

Kim, C., Song, S., Park, C., Al, K.I.M.E.T., 1997. The D -Allose Operon of Escherichia coli K-12. J. Bacteriol. 179, 7631–7637.

Kloosterman, H., Vrijbloed, J.W., Dijkhuizen, L., 2002. Molecular, biochemical, and functional characterization of a Nudix hydrolase protein that stimulates the activity of a nicotinoprotein alcohol dehydrogenase. J. Biol. Chem. 277, 34785–34792. doi:10.1074/jbc.M205617200

Koopman, F.W., De Winde, J.H., Ruijssenaars, H.J., 2009. C1 compounds as auxiliary substrate for engineered Pseudomonas putida S12. Appl. Microbiol. Biotechnol. 83, 705–713. doi:10.1007/s00253-009-1922-y

Kotrbova-Kozak, A., Kotrba, P., Inui, M., Sajdok, J., Yukawa, H., 2007. Transcriptionally regulated adhA gene encodes alcohol dehydrogenase required for ethanol and n-propanol utilization in Corynebacterium glutamicum R. Appl. Microbiol. Biotechnol. 76, 1347–1356. doi:10.1007/s00253-007-1094-6

Kozlowski, J.T., Davis, R.J., 2013. Heterogeneous catalysts for the guerbet coupling of alcohols. ACS Catal. 3, 1588–1600. doi:10.1021/cs400292f

Krog, A., Heggeset, T.M.B., Müller, J.E.N., Kupper, C.E., Schneider, O., Vorholt, J.A., Ellingsen, T.E., Brautaset, T., 2013. Methylotrophic Bacillus methanolicus Encodes Two Chromosomal and One Plasmid Born NAD+ Dependent Methanol Dehydrogenase Paralogs

with Different Catalytic and Biochemical Properties. PLoS One 8. doi:10.1371/journal.pone.0059188

Lan, E.I., Ro, S.Y., Liao, J.C., 2013. Oxygen-tolerant coenzyme A-acylating aldehyde dehydrogenase facilitates efficient photosynthetic n-butanol biosynthesis in cyanobacteria. Energy Environ. Sci. 6, 2672. doi:10.1039/c3ee41405a

Lee, Y., Lafontaine Rivera, J.G., Liao, J.C., 2014. Ensemble Modeling for Robustness Analysis in engineering non-native metabolic pathways. Metab. Eng. 25, 63–71. doi:10.1016/j.ymben.2014.06.006

Leßmeier, L., Pfeifenschneider, J., Carnicer, M., Heux, S., Portais, J., Wendisch, V.F., 2015. Production of carbon-13-labeled cadaverine by engineered Corynebacterium glutamicum using carbon-13-labeled methanol as co-substrate. Appl. Microbiol. Biotechnol. 10163–10176. doi:10.1007/s00253-015-6906-5

Long, C.P., Gonzalez, J.E., Sandoval, N.R., Antoniewicz, M.R., 2016. Characterization of physiological responses to 22 gene knockouts in Escherichia coli central carbon metabolism. Metab. Eng. 37, 102–113. doi:10.1016/j.ymben.2016.05.006

Lutz, R., Bujard, H., 1997. Independent and tight regulation of transcriptional units in Escherichia coli via the LacR/O, the TetR/O and AraC/I1-I2 regulatory elements. Nucleic Acids Res. 25, 1203–10. doi:10.1093/nar/25.6.1203

Lyngstadaas, A., Sprenger, G.A., Boye, E., 1998. Impaired growth of an Escherichia coli rpe mutant lacking ribulose-5-phosphate epimerase activity. Biochim. Biophys. Acta - Gen. Subj. 1381, 319–330. doi:10.1016/S0304-4165(98)00046-4

Mani, J.C., Pietruszko, R., Theorell, H., 1970. Methanol activity of alcohol dehydrogenases from human liver, horse liver, and yeast. Arch. Biochem. Biophys. 140, 52–59. doi:10.1016/0003-9861(70)90009-3

Marçal, D., Rêgo, A.T., Carrondo, M.A., Enguita, F.J., 2009. 1,3-Propanediol dehydrogenase from Klebsiella pneumoniae: Decameric quaternary structure and possible subunit cooperativity. J. Bacteriol. 191, 1143–1151. doi:10.1128/JB.01077-08

McCann, D.M., Lesthaeghe, D., Kletnieks, P.W., Guenther, D.R., Hayman, M.J., Van Speybroeck, V., Waroquier, M., Haw, J.F., 2008. A complete catalytic cycle for supramolecular methanol-to-olefins conversion by linking theory with experiment. Angew. Chemie - Int. Ed. 47, 5179–5182. doi:10.1002/anie.200705453

Montella, C., Bellsolell, L., Pe, R., Badı, J., Baldoma, L., 2005. Crystal Structure of an Iron-Dependent Group III Dehydrogenase That Interconverts L -Lactaldehyde and L -1 , 2-Propanediol in Escherichia coli †. Society 187, 4957–4966. doi:10.1128/JB.187.14.4957

Moon, J.H., Lee, H.J., Park, S.Y., Song, J.M., Park, M.Y., Park, H.M., Sun, J., Park, J.H., Kim, B.Y., Kim, J.S., 2011. Structures of iron-dependent alcohol dehydrogenase 2 from zymomonas mobilis ZM4 with and without NAD+cofactor. J. Mol. Biol. 407, 413–424. doi:10.1016/j.jmb.2011.01.045

Motoyama, H., Anazawa, H., Katsumata, R., Araki, K., Teshiba, S., 1993. Amino acids production from methanol by methylobaccilus glycogenes mutants: isolation of L-glutamic acid hyper-producing mutants from M. glycogenes strains, and derivation of L-threonine and L-lysine-producing mutants from them. Chem. Pharm. Bull. (Tokyo). 37, 3229–3235.

doi:10.1248/cpb.37.3229

Motoyama, H., Yano, H., Ishino, S., Anazawa, H., Teshiba, S., 1994. Effects of the amplification of the genes coding for the L-threonine biosynthetic enzymes on the L-threonine production from methanol by a gram-negative obligate methylotroph, Methylobacillus glycogenes. Appl. Microbiol. Biotechnol. 42, 67–72. doi:10.1007/s002530050218

Motoyama, H., Yano, H., Terasaki, Y., Anazawa, H., 2001. Overproduction of L-Lysine from Methanol by Methylobacillus glycogenes Derivatives Carrying a Plasmid with a Mutated dapA Gene. Appl. Environ. Microbiol. 67, 3064–3070. doi:10.1128/AEM.67.7.3064-3070.2001

Müller, J.E.N., Meyer, F., Litsanov, B., Kiefer, P., Potthoff, E., Heux, S., Quax, W.J., Wendisch, V.F., Brautaset, T., 2015. Engineering Escherichia coli for methanol conversion. Metab. Eng. 28, 190–201. doi:10.1016/j.ymben.2014.12.008

Müller, J.E.N., Meyer, F., Litsanov, B., Kiefer, P., Potthoff, E., Heux, S., Quax, W.J., Wendisch, V.F., Brautaset, T., Portais, J.-C., Vorholt, J.A., 2015. Engineering Escherichia coli for methanol conversion. Metab. Eng. 28, 190–201. doi:10.1016/j.ymben.2014.12.008

Naerdal, I., Pfeifenschneider, J., Brautaset, T., Wendisch, V.F., 2015. Methanol-based cadaverine production by genetically engineered *B acillus methanolicus* strains. Microb. Biotechnol. 8, 342–350. doi:10.1111/1751-7915.12257

Nakahigashi, K., Toya, Y., Ishii, N., Soga, T., Hasegawa, M., Watanabe, H., Takai, Y., Honma, M., Mori, H., Tomita, M., 2009. Systematic phenome analysis of Escherichia coli multiple-knockout mutants reveals hidden reactions in central carbon metabolism. Mol. Syst. Biol. 5,

1–14. doi:10.1038/msb.2009.65

Nnyepi, M.R., Peng, Y., Broderick, J.B., 2007. Inactivation of E. coli pyruvate formate-lyase: Role of AdhE and small molecules. Arch. Biochem. Biophys. 459, 1–9. doi:10.1016/j.abb.2006.12.024

Notredame, C., Higgins, D.G., Heringa, J., 2000. T-coffee: A novel method for fast and accurate multiple sequence alignment. J. Mol. Biol. 302, 205–217. doi:10.1006/jmbi.2000.4042

Ochsner, A.M., Müller, J.E.N., Mora, C.A., Vorholt, J.A., 2014. In vitro activation of NAD-dependent alcohol dehydrogenases by Nudix hydrolases is more widespread than assumed. FEBS Lett. 588, 2993–2999. doi:10.1016/j.febslet.2014.06.008

Ohta, K., Beall, D.S., Mejia, J.P., Shanmugam, K.T., Ingram, L., 1991. Genetic Improvement of Escherichia coli for ethanol production: Chromosomal integration of zymomonas mobilis genes encoding pyruvate decarboxylase and alcohol dehydrogenase II. Appl. Environ. Microbiol. 57, 893–900.

Ott, J., Gronemann, V., Pontzen, F., Fiedler, E., Grossmann, G., Kersebohm, D.B., Weiss, G., Witte, C., 2012. Methanol, in: Ullmann's Encyclopedia of Industrial Chemistry. Wiley-VCH Verlag GmbH & Co. KGaA, Weinheim, Germany. doi:10.1002/14356007.a16_465.pub3

Park, C.S., Yeom, S.J., Lim, Y.R., Kim, Y.S., Oh, D.K., 2011. Substrate specificity of a recombinant ribose-5-phosphate isomerase from Streptococcus pneumoniae and its application in the production of l-lyxose and l-tagatose. World J. Microbiol. Biotechnol. 27, 743–750. doi:10.1007/s11274-010-0511-7

Price, J.V., Chen, L., Whitaker, W.B., Papoutsakis, E., Chen, W., 2016. Scaffoldless engineered enzyme assembly for enhanced methanol utilization. Proc. Natl. Acad. Sci. 113, 12691–12696. doi:10.1073/pnas.1601797113

Robert, X., Gouet, P., 2014. Deciphering key features in protein structures with the new ENDscript server. Nucleic Acids Res. 42, 320–324. doi:10.1093/nar/gku316

Roggenkamp, R., Sahm, H., Hinkelmann, W., Wagner, F., 1975. Alcohol Oxidase and Catalase in Peroxisomes of Methanol-Grown Candida boidinii. Eur. J. Biochem. 59, 231–236. doi:10.1111/j.1432-1033.1975.tb02446.x

Ruzheinikov, S.N., Burke, J., Sedelnikova, S., Baker, P.J., Taylor, R., Bullough, P. a., Muir, N.M., Gore, M.G., Rice, D.W., 2001. Glycerol Dehydrogenase. Structure 9, 789–802. doi:10.1016/S0969-2126(01)00645-1

Salis, H.M., Mirsky, E. a, Voigt, C. a, 2010. Automated Design of Synthetic Ribosome Binding Sites to Precisely Control Protein Expression. Nat Biotechnol 27, 946–950. doi:10.1038/nbt.1568.Automated

Schrader, J., Schilling, M., Holtmann, D., Sell, D., Filho, M.V., Marx, A., Vorholt, J.A., 2009. Methanol-based industrial biotechnology: Current status and future perspectives of methylotrophic bacteria. Trends Biotechnol. 27, 107–15. doi:10.1016/j.tibtech.2008.10.009

Schramm, M., Klybas, V., Racker, E., 1958. Phosphorolytic Cleavage of Fructose-6-phosphate by Fructose-6-phosphate Phosphoketolase from Acetobacter xylinum. J. Biol. Chem. 233, 1283–1288.

Schürmann, M., Sprenger, G.A., 2001. Fructose-6-phosphate Aldolase is a Novel Class I Aldolase from Escherichia coli and is Related to a Novel Group of Bacterial Transaldolases. J. Biol. Chem. 276, 11055–11061. doi:10.1074/jbc.M008061200

Shaked, Z., Whitesides, G.M., 1980. Enzyme-Catalyzed Organic Synthesis: NADH Regeneration by Using Formate Dehydrogenase. J. Am. Chem. Soc. 102, 7104–7105. doi:10.1021/ja00543a038

Sheehan, M.C., Bailey, C.J., Dowds, B.C., McConnell, D.J., 1988. A new alcohol dehydrogenase, reactive towards methanol, from Bacillus stearothermophilus. Biochem. J. 252, 661–666. doi:10.1042/bj2520661

Shen, C.R., Lan, E.I., Dekishima, Y., Baez, A., Cho, K.M., Liao, J.C., 2011. Driving Forces Enable High-Titer Anaerobic 1-Butanol Synthesis in Escherichia coli. Appl. Environ. Microbiol. 77, 2905–2915. doi:10.1128/AEM.03034-10

Sonntag, F., Kroner, C., Lubuta, P., Peyraud, R., Horst, A., Buchhaupt, M., Schrader, J., 2015. Engineering Methylobacterium extorquens for de novo synthesis of the sesquiterpenoid α-humulene from methanol. Metab. Eng. 32, 82–94. doi:10.1016/j.ymben.2015.09.004

Sørensen, K.I., Hove-Jensen, B., 1996. Ribose catabolism of *Escherichia coli*: characterization of the *rpiB* gene encoding ribose phosphate isomerase B and of the *rpiR* gene, which is involved in regulation of *rpiB* expression. J. Bacteriol. 178, 1003–11.

Stöcker, M., 1999. Methanol-to-hydrocarbons: catalytic materials and their behavior1. Microporous Mesoporous Mater. 29, 3–48. doi:10.1016/S1387-1811(98)00319-9

Summers, D.P., Leach, S., Frese, K.W., 1986. The electrochemical reduction of aqueous carbon dioxide to methanol at molybdenum electrodes with low overpotentials. J. Electroanal. Chem. 205, 219–232. doi:10.1016/0022-0728(86)90233-0

Thomason, L.C., Costantino, N., Court, D.L., 2007. *E. coli* Genome Manipulation by P1 Transduction. Curr. Protoc. Mol. Biol. 1.17.1-1.17.8. doi:10.1002/0471142727.mb0117s79

Welch, P., Scopes, R.K., 1985. Studies on cell-free metabolism: Ethanol production by a yeast glycolytic system reconstituted from purified enzymes. J. Biotechnol. 2, 257–273. doi:10.1016/0168-1656(85)90029-X

Whitaker, W.B., Jones, J.A., Bennett, R.K., Gonzalez, J., Vernacchio, V.R., Collins, S.M., Palmer, M.A., Schmidt, S., Antoniewicz, M.R., Koffas, M.A.G., Papoutsakis, E.T., 2016. Engineering the biological conversion of methanol to specialty chemicals in Escherichia coli. Metab. Eng. doi:10.1016/j.ymben.2016.10.015

Whitaker, W.B., Jones, J.A., Bennett, R.K., Gonzalez, J.E., Vernacchio, V.R., Collins, S.M., Palmer, M.A., Schmidt, S., Antoniewicz, M.R., Koffas, M.A., Papoutsakis, E.T., 2017. Engineering the biological conversion of methanol to specialty chemicals in Escherichia coli. Metab. Eng. 39, 49–59. doi:10.1016/j.ymben.2016.10.015

Whitaker, W.B., Sandoval, N.R., Bennett, R.K., Fast, A.G., Papoutsakis, E.T., 2015. Synthetic methylotrophy: engineering the production of biofuels and chemicals based on the biology of aerobic methanol utilization. Curr. Opin. Biotechnol. 33, 165–175. doi:10.1016/j.copbio.2015.01.007

Wierenga, R.K., Terpstra, P., Hol, W.G., 1986. Prediction of the occurrence of the ADP-binding

beta alpha beta-fold in proteins, using an amino acid sequence fingerprint. J. Mol. Biol. 187, 101–107. doi:10.1016/0022-2836(86)90409-2

Witthoff, S., Mühlroth, A., Marienhagen, J., Bott, M., 2013. C1 metabolism in Corynebacterium glutamicum: An endogenous pathway for oxidation of methanol to carbon dioxide. Appl. Environ. Microbiol. 79, 6974–6983. doi:10.1128/AEM.02705-13

Witthoff, S., Schmitz, K., Niedenführ, S., Nöh, K., Noack, S., Bott, M., Marienhagen, J., 2015. Metabolic engineering of Corynebacterium glutamicum for methanol metabolism. Appl. Environ. Microbiol. 81, 2215–2225. doi:10.1128/AEM.03110-14

Wu, T.Y., Chen, C.T., Liu, J.T.J., Bogorad, I.W., Damoiseaux, R., Liao, J.C., 2016. Characterization and evolution of an activator-independent methanol dehydrogenase from Cupriavidus necator N-1. Appl. Microbiol. Biotechnol. 100, 4969–4983. doi:10.1007/s00253-016-7320-3

Ye, X., Honda, K., Sakai, T., Okano, K., Omasa, T., Hirota, R., Kuroda, A., Ohtake, H., 2012. Synthetic metabolic engineering-a novel, simple technology for designing a chimeric metabolic pathway. Microb. Cell Fact. 11. doi:10.1186/1475-2859-11-120

Yomano, L.P., York, S.W., Zhou, S., Shanmugam, K.T., Ingram, L.O., 2008. Re-engineering Escherichia coli for ethanol production. Biotechnol. Lett. 30, 2097–2103. doi:10.1007/s10529-008-9821-3

Zhang, J.., Chung, T.D.., Oldenburg, K.., 1990. A simple statistical parameter for use in evaluation and validation of high throughput screening assays. J. Biomol. Screen. 4, 67–73. doi:0803973233

Zhang, W., Zhang, T., Wu, S., Wu, M., Xin, F., Dong, W., Ma, J., Zhang, M., Jiang, M., 2017. Guidance for engineering of synthetic methylotrophy based on methanol metabolism in methylotrophy. RSC Adv. 7, 4083–4091. doi:10.1039/C6RA27038G

Zhang, X., Jantama, K., Moore, J.C., Jarboe, L.R., Shanmugam, K.T., Ingram, L.O., 2009. Metabolic evolution of energy-conserving pathways for succinate production in Escherichia coli. Proc. Natl. Acad. Sci. 106, 20180–20185. doi:10.1073/pnas.0905396106

Zhang, Y.H.P., Evans, B.R., Mielenz, J.R., Hopkins, R.C., Adams, M.W.W., 2007. High-yield hydrogen production from starch and water by a synthetic enzymatic pathway. PLoS One 2, 2–7. doi:10.1371/journal.pone.0000456

Zhang, Y.H.P., Sun, J., Zhong, J.J., 2010. Biofuel production by in vitro synthetic enzymatic pathway biotransformation. Curr. Opin. Biotechnol. 21, 663–669. doi:10.1016/j.copbio.2010.05.005

Zhao, G., Winkler, M.E., 1994. An Escherichia coli K-12 tktA tktB mutant deficient in transketolase activity requires pyridoxine (vitamin B6) as well as the aromatic amino acids and vitamins for growth. J. Bacteriol. doi:10.1128/jb.176.19.6134-6138.1994

Zhu, X., Tan, Z., Xu, H., Chen, J., Tang, J., Zhang, X., 2014. Metabolic evolution of two reducing equivalent-conserving pathways for high-yield succinate production in Escherichia coli. Metab. Eng. 24, 87–96. doi:10.1016/j.ymben.2014.05.003